

ulm university universität
uulm

Universität Ulm
Institut für Theoretishe Chemie
Leiter: Prof. Dr. Axel Groß

First-principles Study of Structures and Processes at Metallic Electrodes

Dissertation zur Erlangung des Doktorgrades Dr. rer. nat.
der Fakultät für Naturwissenschaften der Universität Ulm

vorgelegt von

Xiaohang Lin
aus Shandong China

Amtierende Dekan:	Prof. Dr. Joachim Ankerhold
Erstgutachter:	Prof. Dr. Axel Groß
Zweitgutachter:	Prof. Dr. Gerhard Taubmann
Tag der Promotion:	21.04.2015

Contents

1 Introduction
2 Theoretical Background
    2.1 Density functional theory
        2.1.1 Kohn-Sham equations
        2.1.2 Exchange-Correlation Functional
        2.1.3 Plane wave basis sets
        2.1.4 Pseudopotential approximation
    2.2 Ab initial molecular dynamics
    2.3 NEB method
    2.4 Physical properties
        2.4.1 Adsorption energies
        2.4.2 Work function
        2.4.3 Charge density difference
        2.4.4 Density of states (DOS)
        2.4.5 Vibrational spectra
3 Computational details
4 Clean metal surfaces: Au Ag and Pb
    4.1 Introduction of experimental data
    4.2 Calculation results of clean surfaces
5 Water-metal interfaces
    5.1 Introduction: Experimental results
    5.2 Adsorption of single water molecule on metal surfaces
    5.3 Single water layer on Au surfaces
    5.4 Single water layer on Ag surfaces
    5.5 Water layers on flat Pb surfaces

6 self-diffusion on Pb flat and stepped surfaces
6.1 Motivation
6.2 single atom adsorbed on Pb surfaces
6.3 Calculation results of self-diffusion
7 Conclusions
Acknowledgments

Chapter1
Introduction

Recently, the development of quantum devices has attracted much attention, which could open perspectives for further developments, especially in computer physical technology [1.1-1.13]. Although many experiments were performed in the fabrication of contacts based on individual molecules or even atoms in recent year, they only focused at the molecule-scale or atom-scale resistors. In this research field, a fundamental point which is hardly addressed, is the development of actively controllable devices such as quantum switches, which allow to control the current through an atom-scale device by an independent gate electrode.

The group of Th. Schimmel reports a series of innovative experiments, which allow the controlled and repeatable switching of an atomic-scale quantum point contacts by means of an independent gate electric field [1.14-1.18].The switch can be applied as a basic functional electric unit, and it shows us an incredible stability at room temperature: after several days and several thousand times transition between the “on state” and ”off state” it still works. It shows great potentialities and probability of application. However the basic principle of such a switch is not clear yet, and the investigation of the process close to the apexes of metal electrodes is rather important to understand the atomic-scale metal reconstruction and electronic properties under the extra electronic field in a liquid environment, which obviously could help us to improve and apply the technology of quantum switch [1.19-1.36].

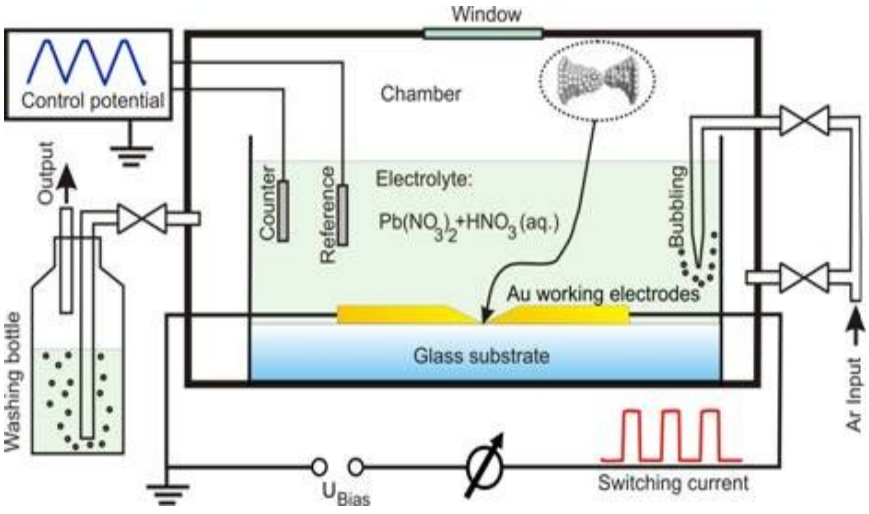


Fig. 1.1 Diagrammatic sketch of the experiment setup. Pb is located on the narrow gap between two Au working electrodes (WE) [1.17].

The diagrammatic sketch of the experiment setup is shown by Fig. 1. Before the beginning of electrochemical deposition, the container is thoroughly streamed with inert gas (Ar) to create a practical Oxygen-free environment, which can prevent the oxidation reaction of lead. To grow the atomic-scale Pb contacts, two polycrystalline gold working electrodes (WEs) are set (thickness approx. 100 nm, 50 nm apart). They were covered with an insulating polymer which can minimize the ionic conduction. The distance between them is approximately 50 nm. The electrolyte is made from 1 mM $Pb(NO_3)_2$ and 0.1 M HNO_3 in bidistilled water. The lead reference electrode (RE) and the counter electrode (CE) (two lead wire with 0.5 mm diameter and 99.998% purity) are set by a computer-controlled potentiostat which the potentials of the WEs are related to. Between two WEs, the voltage of -12.9 mV is used to measure the conductance.

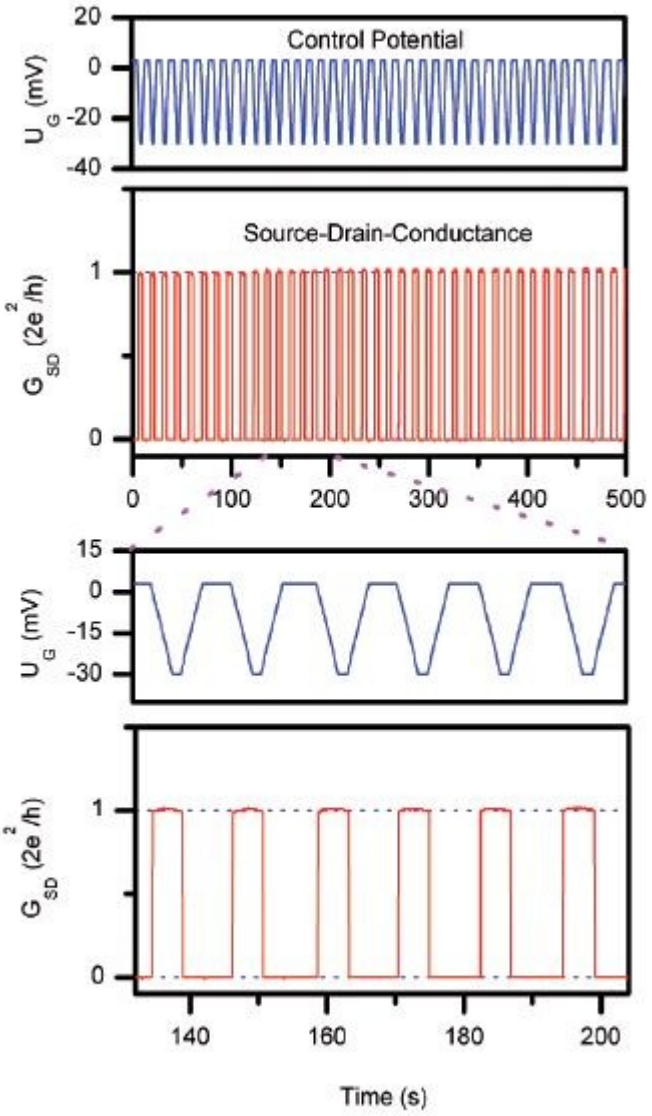


Fig. 1.2 The Ag quantum switch working process [1.37].

The gate potential (U_G) (blue curves) control the source-drain conductance G_{sd} of the Ag atomic-scale quantum switch (red curves) directly. The last two figures in fig.1.2 show us the details of U_G and G_{sd} changes from 140s to 200s in the figures above [1.37].

The size of the switch is rather small, the distance between two contacts is on the scale of the electron wavelength, the quantum effect of the electron is notable and can be observed directly. The conductance of such switches is quantized, the value of the conductance is multiples of the conductance quantum G_0 , which is equal to the $2e^2/h$. E is the charge of an electron and h is Planck's constant.

Fig. 1.2 shows us a stable switch process observed on silver atomic-scale quantum switch, similar results are also observed for lead. The source-drain conductance changes between the "off state" (insulation state) and "on state" ($G_{sd} = G_0$), which obviously is controlled by the gate potential directly. The switch open potential is in the range between -18 mV and -36 mV and closed by the control potential between 6 mV and 15 mV [1.14, 1.17, 1.37].

The switching process between 0 to G_0 costs only about 50 μs after the control potential is changed, different switches have characteristic differences depending on the different geometry of contact and ion concentration of the environment. However these switch processes are highly repeatable, more than 1000 switching events were recorded from the experiments of numerous different contacts [1.14, 1.17, 1.37].

The experimental data indicate several important points:

First, the geometries of the contacts should be well-ordered, most probably in a "crystallized" structure, after several dissolution-deposition processes. Here we address a general idea of the structures of contacts (Fig. 1.3). Most possibly, contacts are formed by (111) surface, (100) surface, in particular stepped surfaces, which were chosen to simulate the contact surfaces in our study (for stepped surfaces (211), (311), (511), (711) are used). More details of these surfaces will be presented in Chapter 4.

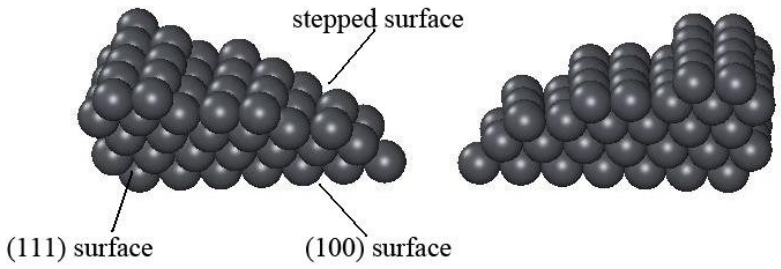


Fig. 1.3 The diagrammatic sketch of the contacts which might be formed by (111) surface, (100) surface and stepped surfaces

Second, the “off state” corresponds to a high stable “phase off” of the switch, and “on state” is related to another stable “phase on” under the control potential. Normally “phase off” is more stable than “phase on”, but the stability relation reverses when the control potential reaches a certain value.

Third, the stability and repeatability of the switch indicate an existence of a stable and certain kind of pathway between “phase off” to “phase on”.

What happens during this switch process? or in other words, what are the differences between these two “phases”? In my opinion, there are three possibilities:

1, Because of the liquid environment, the structures of water layers near the contacts may change when the extra potential changes, and this may cause the difference of the electric properties. In Chapter 5, we investigate the metal-water interface, and compare the results with some experimental data.

2, Under potential control , the barriers of self-diffusion may change and this make it possible to transform the structure to a more stable structure. In Chapter 6, the processes of self-diffusion on different surfaces are investigated.

3, The deposition of the metal ions in the solution and dissolution of the contact may happen, and make the transformation between the “on” and “off” phase. This situation is more complicated than the two above, and it is the next step of our investigation.

The main purpose of our study is to find one or several primary mechanisms of the quantum switch. Finally we summarize our results in Chapter 7.

Bibliography

[1.1] N. Agrait, A. Levy Yeyati, and J. M. van Ruitenbeek, *Phys. Rep.* **377**, 81 (2003).

[1.2] N. Agrait, J. G. Rodrigo, and S. Vieira, *Phys. Rev. B* **47**, 12345 (1993).

[1.3] J. I. Pascual et al, *Phys. Rev.Lett.* **71**, 1852 (1993).

[1.4] J. M. Krans et al, *Phys. Rev. B* **48**, 14721 (1993).

[1.5] J. M. Krans et al, *Nature (London)* **375**, 767 (1995).

[1.6] D. P. E. Smith, *Science* 269, 371 (1995)

[1.7] E. Scheer et al, *Nature (London)* 394, 154 (1998)

[1.8] U. Landman, W. D. Luedtke, B. E. Salisbury, and R. L. Whetten, *Phys. Rev.Lett.* **77**, 1362 (1996)

[1.9] C. Z. Li, and N. J. Tao, *Appl. Phys. Lett.* **72**, 894 (1998)

[1.10] C. Z. Li, A. Bogozi, W. Huang, and N. J. Tao, *Nanotechnology* **10,** 221 (1999)

[1.11] A. F. Morpurgo, C. M. Marcus, and D. B. Robinson, *Appl. Phys. Lett.* 74, 2084 (1999)
[1.12] C. Z. Li, H. X. He, and N. J. Tao, *Appl. Phys. Lett.* 77, 3995 (2000)
[1.13] F. Elhoussine, S. Matefi-Tmpfi, A. Encinas, and L. Piraux, *Appl. Phys. Lett.* 81, 1681 (2002)
[1.14] F. -Q. Xie, L. Nittler, Ch. Obermair, and Th. Schimmel, *Phys. Rev.Lett.* **93,** 128303 (2004)
[1.15] F. -Q. Xie, Ch. Obermair, Th. Schimmel, *Nanoscale Devices-Fundamentals and Applications*, 153-162 (2006)
[1.16] F. -Q. Xie, R. Maul, S. Brendelberger, Ch. Obermair, E. B. Starikov et al. *Appl. Phys. Lett.* **93** 043103 (2008)
[1.17] F. -Q. Xie, F. Hueser, F. Pauly, Ch. Obermair, G. Schoen, and Th. Schimmel, *Phys. Rev. B* **82,** 075417 (2010)
[1.18] F. -Q. Xie, R. Maul, Ch. Obermair, W. Wenzel, G. Schoen, and Th. Schimmel, *Adv. Mater* **22,** 2033 (2010)
[1.19] F. May, M. R. Wegewijs, W. Hofstetter, *Beilstein J. Nanotechnol.* **2***,* 693–698 (2011)
[1.20] C. A. Martin, D. Ding,J. K. Sørensen, T. Bjørnholm, J. M. van Ruitenbeek, H. S. J. van der Zant, *J. Am. Chem. Soc.* **130**, 13198-13199 (2008)
[1.21] W. -J Hong, H. Valkenier, G. Mészáros, D. Zsolt Manrique, A. Mishchenko, A. Putz, P. Moreno Garcia, C. Lambert, J. C. Hummelen, T. Wandlowski, *Beilstein J. Nanotechnol.* **2011**, *2*, 699-713.
[1.22] E. Lörtscher, H. B. Weber, H. Riel, *Phys. Rev. Lett.* **98**, 176807 (2007)
[1.23] T. N. Todorov, D. Dundas, A. T. Paxton, and A. P. Horsfield, *Beilstein J. Nanotechnol.* **2***,* 727–733 (2011)
[1.24] T. Shiota, A. I. Mares, A. M. C. Valkering, T. H. Oosterkamp, and J. M. van Ruitenbeek, *Phys. Rev. B* **77**, 125411 (2008)
[1.25] M. L. Perrin, C. A. Martin, F. Prins, A. J. Shaikh, R. Eelkema, J. H. van Esch, J. M. van Ruitenbeek, H. S. J. van der Zant, and D. Dulić, *Beilstein J. Nanotechnol*. **2**, 714-719 (2011)
[1.26] S. Y. Quek, M. Kamenetska, M. L. Steigerwald, H. J. Choi, S. G. Louie, M. S. Hybertsen, J. B. Neaton, and L. Venkataraman, *Nature Nanotech.* **4**, 230-234 (2009)
[1.27] M. Strange, and K. S. Thygesen, *Beilstein J. Nanotechnol.* **2***,* 746–754 (2011)
[1.28] M. Kamenetska, M. Koentopp, A. C. Whalley, Y. S. Park, M. L. Steigerwald, C. Nuckolls, M. S. Hybertsen, and L. Venkataraman, *Phys. Rev. Lett.* **102**, 126803 (2009)
[1.29] S. Nakashima, Y. Takahashi, and M. Kiguchi, *Beilstein J. Nanotechnol.* **2***,* 755–759 (2011)
[1.30] H. Song, Y. Kim, J. Ku, Y. H. Jang, H. Jeong, and T. Lee, *Appl. Phys. Lett.* **94**, 103110 (2009)
[1.31] J. -T. Lü, T. Gunst, P. Hedegård, and M. Brandbyge, *Beilstein J. Nanotechnol.* **2***,* 814–823 (2011)
[1.32] M. Häfner, J. K. Viljas, and J. C. Cuevas, *Phys. Rev. B* **79**, 140410 (2009)

[1.33] G. C. Solomon, J. P. Bergfield, C. A. Stafford, and M. A. Ratner, *Beilstein J. Nanotechnol.* **2***,* 862–871 (2011)
[1.34] J. Edwin Hobi, A. Fazzio, and A. J. R. da Silva, *Phys. Rev. Lett.* **100**, 056104 (2008)
[1.35] J. P. Bergfield, J. D. Barr, and C. A. Stafford, *Beilstein J. Nanotechnol.* **3**, 40-51 (2012)
[1.36] N. Bode, S. V. Kusminsky, R. Egger, F. von Oppen *Beilstein J. Nanotechnol.* **3**, 144-162 (2012)
[1.37] Ch. Obermair, F.-Q. Xie and Th. Schimmel *Europhysics News* **41**, 4 (2010)

Chapter 2
Theoretical Background

In the research area of computational simulation, there are two basic kinds of methods: ab initio simulation and empirical methods. Ab initio simulations are often based on three basic postulate - non-relativistic approximation, Born-Oppenheimer approximation and orbital approximation. Without any other assumption, ab initio simulations can get the physical parameter of the systems from solving the Schoerdinger equation accurately, such as the electron density, total energy and so on. This method has high accuracy, and the results normally show agreement with the experimental data. Correspondingly, the system which is suitable for it is rather small, only about several hundred of atoms. Empirical methods calculate the physical parameter of the system by using empirical parameter. Although the accuracy of this method is limited, nowadays for large scale systems (several thousand of atoms or even larger) it is still necessary. It is widely used in biology area.

2.1 Density functional theory

Hohenberg and Kohn first laid out the core of density functional theory (DFT) in the 60s of the twentieth century [2.5]. Nowadays, DFT is widely used in physics, chemistry and biology simulation, because of many advantages of DFT, such as fast convergence, little memory requirement and so on. Kohn won the Nobel Prize for his contribution in DFT area in 1999.

2.1.1 Hartree-Fock Theory

Although in my work, Density functional theory (DFT) simulation is used, I have to start with the introduction of Hartree-Fock theory, not only for following the history of ab initio simulations [2.1, 2.2], but also for introducing important concepts such as self-consistency and electron exchange and correlation [2.3].

One of the main aim of the whole chapter is to solve the time independent Schroedinger equation

$$\hat{H}\Psi = E\Psi \tag{2.1}$$

$\hat{H}$ is the Hamiltonian, Ψ is the eigen wave function of the system and E is corresponding eigen energy.

The Hamiltonian of the Schroedinger equation for chemical systems can be written in a well-defined form,

$$\hat{H} = T_{nucl} + T_{el} + V_{nucl-nucl} + V_{nucl-el} + V_{el-el} \tag{2.2}$$

In the system with many atoms, the Hamiltonian should include the kinetic energy of the nuclei and the electrons (the first and second part of the formula 2.2) respectively, and also the potential energy between nuclei-nuclei, nuclei-electrons and electrons-electrons (the last three terms, respectively). The details form of each part can be given as follow,

$$T_{nucl} = \sum_{1}^{L} \frac{P_I^2}{2\mathrm{M}_I} \tag{2.3}$$

$$T_{el} = \sum_{1}^{N} \frac{P_i^2}{2\mathrm{m}} \tag{2.4}$$

$$V_{nucl-nucl} = \frac{1}{2} \sum_{I \neq J} \frac{Z_I Z_J e^2}{|R_I - R_J|} \tag{2.5}$$

$$V_{nucl-el} = -\sum_{i,I} \frac{Z_I e^2}{|r_i - R_I|} \tag{2.6}$$

$$V_{el-el} = \frac{1}{2} \sum_{i \neq j} \frac{e^2}{|r_i - r_j|} \tag{2.7}$$

The nuclei are numbered by capital letter, and electrons are marked by lowercase one. Thus Z_I stands for the charge of the I-th nucleus and r_i means the displacement of i-th electron. The parameter $\frac{1}{2}$ in equation 2.5 and 2.7 is to make sure that the interaction between same pair is not counted twice.

In principle, what is left to do is only to solve this many body Schroedinger equation. Unfortunately, it is impossible to solve it exactly nowadays. So it is necessary to make some approximations that will make it possible to solve the Schroedinger equation at least within a reasonable accuracy. The following part will be devoted to three basic postulate - non-relativistic approximation, Born-Oppenheimer approximation and Hartree-Fock approximation.

The central idea of non-relativistic approximation is to neglected the relativistic effects, except heavy elements with localized wave function for the core electrons because of the high kinetic energies. In other words, normally the mass of the electrons can be seen as a constant value.

Born-Oppenheimer approximation can be described as follows. Since the mass of atomic nucleus is far larger than the mass of electrons, the atomic nucleus' velocity is significantly slower than electrons'. In Born-Oppenheimer approximation, the motion of the nucleus can be seen as non-correlated with the motion of electrons, in other words, the motion of electrons can be dealt with in a static picture with respect to the nuclei. In this way, the eigen wave function of the system Ψ can be divided into two parts.

$$\Psi(r,R)=\Phi(R)*\Phi(r) \tag{2.8}$$

Put formula (2.8) into the Schroedinger equation (2.2), we can get the equation of nucleus and electrons separately.

$$-\sum_{A}\frac{1}{2\mathrm{M}_a}\nabla_A^2\Phi(R)+E_t(R)\Phi(R)=E\Phi(R) \tag{2.9}$$

$$-\sum_{P}\frac{1}{2}\nabla_P^2\Phi(r,R)+V(r,R)\Phi(r,R)=E_t\Phi(r,R) \tag{2.10}$$

$\Phi(R)$ is the wave function of nucleus formula (2.9) is the eigen equation of nuclei, and $\Phi(r,R)$ is the electrons' wave function, formula (2.10) is the eigen equation of electrons. From the discussion above, we can easily understand that the nuclei should be fixed in formula (2.10), in other words, the distances between nuclei should be constant. The Hamiltonian of electrons can be written as follows,

$$\hat{H}=\sum_{p}\frac{1}{2}\nabla_p^2-\sum_{p<q}\frac{1}{r_{pq}}-\sum_{A}\sum_{p}\frac{Z_A}{r_{pA}} \tag{2.11}$$

and we can also get the eigen energy of electrons E(R)

$$E(R)=E_t(R)-\sum_{A<B}\frac{Z_A Z_B}{R_{AB}} \tag{2.12}$$

We separate the motion of electrons and nucleus, and get the electrons' and nuclei' equation separately.

Hartree approximation. Although we separate the equation of electrons and nuclei, it is still a hard work to solve the many-electron system. As a first approximation we assume,

$$\Phi(q_1, q_2, \ldots q_3) = \Phi_1(q_1)\,\Phi_2(q_2)\ldots\Phi_3(q_3) \tag{2.13}$$

This equation means that the total wave function of the electron system can be described as the product of every single electron wave function separately, and every single electron wave function is only related to the coordinate itself. The physical meaning of this approximation is that every single electron can be described as a electron in the average field created by nuclei and all electrons including the particular electron itself. In this way, the Hamiltonian of electrons' system can be written as the sum of effective single electron operator $\hat{F}(i)$:

$$\hat{H} = \sum_i \hat{F}(i) \tag{2.14}$$

The single electron operator $\hat{F}(i)$ includes the kinetic energy and potential energy of single electron. From equation (2.13) and (2.14), we can easily get the single electron's equation so called Hartree equations [2.4].

$$\hat{F}(i)\phi_i = \zeta_i \phi_i \tag{2.15}$$

ζ_i is the eigen energy of single electron (orbital energy).

Obviously, the single electron operator $\hat{F}(i)$ include the kinetic energy and potential energy of single electron V(i) which was established by all electrons including the particular electron itself, in other words, V(i) can be seen as a function of the other electrons' distribution. Interestingly enough, this forms a cycle: To get the distribution of the electrons, we have to solve the single electron's Schroedinger equations, but solving the equations ask for the distribution of the electrons also. The normal way to deal with this kind of problem is as follow: We start with some random guess for the wave functions which enter the effective one-particle Hamiltonian. In this way, the Hartree equations can be solved to get the new wave functions. This cycle will continue repeatedly until the self-consistency is reached, for example, the difference between the old and new eigen value smaller than a certain tiny number which can be seen as the results would not change any more. This method is called self-consistent field (SCF) method.

Although the Hartree ansatz obey the Pauli prinple which every electronic state only can and only can be occupied by one electron, the anti-symmetry of the electronic many-body wave function is not fulfilled. The anti-symmetry requirement is to replace

the product wave function by a single Slater determinant. Considering this antisymmetry part, we will get Hartree-Fock equation

$$\hat{F}(i)\Phi_i = \sum_i \zeta_i \Phi_i \tag{2.16}$$

$$\hat{F} = -\frac{h^2}{2\mathrm{m}} \nabla^2 + V_{ext} + V_H - V_X \tag{2.17}$$

The V_{ext} correspond to the potential energy of nuclei interaction. The so called Hartree energy V_H is related to the classical electrostatic energy of the electronic charge distribution. The V_X part which is called exchange term which is caused by the antisymmetry of electronic wave function.

2.1.2 Kohn-Sham equations

The basic idea of density functional theory can be described as follow: All of the properties of a many electron system including the total energy can be regarded according to the Hohenberg-Kohn theorem as a functional of electron density $\rho(r)$. It is based on the Rayleigh-Ritz variational principle which states that the expectation value of the total energy of system with the ground state energy (the electron density $\rho_0(r)$) is always smaller than the expectation value using other states (the electron density $\rho_i(r)$).

As a first step, by the derivation Schroedinger equation for electrons (formula 2.1) is solved. Using this wave function, the energy of electrons follows from the definition of DFT

$$E = \int \rho(r)\hat{V}_{ne}(r)d(r) + \langle \Psi | \hat{T}_e + \hat{V}_{ee} | \Psi \rangle \tag{2.18}$$

In this formula, $\hat{V}_{ne}(r)$ is the potential energy between nuclei and electrons and $\hat{V}_{ee}(r)$ is the electron-electron potential energy. The electron density is defined as:

$$\rho(r) = N \int |\Psi(r_{1,} r_{2,} .. r_n)|^2 dr_{1,} dr_{2,} .. dr_n \tag{2.19}$$

The electronic Hamiltonian can be specified by the number of the electrons and the potential $V_{ne}(r)$. Hence the electronic wave function and other properties are also determined by these two parts. Like the electronic energy:

$$E = E[N, V_{ne}] \tag{2.20}$$

Hohenberg and Kohn first put forward the Hohenberg-Kohn theorem [2.5].

1. If two electron systems, one subject to the potential $v_1(\vec{r})$ and the other to $v_2(\vec{r})$ have the same ground state density, then necessarily

$$v_1(\vec{r}) - v_2(\vec{r}) = const \tag{2.21}$$

We can easily get the following corollary. The ground state density uniquely determines the potential and thus all properties of the system, including the system wave function.

2. For any positive integer N and potential $v(\vec{r})$, it exists a density functional $F[\rho]$ with the form

$$E_{(v,N)}[\rho] = F[\rho] + \int v(\vec{r})\rho(\vec{r})d^3r \tag{2.22}$$

Formula (2.22) yields the minimal value of $E_{(v,N)}[n]$ at the ground state density of N electrons in the potential $v_0(\vec{r})$. The minimal value of $E_{(v,N)}[n]$ is then the ground state energy of this system.

Hence, for any electron density $\rho(r)$ that satisfies the normalizing condition, we can get:

$$E[\rho'] \geqslant E_0[\rho_0] \tag{2.23}$$

Obviously, as the electron density determines the number of electrons, we can get the electron energy by electron density from formula (2.22)

$$E[\rho] = \int \rho(r)\hat{V}_{ne}(r)d(r) + F_{HK}[\rho] \tag{2.24}$$

In this formula, $F_{HK}[\rho]$ includes electronic kinetic energy and the repulsive energy between electrons. The repulsive energy can be divided into the Coulomb repulsive energy and the exchange correlation potential

$$F_{HK}[\rho] = T_e[\rho] + V_{ee}[\rho] = T_e[\rho] + (J[\rho] + \zeta_{xc}[\rho]) \tag{2.25}$$

Then, we can easily get the chemical potential μ :

$$\mu = V_{ne} + \frac{\partial F_{HK}[\rho]}{\partial \rho} \tag{2.26}$$

Kohn and Sham divide the energy function into two parts [2.6-2.8], one can be expressed analytically, all other parts were put together into the so called exchange-correlation part. In a local effective external potential V_{eff} (Kohn–Sham potential), we could create a fictitious system of non-interacting particles (typically electrons) that generate the same density as any given system. For the created system, the Schroedinger equation can be written as:

$$(\frac{-\hbar^2}{2\mathrm{m}}\nabla^2 + V_{eff}(r))\psi_i(r) = e_i\psi_i \tag{2.27}$$

The electron density can be expressed as:

$$\rho(r) = \sum_i^N |\psi_i(r)|^2 \tag{2.28}$$

Then the formula 2.25 can be be written as:

$$\mu_s = V_{eff} + \frac{\partial T_s[\rho]}{\partial \rho} \tag{2.29}$$

where T_s is the kinetic energy of the fictitious system ,so called the Kohn-Sham kinetic energy, which can be written as the following expression:

$$T_s[\rho] = \sum_{i=1}^N \int dr\, \psi_i^*(r)(\frac{-\hbar^2}{2\mathrm{m}}\nabla^2)\psi_i(r) \tag{2.30}$$

.

The total energy of the real system is expressed as a functional of the charge density as:

$$E[\rho] = \int \rho(r)V_{ne}(r)d(r) + T_s[\rho] + J[\rho] + E_{xc}[\rho] \tag{2.31}$$

V_{ne} is the external potential acting on the real system (for example,the electron-nuclei interaction potential for a molecular system.) $J(\rho)$ is the Coulomb energy, and $E_{xc}[\rho]$ is so-called the exchange-correlation energy

Then, we can get the expression of the Kohn–Sham potential V_{eff}

$$V_{eff} = V_{ne} + \frac{\partial J[\rho]}{\partial \rho} + \frac{\partial}{\partial \rho}(T_e[\rho] - T_s[\rho] + \zeta_{xc}[\rho])$$
$$V_{eff} = V_{ne} + \frac{\partial J[\rho]}{\partial \rho} + V_{xc} \tag{2.32}$$

where the last term

$$V_{xc} \equiv \frac{\partial E_{xc}[\rho]}{\partial \rho(r)} \tag{2.33}$$

is the exchange-correlation potential.

Formula 2.26 and 2.27 are the Kohn-Sham equation. The most significant point of Kohn-Sham approach is using a fictitious system of non-interacting elecrons to replace the respective term of the Hamiltonian in real system. Thus, all remaining terms are included in the exchange-correlation potential, which is the only unknown in the Kohn-Sham approach. Then the form of the exchange-correlation functionals is the next issue we must deal with in DFT.

2.1.3 Exchange-Correlation Functional

From the last section, the major problem of DFT consists of finding an expression of exchange-correlation functional. Nowadays, the most widely used approximated functional are the local density approximation (LDA) and generalized gradient approximation (GGA).

LDA is the approximation which is generally synonymous with a functional based on the homogeneous electron gas (HEG) model. In general, the LDA can be written as follow

$$E_{xc}^{LDA}[\rho] = \int \rho(r)\xi_{xc}(\rho)\,dr \tag{2.34}$$

where ξ_{xc} which is also a function of electron density, is the exchange-correlation energy density in a homogeneous electron gas, whose density is only taken at the position r. In other words, the LDA potential is a totally local function only related to $\rho(r)$. The exchange-correlation energy can be decomposed into two parts, exchange term and correlation term,

$$E_{xc} = E_x + E_c \tag{2.35}$$

The exchange energy part of the homogeneous electron gas is analytically known. The exchange energy density employs expression [2.7, 2.11].

$$\xi_x[\rho] = -\frac{3}{4}\left(\frac{3}{\pi}\right)^{\frac{1}{3}}\rho^{\frac{1}{3}} \tag{2.36}$$

Hence, the expression of the exchange energy is

$$E_x^{LDA}[\rho] = \int \rho(r)\xi_x(\rho)\,dr = -\frac{3}{4}\left(\frac{3}{\pi}\right)^{\frac{1}{3}}\int \rho^{\frac{4}{3}}\,dr \tag{2.37}$$

Analytic expressions of the correlation part can not be derived. Normally, we get the numerical values from different electron densities in order to fit the analytic formula. Thus, there are several LDA functional with different analytic forms for correlation energy, like Vosko-Wilk-Nusair (VWN) [2.12], Perdew-Zunger (PZ81) [2.13] and Perdew-Wang (PW92) [2.14].

The LDA functional shows rather satisfactory results on lattice constant and geometries calculations. But still some results are not good enough, like the binding energy and chemical reaction barriers[2.16, 2.17]. In order to improve the accuracy of inhomogeneous systems, the GGA approach is widely used. Comparing with the LDA, although the GGA approach is still local, it introduces the gradient of electron density in order to correct the heterogeneity of electron density, which has the following form

$$\xi_{x/c}^{GGA}(\rho) = \xi_{x/c}^{LDA}(\rho) + \Delta\xi_{x/c}\left(\frac{|\nabla\rho|}{\rho^{4/3}}\right) \tag{2.38}$$

The results of binding energy are significantly improved bu using the GGA functional, the absolute error of small molecules is also satisfactory [2.18]. There are several GGA functional with different $\Delta\xi_{x/c}$, such as Perdew and Wang functional (PW91) [2.19] and Perdew-Burke-Ernzerhof functional (PBE) [2.20], which are all widely used.

2.1.4 Plane wave basis sets

Most of the problems related to the Schroedinger equation has already been addressed in the section above, but still an important one remains. For the systems with finite number of electrons, like molecules and clusters, the Kohn-Sham equations can be

solved in the real space mesh [2.21]. But how should one deal with a periodic system? For such systems, we usually expand the wave function with a discrete plane wave basis set.

$$\phi_{\boldsymbol{K},i}(r)=\sum_{\boldsymbol{G}} c_{\boldsymbol{K}+\boldsymbol{G},i}\, e^{i(\boldsymbol{K}+\boldsymbol{G})\cdot\boldsymbol{r}} \tag{2.39}$$

That wave function 2.39 satisfies the Bloch's theorem, **K** is the wave vector within the first Brillouin zone, G is the reciprocal lattice vector. For technical reasons, it is not possible and also not necessary to expand the wave function with the whole plane wave basis set, because one basis set includes infinite number of plane waves. What one usually does is setting an energy maximum of plane wave, so called cutoff energy. Then the accuracy of the calculations can be easily controlled by the value of the cutoff energy

$$E_{cutoff}=\frac{\hbar^2}{2\mathrm{m}}|\boldsymbol{K}+\boldsymbol{G}|^2 \tag{2.40}$$

For the infinite systems, of course, the number of k points are also infinite. However, wave functions at the k points close enough to each other can be seen as identical, so that representing the total wave function using only finite number of k points become possible. Considering the system symmetries, some special k points which are first described by Monkhorst and Pack, can simply consist of an equispaced grid of k points [2.22]. Then it is possible to calculate any expectation value by the formula 2.41, using the integral over the reciprocal unit cell volume V and summation over all bands n, by simply replacing the integral with a finite summation of the given k point set.

$$\langle X\rangle=\frac{1}{V}\sum_{n}\int_{V} d\,\boldsymbol{k}\, X_n(\boldsymbol{k})\, f(\xi_n(\boldsymbol{k})) \tag{2.41}$$

2.1.5 Pseudopotential approximation

Generally speaking, the physical and chemical properties of materials are mainly determined by the outer electrons, so called valence electrons [2.23]. To increase the calculation efficiency, it is reasonable to distinguish between valence and core electrons, and replace the core electrons together with the nucleus by an effective core potential.

This approximation is illustrated in detail in Fig. 2.1. It clearly shows that the core electrons potentials are replaced by a weaker and smoother one within the core region, determined by the core radius r_c . Both the pseudopotential and the wave function are almost identical to the real one outside the core region. A pseudopotential with larger cutoff radius means more rapidly convergent but less transferable,which is less accurate to reproduce realistic feature. Inside the core radius, although all of the wave functions are replaced, the pseudo wave function preserves the norm and scattering properties of all electrons system. The following formula shows us the form of the norm-conserving pseudopotential

$$V_{pseudo}(\boldsymbol{r}) = \sum_{lm} |Y_{lm}\rangle V_l(\boldsymbol{r}) \langle Y_{lm}| \tag{2.42}$$

$|Y_{lm}\rangle$ denotes spherical harmonics, which are called semi-local functions, because they are only located in the radial part, but not in the angular part.

The pseudopotential approach decreases the number of the electrons which should be calculated, the simulation efficiency is improved significantly.

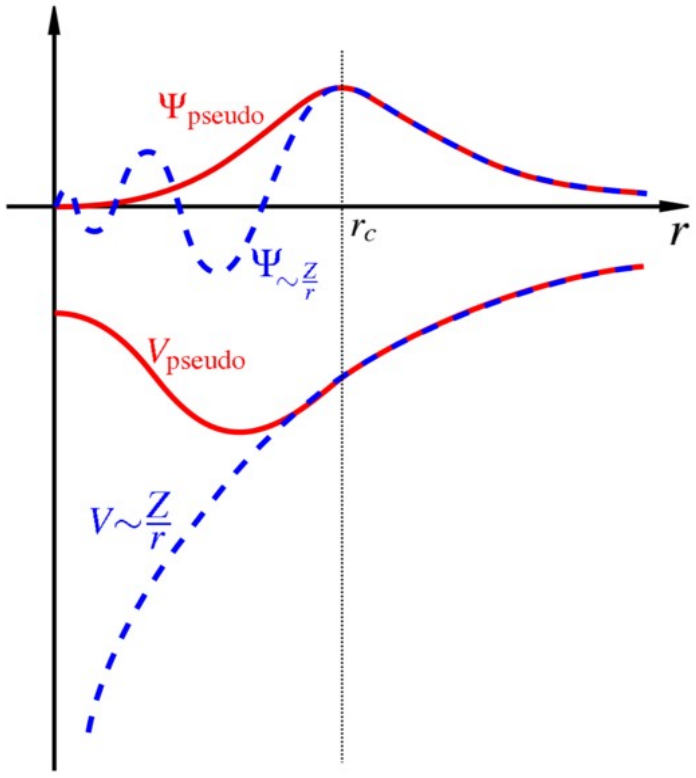


Fig. 2.1 An example of pseudopotential approximation [2.24]. The wave funcrion (the above curves) and potential (the below part) comparison between all electrons system (blue and dashed lines) and pseudopotential approximation one (red and solid lines).

2.1.6 Supercell approach

From the section above, we can easily conclude that the model we build up has to be periodic in all three dimensions, because of both the Bloch's theorem and the plane wave basic set we employed. It is satisfied for bulk calculation, but how can we deal with surface systems which are the subject of my study?

For surface systems, one has to deal with the half-infinite vacuum perpendicular with the surface and also a half-infinite bulk along this direction(usually the vacuum is along z direction). What I have done is to use the supercell approach: using a finite number of layers to simulate the half-infinite bulk part, of course with sufficient thickness. And these finite layers can be repeated, the repeated parts are separated by adding a sufficiently large vacuum between them (fig.2.2)

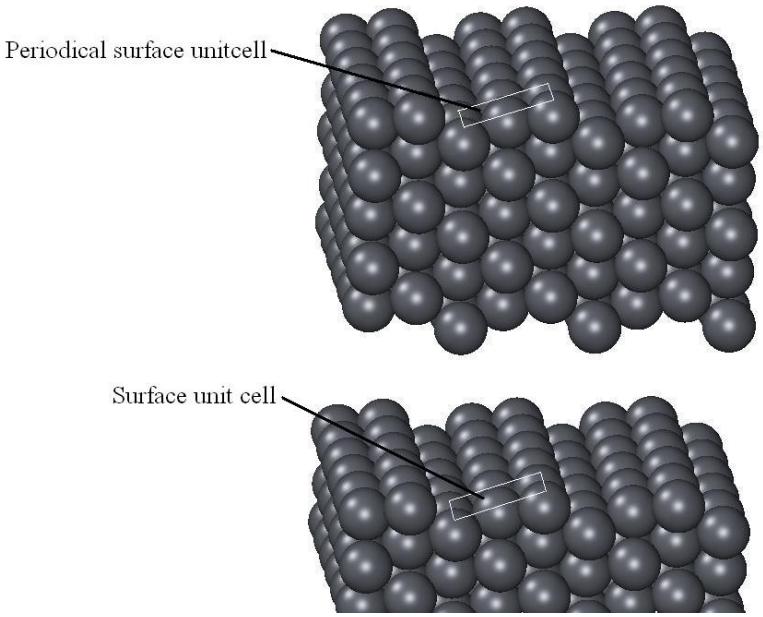


Fig.2.2 Sketch of supercell approach: Using a repeated slab of finite thickness and a large vacuum periodically in Z direction to model the metal surfaces [2.3]. In this figure, Pb(211) surface is used as an example.

For the reliability of this surface model, the thickness of the vacuum and slab layers is rather important. The vacuum area must be large enough (at least 10Å) to avoid the interaction between opposing surfaces/ adsorbates. In my work, even a much larger vacuum (usually 20Å) is needed, because of the stepped surfaces and the water adsorbates. To check whether the thickness of layers is enough will be discussed in detail in next chapter.

2.2 Ab initio molecular dynamics

Molecular dynamics (MD) is a computer simulation method which yields the physical movements of atoms and molecules in a period of time. From the MD simulation, one can get not only the trajectories of atoms but also the processes of some physical phenomenons of systems, in particular, the non-equilibrium system in a relatively short period of time (normally 1 to 10 ps). As some details of the atoms can not be observed directly in the experiments, the MD simulation becomes a good supplement of experiments. Because of this advantage, MD method is widely used in the study of condensed matter physics area, such as the growth of crystal [2.25], epitaxy [2.26], diffusion process [2.27], surface and phase reconstruction [2.28, 2.29] and so on.

In the normal MD simulation, the trajectories of atoms are given by the interaction of the atoms and molecules, which is determined by numerically solving the Newton's equation of motion. But the MD simulation with the empirical/semi-empirical force fields has some problems which might lead to significant error. First, the electron polarization is typically ignored. Second, the empirical potential can not get the electron properties, like bonding properties, because the empirical potential ignores the interaction between the local electron structure. Third, the accuracy of the simulation results directly depend on the chosen potential model and parameter. Different potential models and parameters usually lead to a totally different results.

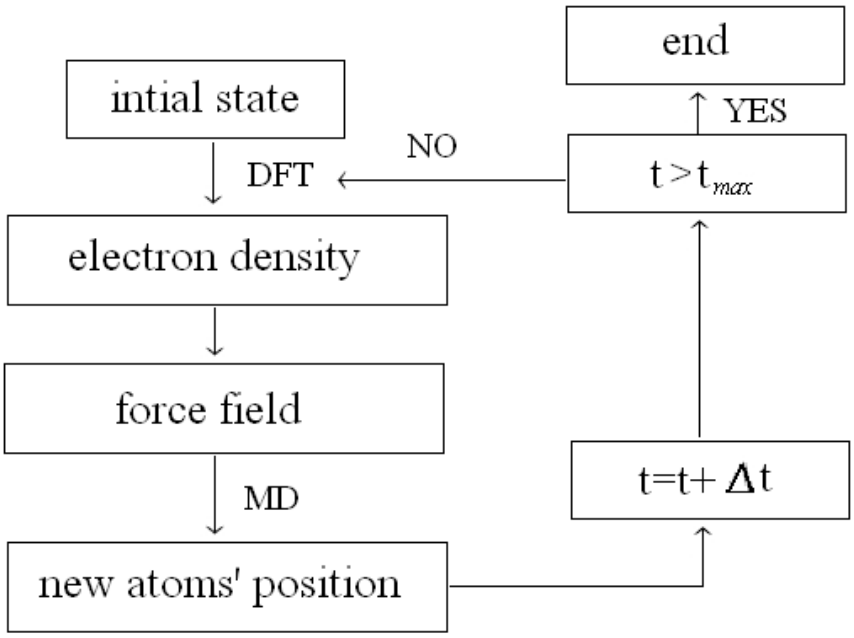


Fig.2.3 Flow-chart diagram of a simple AIMD simulation

To solve these problems, the most important point is a new potential which does not depend on any empirical data and parameter. Undoubtedly, DFT is a good choice. In 1985, R. Car and M. Parrinello theorized the ab initial molecular dynamics (it is also called CP method) which combine the DFT and MD for the first time [2.30]. Since then, AIMD becomes one of the most important method in the simulation area.

The main idea of the AIMD is rather simple which is shown by figure 2.3 clearly. The whole simulation is divide into two steps. First step, get the potential which depend on the electron density by DFT calculation. Second step, from the potential, one can easily get the state of atoms at time $t+\Delta t$ by a numerical scheme to solve the classical equations of motion using the positions and forces we get in the first step. Then we repeat the process until the period of the time $t > t_{max}$, t_{max} is the run time we set at the very beginning.

In my research, AIMD is used to check the stability of the water structures on the substrates, and get the vibrational spectra under different temperature to compare with the experimental data.

2.3 Nudged elastic band method

To determine a lowest energy path for the atoms rearrangement from one stable state to another is an important and interesting area in theoretical chemistry and in condensed matter physics. Chemical reactions and diffusion processes are the common examples of this area, which are all defined by a reaction coordinate for transition state [2.31]. The saddle point energy which is the potential energy maximum along the minimum energy path (MEP) is also important. It shows the activation energy barrier [2.32], which determine the transition rates within harmonic transition state theory [2.33]. There are several different methods for finding the MEP [2.34]. In my work, the so called nudged elastic band (NEB) method is used, which has already been proofed solving a wide range of problems successfully [2.35, 2.36], such as the diffusion processes at metal surfaces [2.37], atoms exchange in sputter deposition [2.38] and formation of a contact [2.39].

The main idea of the NEB method is rather simple. First several initial configurations (we call these configurations 'images') between initial and final states are selected. All of these images are connected by spring forces along the 'expected band', which is set by the option 'SPRING' in the VASP code. In my work, the spring forces are set to be equal to $-5.0 eV/A^2$. Another component of the force which is perpendicular to the 'band' is created by the system potential. When the routine runs, each image optimizes while maintaining equal spacing to neighboring images.

Generally speaking, at least 8 images are needed for a complex system to get both the reaction path and the barrier. But the convergence usually is very slow if 8 images are used at the very beginning, because nobody can make sure that the initial guesses are close enough to the final results. Actually, the guesses are usually rather 'bad' in some complicated system. What I have done is to divide the calculation into two steps. First, only one image is chosen. The result of first step will point out the MEP. And then the other images which are added around this optimized image should not far away from the reality answer.

2.4 Physical properties

Using the methods described before, it is now possible to solve a large number of surface science problems. In the following part, I will roughly address some physical properties and concepts which are widely used in theoretical surface science. Some of these properties can directly be compared with experimental data to confirm the details of the experimental phenomenon, such as adsorption energy, work function changes, vibrational spectra, band structure and so on. Others like density of states (DOS), or charge density difference, though these properties are not corresponding to the measured data, they are proved to be valuable theoretical tools to understand and predict the reality phenomenons.

2.4.1 Adsorption energies

Adsorption is a very important process in the field of surface science. Adsorption process is involved in a large number of physical phenomenons, such as the growth of crystal, heterogeneous catalysis and so on.

Adsorption is a process in which atoms, ions or molecules from gas, liquid or dissolved solid stick to a surface. Generally speaking, adsorption is a consequence of surface properties. In a ideal bulk system, all the bonding requirements of the atom are already filled. However, the atoms on the surface are not fully coordinated, so that they can bind adsorbates. There are two kind of adsorption, physisorption in which the interaction between surface and adsorbates is due to van der Waals forces and chemisorption in which the adsorbates form chemical bonds with the surfaces. The exact nature of the adsorption depends on the details of the species involved [2.40].

The definition of adsorption energy is the energy change during the adsorption process. In the DFT calculation, the adsorption energy is defined as the total energy difference between the separated two systems, clean substrate and the adsorbates in the vacuum, and the adsorbate system. It can be described by the following formula 2.39

$$E_{ads} = E_{tot} - E_{clean\ surface} - E_{adsorbates} \tag{2.43}$$

where E_{tot} is the total energy of the substrate with the atoms/molecule adsorbed on it, $E_{adsorbates}$ is the total energy of isolate adsorbates in the vacuum.

Although adsorption energy can not give a full description of the adsorption process, it indicates the interaction strength between substrate and adsorbates, and shows the properties of surfaces indirectly.

2.4.2 Work Function

In solid-state physics, the work function is defined as the minimum energy needed to remove an electron from a solid at 0K.

At the very beginning, the definition of work function comes from the thermionic emission experiment. This experiment shows the phenomenon that a large number of electrons are able to escape at a sufficiently high temperature. From the experiment, the relationship between the emission current and the temperature is as follow,

$$i = a\, e^{-\frac{W}{k_B T}} \tag{2.44}$$

In formula 2.40, W is the work function.

First, we try to explain this phenomenon by classical statistical mechanics. In classical electronic theory, the electrons in metal can be seen as free particles in a certain potential well (fig.2.4 a)). The depth of the potential well V indicates the minimum necessary work needed to remove electron from the metal. The electrons in the potential well obey the classical distribution. The velocity distribution is,

$$dn = n_0 \left(\frac{m}{2\pi k_B T}\right)^{3/2} e^{-\frac{mv^2}{2k_B T}}\, d\boldsymbol{v} \tag{2.45}$$

where dn is the electron density in the velocity zone form $\boldsymbol{v}$ to $\boldsymbol{v}+d\boldsymbol{v}$. $d\boldsymbol{v} = dv_x dv_y dv_z$. n_0 is the number of electrons in a volume unit. Hence, we can get the emission current from formula 2.41, if we set x coordinate axis as the emission direction.

$$i = n_0 \left(\frac{m}{2\pi k_B T}\right)^{3/2} \int_{-\infty}^{\infty} dv_y \int_{-\infty}^{\infty} dv_z \int_{\frac{1}{2}mv^2 > V} dv_x (-qv_x) e^{-\frac{mv^2}{2k_B T}} \tag{2.46}$$

Because only the electron with kinetic energy larger than V can move outside the metal, at x direction only these electrons are counted. The result of formula 2.42 is,

$$i = n_0 q \left(\frac{k_B T}{2\pi m}\right)^{1/2} e^{-\frac{V}{k_B T}} \tag{2.47}$$

Comparing formula 2.43 with 2.40, the result from classical electronic theory agree with the experimental data, and also explain the physical meaning of work function, which is the depth of the potential well V.

Although formula 2.43 describes the relationship between emission current and temperature quite well, the work function given by this model shows a rather large error. Why? Because the classical model can not describe the metal system correctly. It is necessary to use a quantum model (fig.2.4 b)). In this model, V gives the necessary work to remove a electron from the bottom of conduction band.

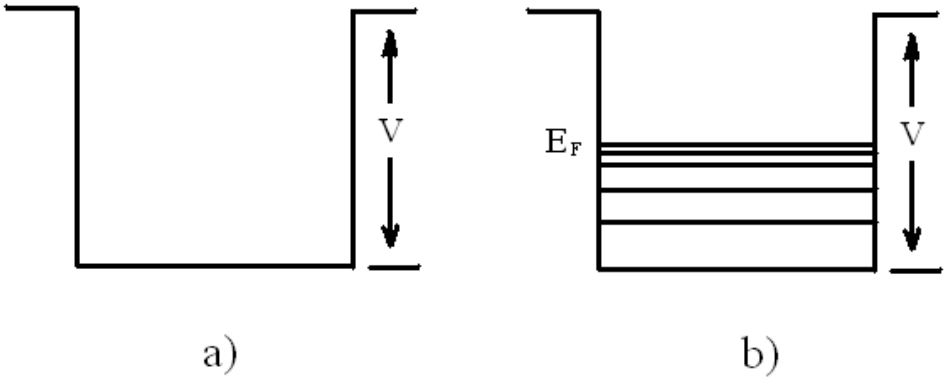


Fig.2.4 a) the potential well of metal in classical model. b) the potential well of metal in quantum model

Similar with the classical theory, we can get the emission current from the velocity distribution. To make it easy to understand, here we consider the simplest condition,

$$E(\boldsymbol{k}) = \frac{\hbar^2 k^2}{2\mathrm{m}} \tag{2.48}$$

For this condition, we can easily get,

$$\begin{aligned} \boldsymbol{v}(\boldsymbol{k}) &= \frac{1}{\hbar}\nabla_k E = \frac{\hbar \boldsymbol{k}}{m} \\ E(\boldsymbol{k}) &= \frac{1}{2} m v^2 \end{aligned} \tag{2.49}$$

From formula 2.45, the quantum states number of a volume unit in $d\boldsymbol{v}$ is,

$$N_s = 2\frac{d\boldsymbol{k}}{(2\pi)^3} = 2\left(\frac{m}{2\pi\hbar}\right)^3 d\boldsymbol{v} \tag{2.50}$$

Then the number of electrons can easily be calculated by multiplying formula 2.46 with the Fermi-Dirac distribution function f(E),

$$dn = 2\left(\frac{m}{2\pi\hbar}\right)^3 \frac{1}{e^{(\frac{1}{2}mv^2 - E_F)/k_B T} + 1} d\boldsymbol{v} \tag{2.51}$$

Because the kinetic energy of electron which escape from the metal ($\frac{1}{2}mv^2$) is larger than V, then actually $(\frac{1}{2}mv^2 - E_F)$ should be much larger than $k_B T$, it mean the number '1' at the denominator can be ignored,

$$dn \approx 2\left(\frac{m}{2\pi\hbar}\right)^3 e^{\frac{E_F}{k_B T}} e^{-\frac{mv^2}{2k_B T}} d\boldsymbol{v} \tag{2.52}$$

The only difference between formula 2.44 and 2.51 is the factor,

$$n_0\left(\frac{m}{2\pi k_B T}\right)^{3/2} \to 2\left(\frac{m}{2\pi\hbar}\right)^3 e^{\frac{E_F}{k_B T}} \tag{2.53}$$

Then the emission current of quantum theory can easily be written from formula 2.43,

$$i = -\frac{4\pi m (k_B T)^2 q}{(2\pi\hbar)^3} e^{-\frac{V - E_F}{k_B T}} \tag{2.54}$$

In the quantum theory, we get a new explanation of work function

$$W = V - E_F \tag{2.55}$$

E_F is the fermi energy. The work function can be understood by another way. As the electrons spill out into the vacuum, the center of the negative and positive

change separate. This creates an electrostatic dipole layer at the surface [2.41]. In order to move the electron through the electric field of the dipole layer at the surface, extra work has to be done. Hence, it is important to point out that the work function is a property of the material surfaces, but not the characteristic of the bulk material alone. There are two contribution to the work function: an intrinsic one due to the binding of the electron and the effect of the dipole layer at the surface [2.3, 2.41].

2.4.3 Charge Density Analysis

In the DFT calculation, the most direct and most important information we get is the charge density. In other words, almost all the other properties could energetically be described by the charge density, such as the geometries of the surfaces, the interaction process and so on. For example, the charge density could directly and clearly reflect the bonding formation and anti-bonding level by the accumulation and depletion of electron density.

For more complicated system, like adsorbate-covered surfaces, the charge density redistribution is not so easy to analysis. In this situation, it is more valuable to analyze the charge density difference, which is given by the following formula:

$$\Delta n = n_{interacting\ system} - \sum_i n_{non-interacting\ system\, i} \tag{2.56}$$

While Δn is the charge density difference, the interacting system is the system which we would like to investigate. The non-interacting system is the isolated system of surface or adsorbate. In this way, the charge density redistribution due to the interaction is clearly illustrated. There are some other analysis of charge density, like "atoms in molecules" theory [2.42, 2.43], using electron localization function to classify bonds [2.44-2.46].

2.4.4 Density of States

Comparing with the band structure, the density of states is a more common tool for the discussion and determination of the bonding processes at surfaces, especially for the understanding of the adsorption process [2.47]. The physical meaning of the density

of states (DOS) is the number of states in the interval of energy $E \sim \Delta E$ per energy difference ΔE . The DOS is closely related to the band structure, it can be seen as the visualization of the band structure. Many properties, such as the electronic specific heat, paramagnetic susceptibility and so on, can directly be related to the DOS. There are some different kind of DOS, like the total density of states, the local density of states and projected density of states.

The local density of states (LDOS) is defined as the

$$n(\boldsymbol{r}, \varepsilon) = \sum_i |\phi_i(\boldsymbol{r})|^2 \delta(\varepsilon - \varepsilon_i) \tag{2.57}$$

which gives the DOS at a local position $\boldsymbol{r}$. From the definition of DOS, we can easily get the expression by the formula 2.53

$$n(\varepsilon) = \int n(\boldsymbol{r}, \varepsilon) d^3 \boldsymbol{r} \tag{2.58}$$

And the electron density could be written by

$$n(\boldsymbol{r}) = \int^{\varepsilon_{fermi}} n(\boldsymbol{r}, \varepsilon) d\varepsilon \tag{2.59}$$

The projected density of states (PDOS) is another rather common tools, which is the density of states projected on a certain orbital, for example, s orbital, p orbital or d orbital. It can be calculated by:

$$n_a(\varepsilon) = \sum_i |\langle \phi_i | \phi_a \rangle|^2 \delta(\varepsilon - \varepsilon_i) \tag{2.60}$$

For the s and p orbital, the PDOS is usually gradual and broad, which means the electron on these orbital is rather delocalized. Although the s electrons also contribute significantly to the molecule-metal interaction, however, this interaction is rather similar for all metals. In contrast, the occupation of the d-band is very element specific, and therefore it is the specific interaction of the d-band with adsorbates that distinguishes one d-band metal from another one.[2.48, 2.49].

The main principle of the d-band model is that the binding energy of an adsorbate to a metal surface closely depend on the electronic structure of the surface. Considering a simple situation: hydrogen adsorbing on a transition metal surface. As shown in figure 2.5, the interaction is formally split into two parts: contribution of the s,p states and contribution of the d state. The s and p states lead to a renormalization of the energy level, which make the atomic level broader and shift it to a lower energies.

The renomalized level then strongly hybridize with the d-states of metal surface, and split into a bonding and a anti-bonding contribution. For the metals, of course, the bonding state is full. The situation of the anti-bonding state which is fully or partially or

non occupied depends on the local electronic structure of the metal at the surface, which could be shown in the surface PDOS. An increased filling of anti-bonding state lead to a weaker interaction between substrate and adsorbates. So a experimentally-determinable parameter which strongly relates to the filling of the anti-bonding state is introduced, so called the center of the d-band [2.50]. A smaller difference between the d-band center and the fermi level indicates a stronger bonding between substrate and adsorbates. Similarly, a larger difference means a weaker bonding.

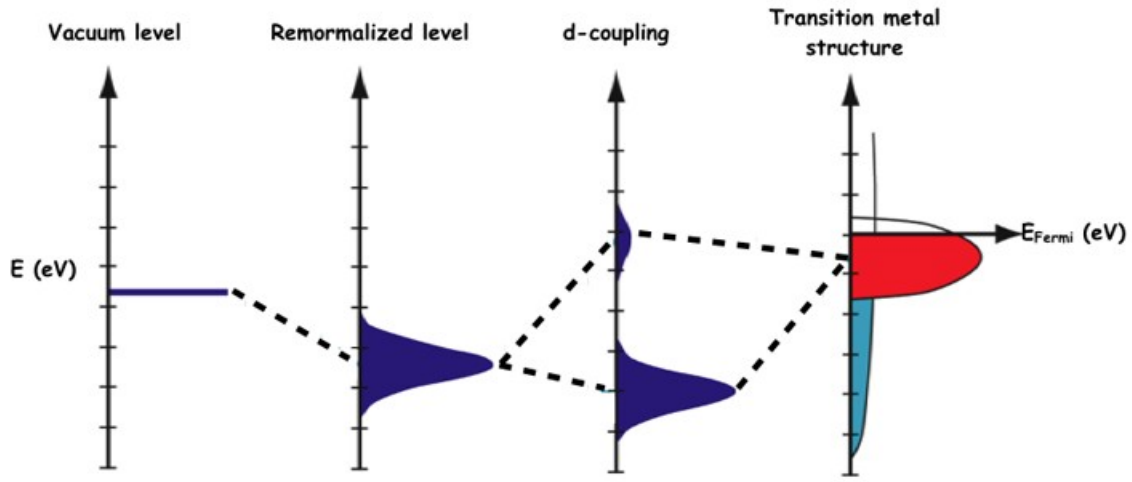


Fig.2.5 Schematic drawing of the interaction of an atomic level with a transition metal surface [2.65].

2.4.5 Vibrational spectra

vibrational spectra constitutes one of the important pillars of modern analytical chemistry which is an important tool in chemical structure determination [2.51-2.54]. Today the theoretical prediction of vibrational spectra become another common tool in the field of computational chemistry [2.55-2.60]. It could directly be compared with the experimental data.

The vibrational spectra simulation under a certain temperature is based on the results of AIMD simulation. Although there are several different spectra simulation, like power spectrum, IR spectrum and Raman spectrum, only the power spectrum which is obtained by a fourier transform of the auto-correlation of the particle velocities [2.61] is used in my work.

All vibrational spectra simulations are calculated by the fourier transform of different auto-correlation functions, power spectrum rely on particle velocities, IR spectrum use the molecular dipole moments and Raman spectrum is derived from

molecular polarizabilities. The auto-correlation function is given by the Wiener-Khintchine theorem [2.62, 2.63].

$$\langle f(\tau) f(t+\tau) \rangle_{\tau} = \frac{1}{2\pi} \int \left| \int f(t) e^{-i\omega t} dt \right|^2 e^{i\omega t} d\omega \qquad (2.61)$$

so that the Fourier transform of f(t) is taken.

The power spectrum relies on the nuclear velocities, which could easily be obtained from a MD simulation. For each atom, the vector auto-correlation functions of the velocity is calculated and the sum of all the correlation function of a molecule is fourier transformed to get the power spectrum of that molecule [2.51, 2.64]. The power spectrum features peak for each normal mode vector, and could be compared with the experimental data directly.

Bibliography

[2.1] D. R. Hartree, Proc. *Cambridge. Philos. Soc*. **24**, 89 (1928)
[2.2] V. Fock, Z. *Phys.* 61 126 (1930)
[2.3] A. Gross, *Theoretical surface science* 21 (2009)
[2.4] D. R. Hartree, Proc. *Cambridge. Philos. Soc*. **24**, 89 (1928)
[2.5] P. Hohenberg and W. Kohn, *Phys .Rev.* B **136**, 864 (1964)
[2.6] W. Kohn and L. J. Sham, *Phys. Rev.* **140**, A1133–A1138 (1965)
[2.7] R. G. Parr, W. Yang, *Density-Functional Theory of Atoms and Molecules* (1994)
[2.9] L. H. Thomas, Proc. Camb. Phil. Soc.**23**, 542 (1927)
[2.10] E. Fermi, *Rend. Accad. Lincei.* **6**, 602 (1927)
[2.11] P. A. M. Dirac, *Proc. Camb. Phil. Soc*. **26**, 376 (1930)
[2.12] S. H. Vosko, L. Wilk and M. Nusair, *Can. J. Phys.* **58**, 8 (1980).
[2.13] J. P. Perdew and A. Zunger, *Phys. Rev. B* **23**, 10 (1981)
[2.14] J. P. Perdew and Y. Wang, *Phys. Rev. B* **45** 23 (1992)
[2.15] A. D. Becke, *Phys. Rev. B* **38**, 3098 (1988)
[2.16] A. J. Cohen and N. C. Handy, *Chem. Phys. Lett.* **45** 566 (2000)
[2.17] B. Hammer, M. Scheffler, K. W. Jacobsen and J. K. Norskov, *Phys. Rev. Lett.* **73** 1400 (1994)
[2.18] S. Kurth, J. P. Perdew, P. Blaha, *Int. J. Quant. Chem.* **75** 889 (1999)
[2.19] J. P. Perdew, J. A. Chevary, S. H. Vosko, K. A. Jackson, M. R. Pederson, D. J. Singh and C. Fiolhais, *Phys. Rev. B* **46** 6671 (1992)

[2.20] J. P. Perdew, K. Burke and M. Ernzerhof, *Phys. Rev. Lett.* **77** 3865 (1996)
[2.21] T. L. Beck, *Rev. Mod. Phys.* **72** 1041 (2000)
[2.22] H. J. Monkhorst, and J. D. Pack, *Phys. Rev. B* **13**, 5188 (1976)
[2.23] U. Barth and C. D. Gelatt, *Phys. Rev. B* **21** 2222 (1980)
[2.24] M. C. Payne, M. P. Teter, D. C. Allan, T. A. Arias, and J. D. Joannopoulos, *Rev. Mod. Phys.* **64** 1045 (1992)
[2.25] A. M. Reilly and H. Briesen, *J. Chem. Phys.* **136**, 034704 (2012)
[2.26] K. Mueller, *Phys. Rev. B* **35**, 7906 (1987)
[2.27] R. Elber and M. Karplus, *J. Am. Chem. Soc.*, **25** 122 (1990)
[2.28] Q. Yu and P. Clancy *Modelling Simul. Mater. Sci. Eng.* **2** 829 (1994)
[2.29] F. Ercolessi and E. Tosatti, *Phys. Rev. Lett*. **57**, 719 (1986)
[2.30] R. Car and M. Parrinello, *Phys. Rev. Lett*. **55**, 2471 (1985)
[2.31] R. Marcus, *J. Chem. Phys.* **45**, 4493 (1966)
[2.32] H. Jónsson, G. Mills, K. W. Jacobsen, *Classical and Quantum Dynamics in Condensed Phase Simulations*, Ed. B. J. Berne, G. Ciccotti and D. F. Coker (World Scientific, 1998), page 385.
[2.33] G. H. Vineyard, *J. Phys. Chem. Solids* **3** 121 (1957)
[2.34] M. L. McKee and M. Page, Reviews in Computational Chemistry Vol. IV (1993)
[2.35] G. Mill and H. Jónsson, *Phys. Rev. Lett.* **72** 1124 (1994)
[2.36] G. Mill, H. Jónsson and G. Schenter, *Surf. Sci.* **324** 305 (1995)
[2.37] M. Villarba and H. Jónsson, *Surf. Sci.* **317** 15 (1994)
[2.38] M. Villarba and H. Jónsson, *Surf. Sci.* **324** 35 (1995)
[2.39] M. R. Sorensen, K. W. Jacobsen and H. Jónsson, *Phys. Rev. Lett.* 77 5067 (1996)
[2.40] L. Ferrari, J. Kaufmann, F. Winnefeld and J. Plank, *J. Colloid Interface Sci.* **347** 15 (2010)
[2.41] N. W. Ashcroft and N. D. Mermin, *Solid State Physics*, 1976
[2.42] R. F. W. Bader, *International Series of Monographs on Chemistry,* volume 22 (1990)
[2.43] R. F. W. Bader, *Phys. Rev. B* **49**, 13348 (1994)
[2.44] A. D. Becke and K. E. Edgecombe, *J. Chem. Phys.* **92**, 5397 (1990)
[2.45] B. Silvi and A. Savin, *Nature*, **371**, 683 (1994)
[2.46] A. Savin, R. Nesper, S. Wengert and T. F. Faessler, Angew. *Chem. Int. Ed. Engl.*, **36**, 1808 (1997)
[2.47] R. Hoffmann, *Rev. Mod. Phys.* **60**, 601 (1988)
[2.48] B. Hammer and J. K. Norskov, *Nature* **376**, 238 (1995)
[2.49] B. Hammer and J. K. Norskov, *Adv. Catal*. **45**, 71 (2000)
[2.50] B. Hammer and J. K. Norskov, *Surf. Sci*. **343**, 211 (1995)
[2.51] M. Thomas, M. Brehm, R. Fligg, P. Voehringer and B. Kirchner, *Phys. Chem. Chem. Phys*. **15** 6608 (2013)
[2.52] T. D. Fridgen, *Mass Spectrom. Rev,* **28** 586 (2009)
[2.53] R. Bhargava, *Appl. Spectrosc.*, **66** 1091 (2012)

[2.54] J, Lindner and P. Voehringer, *Femtosecond Vibrational Spectroscopies and Application to Hydrogen-Bond Dynamics in Condensed Phases*, pp. 643-686 (2012)
[2.55] T. Weymuth, M. P. Haag, K. Kiewisch, S. Luber, S. Schenk, C. R. Jacob, C. Herrmann, J. Neugebauer and M. Reiher, *J. Comput. Chem.*, **33**, 2186 (2012)
[2.56] F. Neese, Coord. *Chem. Rev.*, **253**, 526 (2009)
[2.57] S. Luber, J. Neugebauer and M. Reiher, *J. Chem. Phys.*, **130**, 064105 (2009)
[2.58] J. J. Lee, S. Hoefener, W. Klopper, T. N. Wassermann and M. A. Suhm, *J. Phys. Chem. C*, **113**, 10929 (2009)
[2.59] J. Neugebauer, M. Reiher, C. Kind and B. A. Hess, *J. Comput. Chem.,* **23**, 895 (2002)
[2.60] R. I. Ovsyannikov, W. Thiel, S. N. Yurchenko, M. Carvajal and P. Jensen, *J. Mol. Spectrosc.*, **252**, 121 (2008)
[2.61] R. Futrelle and D. McGinty, *Chem. Phys. Lett*., **12**, 285 (1971)
[2.62] N. Wiener, *Acta Math.*, **55**, 117 (1930)
[2.63] A. Khintchine, *Math. Ann.*, **109**, 604 (1934)
[2.64] K. Wendler, M. Brehm, F. Malberg, B. Kirchner and L. DelleSite, *J. Chem. Theory Comput.*, **8**, 1570 (2012)
[2.65] JK. Norskov, F. Abild-Pedersen, F. Studt, T. Bligaard, *Proceedings of the National Academy of Sciences of the United States of America*, **108** 3 (2011)

Chapter 3
Computational details

All DFT calculations in this thesis were performed using the Vienna ab initio simulation package (VASP) [3.1, 3.2] within the generalized gradient approximation (GGA) to describe the exchange-correlation effects, employing the Perdew, Burke and Ernzerhof (PBE) exchange–correlation functional [3.3]. It has already been shown that this functional gives a reasonable description of water systems [3.4, 3.5, 3.6].

Generally speaking, there are two methods to model the surface: fixed several layers with the bulk structure to simulate the part which is far away from the surface, and some relaxed layers either on one side (Fig.3.1.a) or on both sides (Fig.3.1.b) to model the part neighboring the superficies.

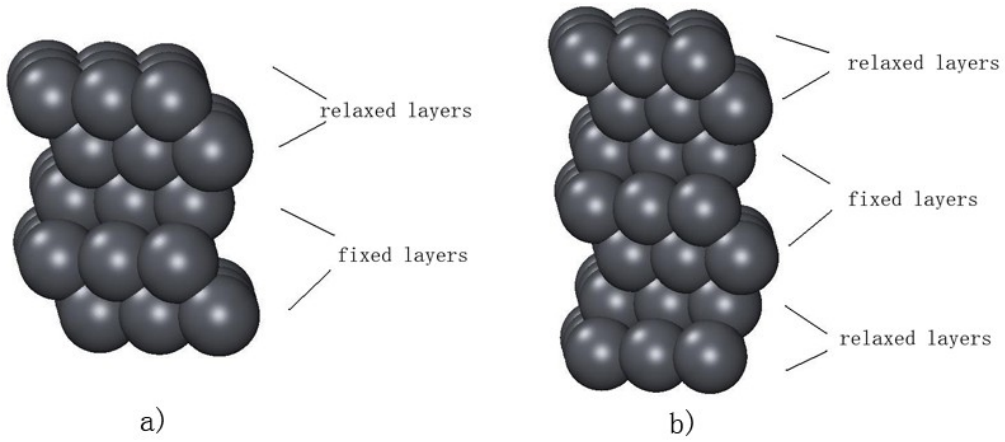


Fig.3.1 The models of Pb(111) surface. a) one-side-relaxation model. b) both-side-relaxation model.

The surface energy of two side model is determined according to

$$E_{surf} = \frac{1}{2}\left(E_{tot} - N * E_{bulk}\right) \tag{3.1}$$

where E_{tot}, N and E_{bulk} are the total energy of the surface system, the number of the atoms in the surface system, and the energy of bulk system per atom. Because there are two side relaxation, it is easy to understand the factor ½ at the front of the formula.

The formula of one side model surface energy can be understood in this way: We do two step separately. First step, we cut a piece from the bulk, the energy is equal to

$$E_1 = \frac{1}{2}\left(E_{unrelax} - N * E_{bulk}\right) \tag{3.2}$$

$E_{unrelax}$ is the total energy of the surface system without relaxation.
The second step is the relaxation, and the energy difference is:

$$E_2 = E_{tot} - E_{unrelax} \tag{3.3}$$

The surface energy is the sum of these two part. So the one side model surface energy can be written as

$$E_{surf} = E_{tot} - \frac{1}{2}E_{unrelax} - \frac{1}{2}N * E_{bulk} \tag{3.4}$$

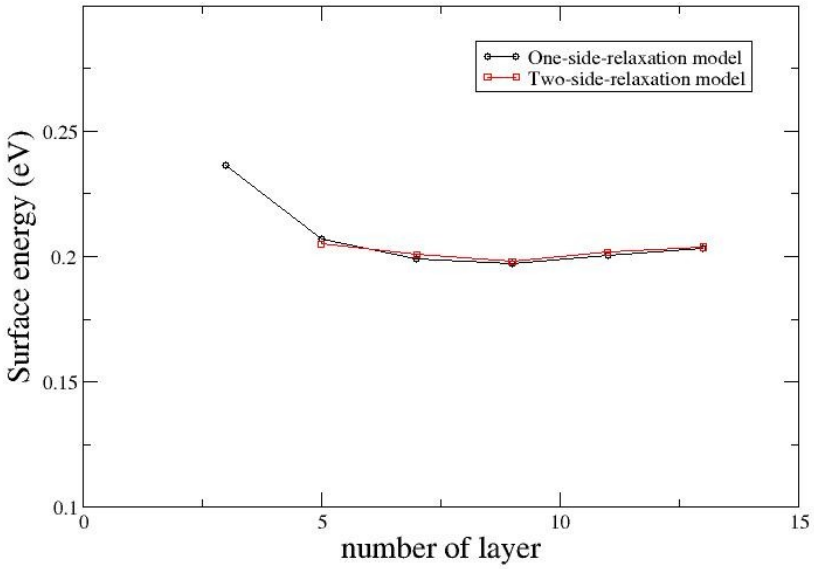


Fig.3.2. The surface energy of Pb(111) surface converge with respect to the number of layers.
The black line use the one side relaxation to simulate the surface and the red line use the both side relaxation model.

In this case, it is necessary to do some calculations to test the surface energy convergence with the number of the layers. A example of Pb(111) surface is shown in Fig.3.2. It is clear that both methods get almost the same results. And after five layers, when the number of layers increases, the surface energy almost does not change. Table 3.1 shows us the necessary layer number for the surfaces, according to our calculation.

Table 3.1. the necessary layer number of the surfaces

surface	(1 1 1)	(1 0 0)	(2 1 1)	(3 1 1)	(5 1 1)	(7 1 1)
Layer number	5	5	15	10	15	20

The number of k-point which is necessary for the calculation depends on the necessary accuracy and the properties of the system. Usually metallic systems require much more k-point than semiconducting and insulating systems. The smearing method is another significant factor of the k-point number, because different methods converge with totally different speed. And the error of the system as a function of k-points depends on the properties of the system. For example, for fcc and bcc metal, a set of 9x9x9 k-points leads to a completely different error. Therefore the convergence with respect to the number of k-points is absolutely necessary.

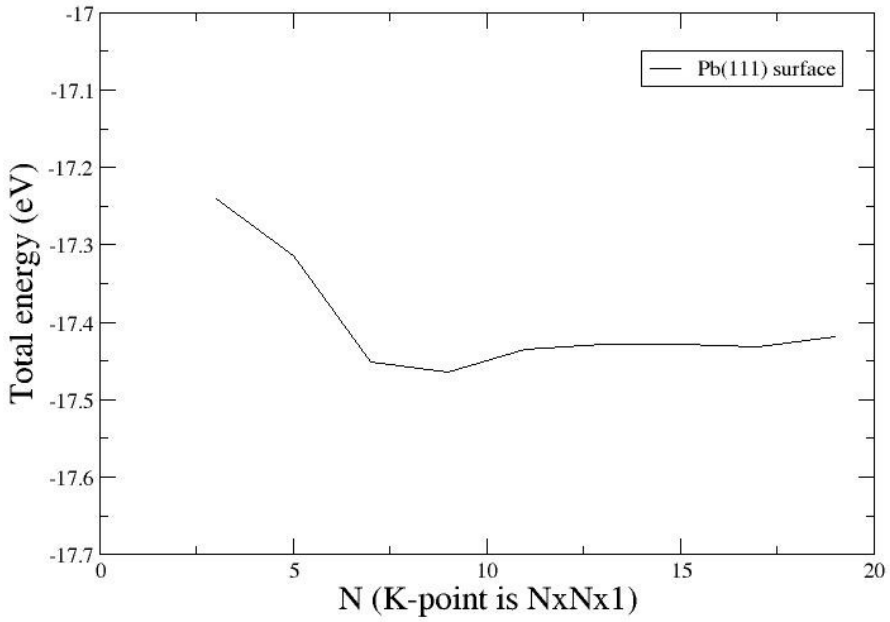


Fig.3.3. The total energy of Pb(111) surface converge with respect to the number of K-point

Fig.3.3. shows us how the total energy of Pb(111) surface converges with respect to the number of k-points. As an example, it is clear that for this system the set of 11x11x1 k-points is enough for the calculations. From our calculations, a k-points set of 11x11x1 is necessary for flat surfaces of all three metals (Au, Ag, Pb).

As we explained in the definition of k-point above, it is easy to understand that the larger the real space we chose, the smaller k-space of this system is. When we use a larger supercell in our calculation, less k-points should be needed. So the total energy of supercell convergence with respect to the number of k-points is also checked. Fig. 3.4 shows us the example of (2X3) Pb(511) supercell. And it demonstrates that a 3x3x1 k-points set yields rather good results. All the supercell simulations in this thesis except some special calculations (for example density of states calculation, band structures calculations) used a 3x3x1 k-points set.

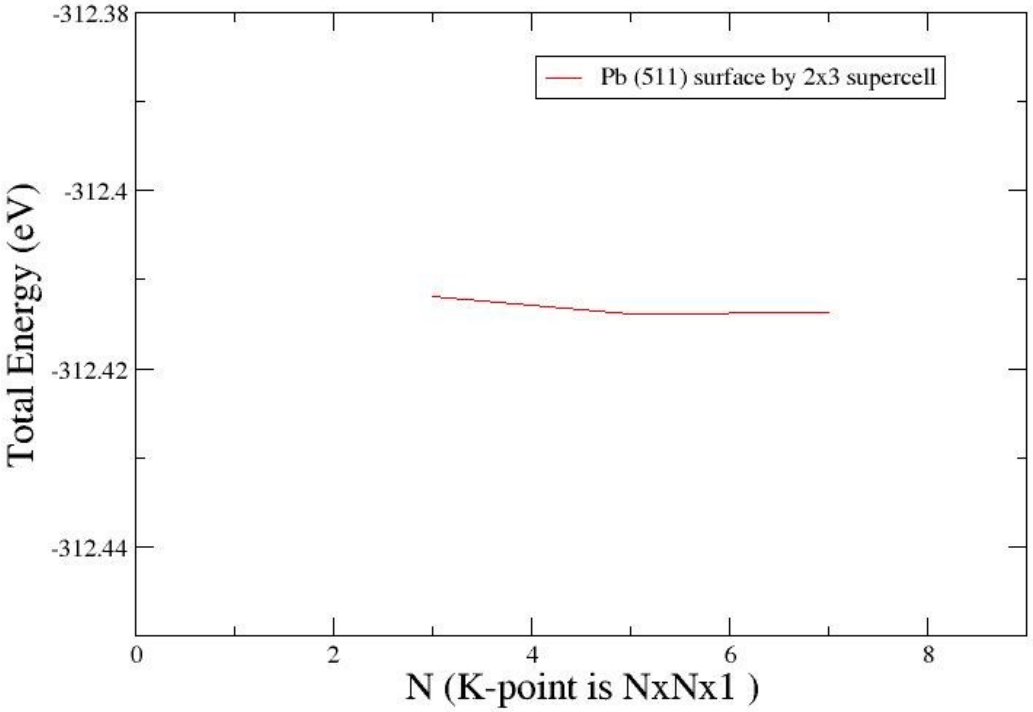


Fig. 3.4. The total energy of Pb(511) surface by two by three supercell converge with respect to the K-point

For a periodic system, the natural way we solve the Kohn-Sham equations, is to expand the wave function in a discrete plane wave basis set.

$$\Phi_{K,i}(\boldsymbol{r}) = \sum \boldsymbol{C}_{\boldsymbol{i.K}} + \boldsymbol{G}\, e^{i(\boldsymbol{K}+\boldsymbol{G})\cdot\boldsymbol{r}} \tag{3.5}$$

where G represent the reciprocal lattice vectors and K is to make sure G lie within the first Brillouin zone. The plane waves in the form above obey the Bloch's theorem completely.

In principle, an infinite number of plane waves could perfectly describe the electronic wave function in the system. In fact, only a limited number of plane waves is used. The Encut-tag specifies the cut-off energy for plane wave basis set in eV in the Vasp. It determines the size of the plane wave basis. All of the plane waves with the kinetic energy smaller than the Encut value are included in the basis set.

In general, the cut-off energy should be chosen according to the pseudopotential, a default value is given in the POTCAR files. But sometime the default cut-off energy in the POTCAR result in serious errors, which means that the basis set is not large enough. Therefore, a test of energy convergence with respect to the cut-off energy is also necessary.

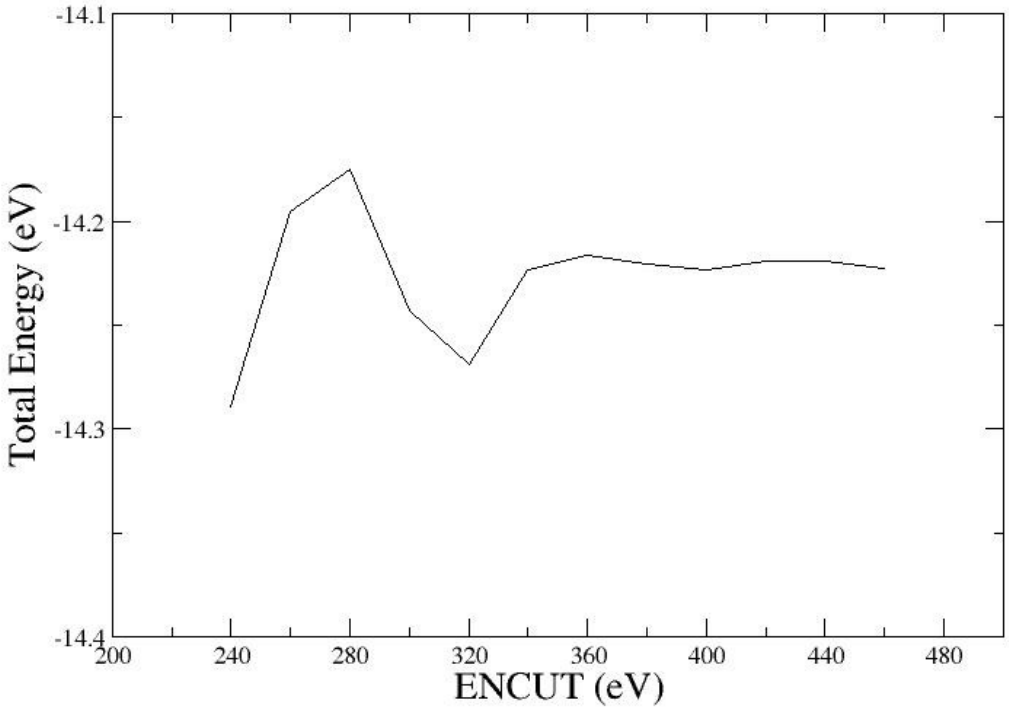


Fig.3.5 The total energy of water molecule converge with respect to the value of the Encut

Next step I have checked the necessary value of Encut. In fig.3.5, the total energy of isolated water molecule increases and decrease rapidly from 240eV to 360eV, and converges at 400eV when the water total energy is equal to -14.22eV, which shows a rather good agreement with other calculation results [3.4, 3.7- 3.10]. And this value will be used frequently in the following chapters. The rapidly changed total energy indicates that the value of Encut is rather important for the accuracy of our calculation. Obviously, default value is not enough and in all of our calculation 400eV is used as the value of Encut.

Since water is a kind of polar molecule, we compare the results of water-metal system with and without dipole-moment correction. The system we used was the single water adsorbed on the lead flat surface. The results are shown in the table 4.2. It is clear that the effect of the dipole-moment correction is rather small in our system. The difference between these two kind of calculations is smaller than 0.001eV (1%). Obviously , it is not necessary to use dipole-moment correction in our calculation.

Table 3.2
comparison of adsorption energy with and without dipole-moment correction

system	without dipole-moment(eV)	with dipole-moment(eV)	difference(%)
Pb(100)	-0.183	-0.183	0.14
Pb(111)	-0.165	-0.164	0.83

In our calculations, all of the surfaces were modeled with a vacuum region of 20 Å. The geometry of the water–metal systems was optimized by relaxing all atoms of the water layers and the uppermost two layers for flat surfaces ((100), (111) surface) the uppermost four layers for (311) surface, five layers for (211) and (511) surface and eight layers for (711) surface.

Bibliography

[3.1] G. Kresse, J. Furthmüller, *Phys. Rev. B: Condens. Matter* **54** 11169 (1996).

[3.2] G. Kresse, J. Furthmüller, *Comput. Mater. Sci.* **6** 15 (1996).
[3.3] J.P. Perdew, K. Burke, M. Ernzerhof, *Phys. Rev. Lett.* **77** 3865 (1996).
[3.4] S. Schnur, A. Groß, *New J. Phys.* **11** 125003 (2009).
[3.5] P. Vassilev, C. Hartnig, M.T.M. Koper, F. Frechard, R.A. van Santen, *J. Chem. Phys.* **115** 9815 (2001).
[3.6]J. VandeVondele, F. Mohamed, M. Krack, J. Hutter, M. Sprik, M. Parrinello, *J. Chem. Phys.* **122** 014515 (2005).
[3.7] A. Michaelides, Appl. Phys. A, 85,415 (2006).
[3.8] P. Vassilev, C. Hartnig, M. T. M. Koper, F. Frechard and R. A. van Santen, J. Chem. Phys., 115 9815-9820 (2001),
[3.9] J. VandeVondele, F. Mohamed, M. Krack, J. Hutter, M. Sprik and M. Parrinello, J. Chem. Phys., 122, 014515 (2005).
[3.10] B. Santra, A. Michaelides, M. Fuchs, A. Tkatchenko, C. Filippi and M. Scheer, J. Chem. Phys., 129, 194111 (2008).

Chapter4
Clean metal surfaces: Au, Ag and Pb

As the first step of my study, we start with the calculation of bulk metal properties. Obviously, the value of the calculation results can not be one hundred percent equal to the experimental one, the similarities of these data is a significant aspect to weigh the accuracy of the calculations. There are two ways to get the lattice constant in principle. Either (A) use the option of "ISIF = 3" in the INCAR file of the DFT simulation, which means that the calculation will change both the shape and the volume of the unit cell automatically to get the optimized bulk structure. Or (B) calculate the energy at many different lattice constants around the experimental value, then get a fitted curve of the "lattice constant- energy", and determine the value with lowest energy.

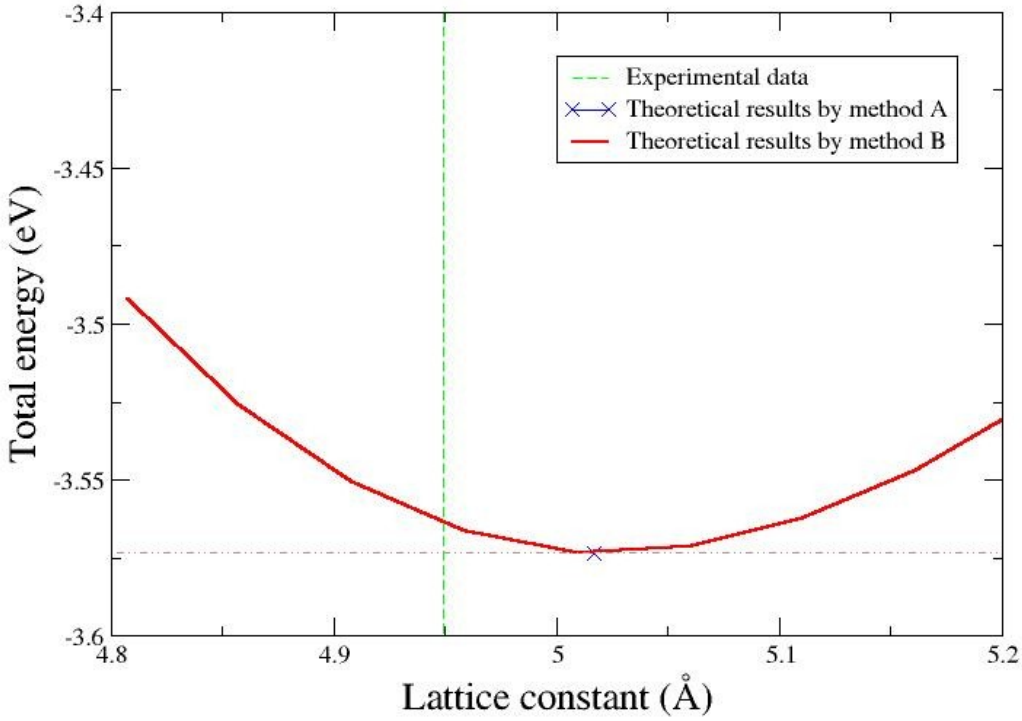


Figure 4.1. The total energy change with the lattice constant (red curve). The blue X point is the result of method B. The dashed line is the experimental result.

All of these three materials we considered are face-centered cubic (fcc) metals. Fig.4.1 shows the lattice constant of lead derived from the two methods. Obviously, the two methods give the same theoretical result of the lattice constant of lead. The value is 5.02 Å, and 1.4% larger than the experimental value of 4.95 Å [4.1] in agreement with previous studies[4.2]. Table 4.1 also shows the lattice constants of Au and Ag, and the error of the theoretical data are all acceptable (all of them are smaller than 3%). Ignoring the overall error due to the exchange-correlation functional, the numerical errors of the lattice constant are rather small. Thus all of the following calculations are based on these theoretical values.

Table 4.1 The lattice constant of Pb Au and Ag

element	Theoretical value(Å)	Experimental value(Å)	error(%)
Pb	5.02	4.95	1.4
Au	4.17	4.08	2.2
Ag	4.16	4.09	1.7

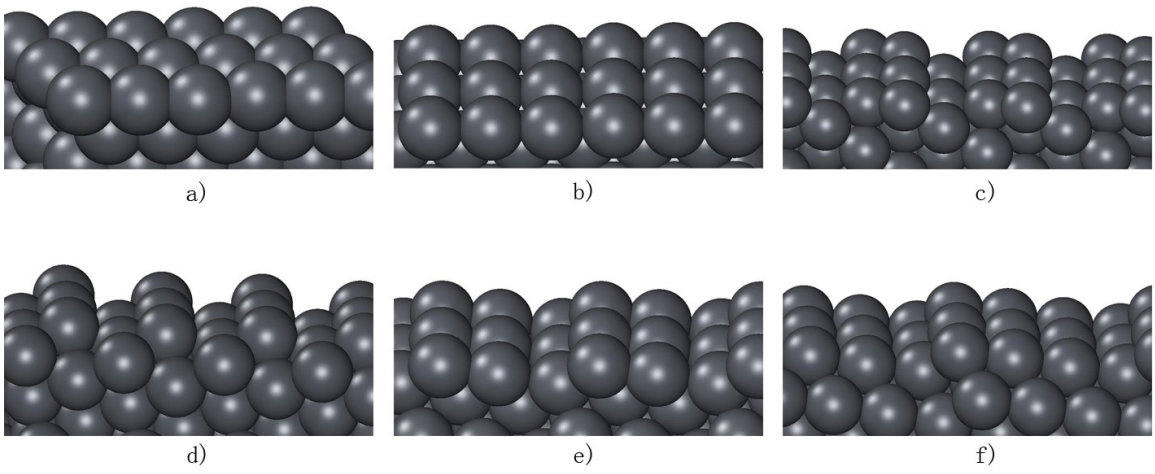


Fig.4.2. The substrates which are used in our calculation. a) (111) surface b) (100) surface c) (211) surface d) (311) surface e) (511) surface f) (711) surface

Figure 4.2 shows us the examples of the substrates we used in the following, including two flat surfaces (a) (111) and b) (100) surface) and four stepped surfaces (c) (211), d) (311), e) (511) and f) (711) surface). Since there will be some atoms or

molecules adsorbed on these substrates, a larger periodic cell which formed by several unit cell, a so called supercell, is necessary in our research. For all of the three metals, if not specified differently, the supercell are set as follow: three by three supercell for flat surfaces and two by three supercell for stepped surfaces

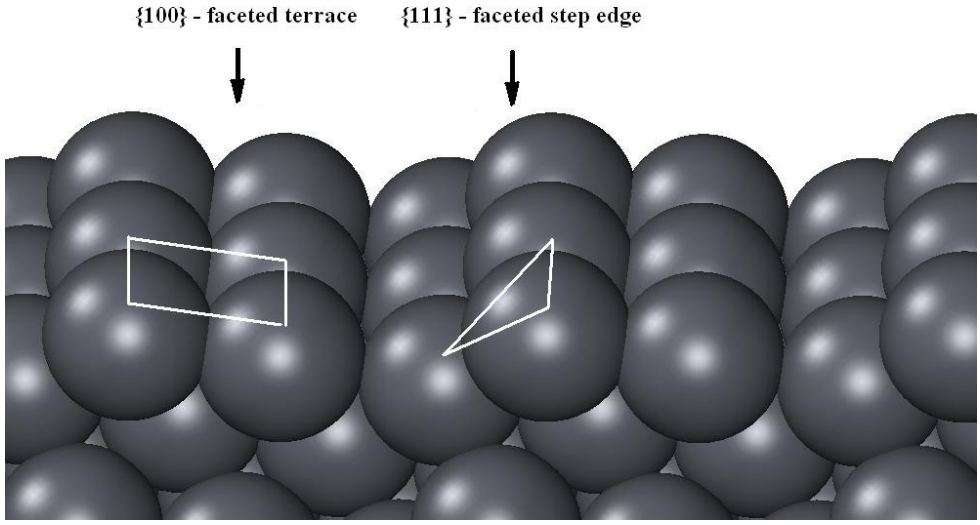


Fig.4.3: {100}- faceted terrace and {111} – faceted step edge on fcc (511) surface

Generally speaking, the stepped surfaces we investigate can be seen as a combination of (111) surface and (100) surface. It is shown clearly in fig.4.3, as a example, (511) surface is composed by a "terrace"({100} orientation) and a step edge ({111} orientation). For a stepped surface (N 1 1), the numerical value N determines the length of the terrace. And whether N is odd or not decides that the terrace is {100} or {111} orientation. Since there are only few experiments addressing stepped surfaces, a main reason in our research to investigate surfaces is to get a general idea of the stepped surfaces' properties. The electronic properties of stepped surfaces particular at step edge will be presented in the following investigation.

The interlayer distance is defined in figure.4.4, which is the distance between two neighboring layers after relaxation. Stepped surfaces are rather open surfaces, especially at the step edge. Since the coordination number of step edge atoms are lower than the atoms at terrace and flat surfaces, the interlayer distances should change considerably comparing with the bulk value. And most importantly, the bulk interlayer distance of the stepped surfaces is rather small, for example , it is only 0.96Å for lead (511) surface. Thus small absolute movement lead to a large relative change. Thus it is also very interesting to investigate the change of the stepped surfaces' layers after relaxation.

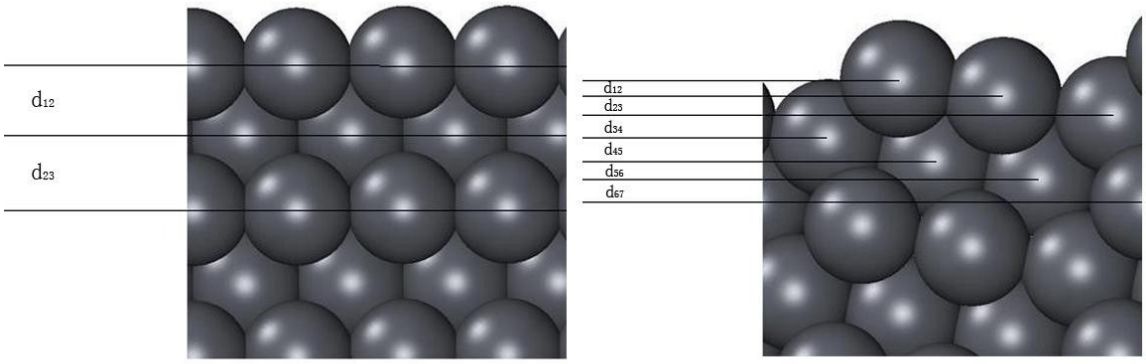


Fig4.4: Definition of the interlayer distance of flat surface (above) and stepped surface (below). The bulk interlayer distance and the obtained values for the interlayer distance d_{ij} are given in Table 4.2.

Table 4.2 Inter-Layer distance of Pb surfaces after the DFT-GGA relaxations. The relative change to the bulk interlayer distance is shown in Fig.4.5 not only for Pb but also for Ag and Au surfaces. All of the values in this table are in the units of Å. Labels are as defined in Fig. 4.4

surface	d_{12}	d_{23}	d_{34}	d_{45}	d_{56}	d_{67}	d_{78}	d_{89}	dbulk
Pb(100)	2.37	2.59	---	---	---	---	---	---	2.50
Pb(111)	2.74	2.93	---	---	---	---	---	---	2.89
Pb(211)	0.88	0.92	1.06	0.98	0.99	1.14	---	---	1.02
Pb(311)	1.22	1.54	1.45	1.59	---	---	---	---	1.51
Pb(511)	0.89	0.97	0.87	1.03	1.00	0.97	---	---	0.96
Pb(711)	0.56	0.74	0.56	0.74	0.62	0.73	0.73	0.75	0.70

In table 4.2 the relaxations of the top crystal layers with respect to the bulk values are tabulated. Generally speaking, a contractive relaxation of the first layer usually happens, because of the smoothing of the electron density at metal surfaces. This trend is clearly shown in the first data column of table 4.2. For the flat (111) and (100) surfaces, because they are relative densely packed, the contraction is rather small, only 5.1% and 5.2% comparing with the lead bulk crystal. But for the stepped surfaces which are more open, it is rather significant, the contraction is 13.7%, 19.2%, 7.2% and 20% (in the order of Pb(211) Pb(311) Pb(511) and Pb(711)). Furthermore, for most of the metal surfaces, the contraction of the first layer leads to an expansion of the second inter-layer distance, such as Pb(100), Pb(111), Pb(311) and Pb(711). But this

phenomenon is not general, which is demonstrated for Pb (211), and Pb(511) and Cu(511)[4.3 4.4]. The other two metals (Au and Ag) show rather similar behavior, and the interlayer distance data are shown in the Appendix A.

For the more open surfaces, in particular the stepped surfaces, the changes after relaxations are more complicated than flat one, but still similar trends exist, especially for the same surfaces of different metals. To make this trend more clearly, fig.4.5 shows the relative change of the optimized inter-layer distance compared with the bulk. The percentage Δ is calculated by the following formula

$$\Delta = \frac{(d_{ij} - d_{bulk})}{d_{bulk}} \times 100\,\% \qquad (4.1)$$

d_{ij} is defined in Fig. 4.4. Negative and positive values represent contraction and expansion of the layers.

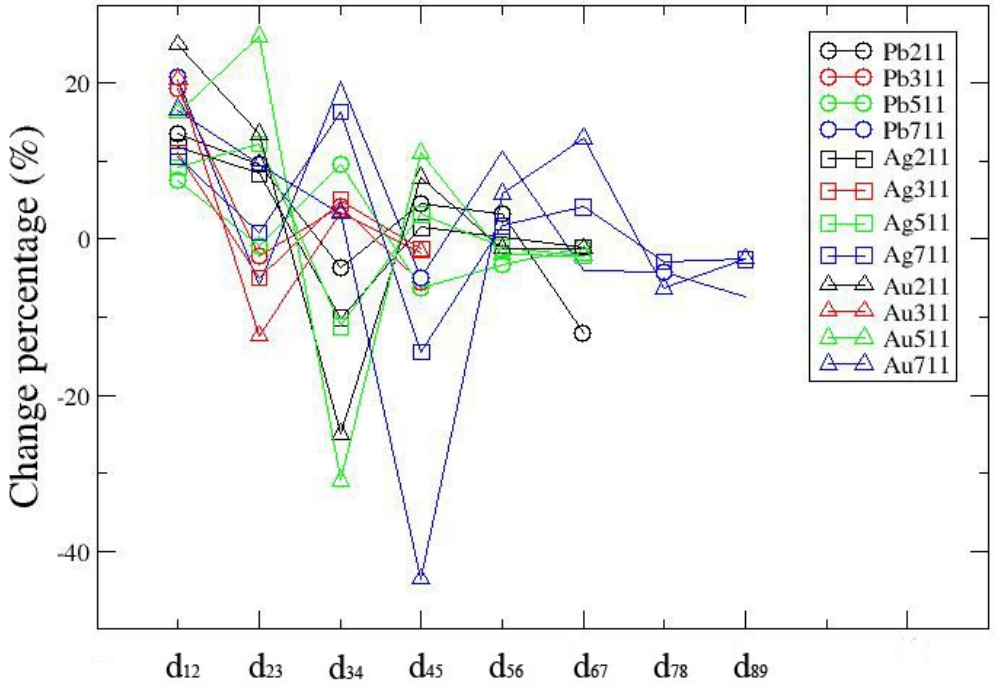


Fig. 4.4 Relative change of the optimized inter-layer distance compared with the bulk. The same kind of surfaces are in the same color, for example, Pb(211), Ag(211) and Au(211) are all in black. The same element are marked in the same geometric drawing, for instance, lead is denoted by circles, silver by squares and gold by triangles.

Although the extent of the contraction and expansion is different, as I mentioned above, the change in the trends of the same kind of surfaces are almost identical except for the Pb(511) surface. I think the main reason is that the electronic structure of lead is rather different to silver and gold, which can cause different properties. We note that at least all of the surfaces have something in common: the first layer distance are all contractive, which can be explained by a simple model proposed by Finnish and Heine[4.5]. In this explanation, as the electrons could move freely in the metal, the electron density should become smooth (as a simple sketch, it is marked as a straight line in fig. 4.5), but not the same as it in the bulk (dashed line in fig.4.5). Hence, the electron should transfer from the "+" part to the "-" part, and this charge redistribution will certainly make the "electrostatic center" lower. The ionic cores will then contract from the original position (the hollow small ball) to a new equilibrium one (the solid one) under the Coulomb force. This simple model can explain the behavior of the first layer quite good, but it can not describe the other layers which is much more complicated. Due to the different electron structures and surfaces, the change of the other layers are totally different (fig.4.4).

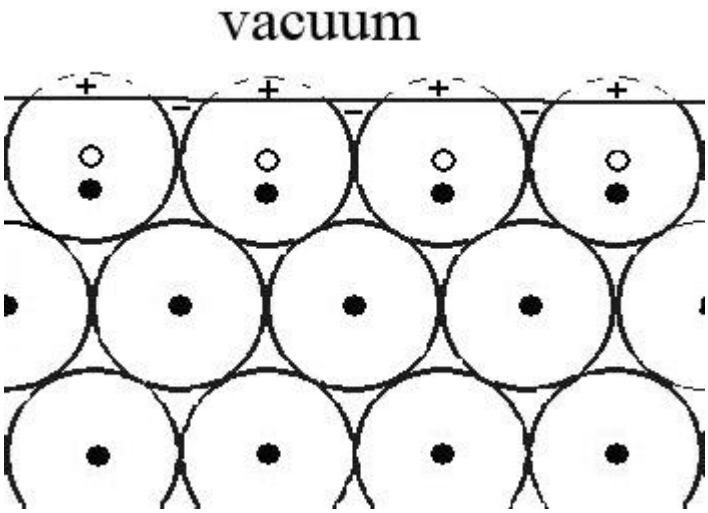


Fig. 4.5 Sketch of the electron smoothing and the first inter-layer contraction at a metal (111) surface.

Table 4.3 shows the main results for all of the surfaces we used in our study, together with experimental data published by Mezey and Gibel [4.6], in order to derive trends among different surfaces and metals. In the experimental results, the surface energies are measured at room temperature and at the melting point. We get the value at 0K linearly by these two point. Although this value is only a roughly approximation, it can give us a general idea and make it comparable with the theoretical results. We

noticed that the theoretical results of surface energies are about 0.5 times the value of the corresponding experimental one extrapolated at T= 0K.

To figure out the reason for this large disagreement between experimental and theoretical results, we should focus on the large uncertainty associated with this kind of experiment. First, the experimental techniques which can determine the surface free energies are mainly based on the measurements of surface liquid-metal tension at melting point. They can only be applied to the isotropic crystal or polycrystalline elements, but not to a particular surface [4.6]. It could be seen as an average surface energy at a given temperature. Second, although in principle the surface energy at 0K can be obtained by extrapolation of experimental data at different temperature, this method might also contribute the uncertainty. At last, of course no experiment is performed in an ideal state. Many conditions could lead to an error, such as defects and impurity.

We then compared our findings with many other computation results. Although the number of studies of stepped surfaces is still limited, it is not so hard to get the reference of the flat surfaces, in particular closed packed surfaces. As a example, the surface energy of Ag(111) for different functionals and basis sets is listed in appendix B. Almost all of the studies using GGA based DFT study with PBE/RPBE exchange-correlation functional have rather similar results compared to ours, such as the value using numeric atomic orbital (NAO)/ exact-muffin-tin-orbital (EMTO) basis sets with PBE functional and in projector augmented wave (PAW)/ NAO with RPBE functional [4.6, 4.10]. On the other hand, LDA based DFT using the full-potential linear- muffin-tin-orbital (FP-LMTO)/ the full charge density (FCD) shows a better agreement with the experimental value[4.7- 4.9]. It is believed that LDA yields these results because of a fortuitous error cancellation.

Table 4.3 Surface energies of flat and stepped Pb/Ag/Au surfaces. The experimental value are extrapolated to different temperatures. T0/ Ta/ Tm are corresponding for the surface energy at 0K/298K/melting temperature.

Surface	Surface energy (eV/atom)	Surface energy (J/m2)
Pb(111)	0.047	0.35
Pb(100)	0.061	0.39
Pb(211)	0.048	0.37
Pb(311)	0.050	0.38
Pb(511)	0.053	0.38
Pb(711)	0.054	0.39
Experimental Pb (T0/Ta/Tm) (J/m2)[4.7]	0.60/0.53/0.47	
Ag(111)	0.075	0.80

Ag(100)	0.093	0.86
Ag(211)	0.079	0.90
Ag(311)	0.082	0.92
Ag(511)	0.086	0.92
Ag(711)	0.087	0.90
Experimental Ag (T0/Ta/Tm) (J/m2)[4.7]	1.38/1.30/1.05	
Au(111)	0.066	0.71
Au(100)	0.091	0.84
Au(211)	0.070	0.79
Au(311)	0.075	0.83
Au(511)	0.079	0.83
Au(711)	0.082	0.84
Experimental Au (T0/Ta/Tm) (J/m2) [4.7]	1.76/1.63/1.35	

According to table 4.3, the trend in the surface energies of the three metals is the same. For the flat surface, E_{surf} (111) < E_{surf} (100) is rather obvious and easy to understand, because the (111) surface is the closed packed surface. Furthermore, the stepped surfaces, (211), (311), (511) and (711), are also considered. For the stepped surface (n 1 1) with odd n, the trend E_{surf} (311) < E_{surf} (511) < E_{surf} (711) is observed. As these kind of surfaces are in fact N(100)X(111) as mentioned above, this phenomenon can be explained easily. When the number of n increase, the (100) part formed in the stepped surface gets larger, the surface energy will get closer to the pure (100) surface. Imagine that if the n is large enough, the (n11) surface energy will approach that of the (100) surface. We noticed that although all of the three metals have this stepped surfaces trend, the surface energies (unit J/m^2) of Ag stepped surfaces are all larger than of Ag(100) as well as metal Cu (appendix C). But for Au and Pb, the values are smaller and rather similar as (100) surface.

Usually, to make a step edge on (100) surfaces needs extra energy, and its' sometimes rather large, that's why the surface energy of Cu/ Ag stepped surfaces[4.4, 4.11] are large. But we should note that, to make a step edge also means to add a (111) surface piece onto the (100) surface, which will decrease the surface energy. For some heavy metal like Au and Pb, this energy decreasing caused by a (111) surface piece maybe even larger than the formation energy of the step edge, which will make the total surface energy lower. Unfortunately, the principle of this phenomena is still not completely clear yet. To make it clear, more elements should be calculated.

The charge density difference of the Pb flat and stepped surfaces comparing with bulk crystal are shown in fig.4.6. At the flat surfaces Pb(100) and Pb(111), the charge distribution is rather delocalized, which the charge density isosurface with the value of 0.01 $eV/\mathring{A}^3$ is smooth and flat covering the surface. The charge accumulation isosurface is a little bit further away from the surface than the depletion one, but the distance is rather small. For stepped surfaces in particular Pb(511) and Pb(711), the charge distribution is localized at the stepped edge, but rather delocalized at the terraces. It indicates that the step edge has unique electron properties which is different from the flat surfaces. This point will be demonstrated in the next two chapters. The other two metals, Ag and Au, show rather similar results compared lead, so that I will not discuss them here.

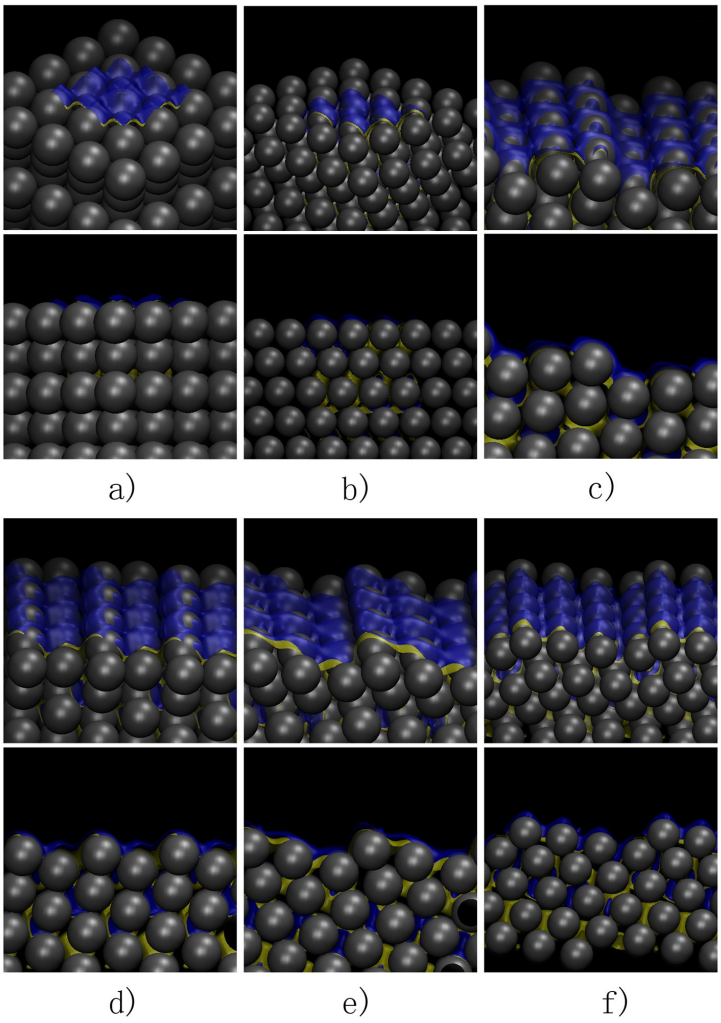


Fig.4.6 Fig. 6. Isosurface plots of charge density differences upon Pb flat surfaces: a) Pb(100), b) Pb(111) and stepped surfaces c) Pb(211), d) Pb(311), e) Pb(511), f) Pb(711). value 0.01 e/Å3. Charge accumulation, i.e. accumulation of electron density, is plotted in blue, charge depletion in yellow. In contrast to the previous figures, the Pb atoms are colored in grey.

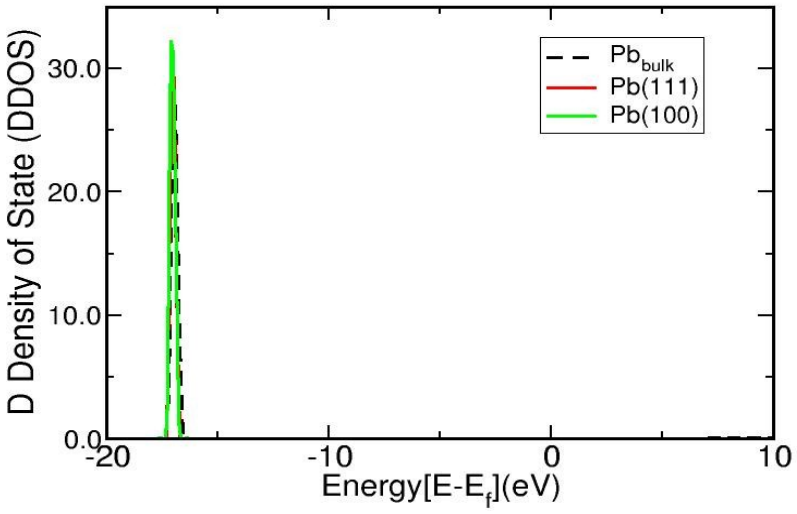


Fig.4.7 d density of state of Pb bulk, Pb(111) and Pb(100) surfaces

The figure of Density of State (DOS) are usually used to analyze the interaction of the substrate and adsorbate. The Newns-Anderson model and the simpler d-band model (details in Chapter 5/ introduction) have been proved particularly useful in the development of an understanding of reactions at the solid-gas or solid-liquid interface. It is particularly important to understand which properties of the surface determine its chemical reactivities. The d-orbital density of states (dDOS) is rather important in the solid-liquid interfaces, some recent studies suggest that the d-band model could explain the strength of the metal-water interaction [4.12]. We all know that Pb's outermost electron structure is 6s26p2, but interestingly enough the water-lead interaction is as strong as other metal like Ag, Au, which will be discussed in detail in the next chapter. Fig. 4.6 shows us the dDOS of Pb surface. It illustrates that the fully occupied d-band of Pb lies far below the Fermi energy indicating that it hardly contributes to the bonding to adsorbates so that the bonding is dominated by the s- and p-orbitals

Bibliography

[4.1] American Institute of Physics Handbook, McGraw-Hill Book Company, Inc. :New York, 1957; pp 2-48

[4.2] C. M. Wei and M. Y. , *Phys. Rev. B,* **66** 233408 (2002)
[4.3] D.A. Walko and I.K. Robinson, Phys. Rev. B 59 1544 (1999)
[4.4] A. Gross, Theoretical surface science 70 (2009)
[4.5] M. W. Finnes, and V. Heine, J. Phys. Chem. B 105, L37 (1973)
[4.6] L. Mancera, J. Behm, and A. Gross, Phys. Chem. Chem. Phys. 15, 1497 (2013)
[4.7] L. Z. Mezey and J. Giber Japanese Journal of Applied Physics 21 11 (1982)
[4.8] M. Methfessel, D. Hennig, and M. Scheffler, Phys. Rev. B 46 4816 (1992)
[4.9] L. Vitos, A. V. Ruban, H. L. Skriver and J. Kollar, Surf. Sci. 411, 186 (1998)
[4.10] M. Ropo, K. Kokko and L. Vitos, Phys. Rev. B 77 195445 (2008)
[4.11] D. Spisak, Surf. Sci. 489, 151 (2001)
[4.12] T. Schiro, O. Takahashi, K. J. Andersson, H. Oestroem, L. G. Pettersson, A. Nilsson and H. Ogasawara, J. Chem. Phys. 132, 094701 (2010)

Chapter 5
Water-metal interfaces

5.1 Introduction

The results with respect to water-Au interfaces of this chapter have been published in Surf. Sci. 606, 886-891, and parts of the text are taken from this reference. The experimental data concerning Au and Ag electrodes are taken from H. Ibach's work[5.5, 5.49].

The atomic level understanding of metal–water interfaces is of strong current interest [5.1– 5.9], not only from a fundamental but also from an applied point of view, in particular in the context of electro-chemistry, corrosion, and atmospheric science [5.10]. Stepped surfaces are particularly interesting [5.11– 5.13] as they are present in any realistic surface and often exhibit specific electronic [5.13], chemical [5.14] and/or catalytic [5.15– 5.17] properties. To systematically study the effects of steps on the properties of metal–water interfaces, vicinal surfaces are well-suited since they have a well-defined step structure.

Although the structure of water layers, especially the stratification of liquid water near electrode surfaces, has been studied intensively, for example by experiments using grazing incidence X-ray and scanning tunneling microscopy (STM) [5.10, 5.18– 5.23], still the structure of water at metal surfaces, in particular at structured surfaces remains unclear. On hexagonal densely-packed (111) substrates, usually it has been assumed that water forms crystalline ice-like layers because of the matching hexagonal geometry [5.18, 5.19, 5.24– 5.29], however, recent ab initio molecular dynamics studies [5.6, 5.30] have indicated that at temperatures above 150 K the water layers start to become disordered. On more strongly interacting metal substrates such as Ru Rh and Ni, water tends to form half-dissociated water-layers [5.7, 5.27, 5.31], however, their formation might be kinetically hindered [5.21].

At non-hexagonal or stepped surfaces, the situation is even less clear since these substrates do not support a hexagonal arrangement of the water molecules. The resulting structure will be a consequence of the balance between water–water and water–metal interactions which are of comparable strength [5.26, 5.32, 5.33] so that it is not trivial to make any structural predictions.

Recently, vibrational spectra of water adsorbed on Au(100), Au(511) and Au (11 1 1) were measured at low temperatures (140 K) using electron energy loss spectrometry (EELS) by H. Ibach [5.5]. This work was motivated by the observed large reduction of the Helmholtz capacitance or inner-layer capacitance on stepped gold and silver surfaces [5.13].

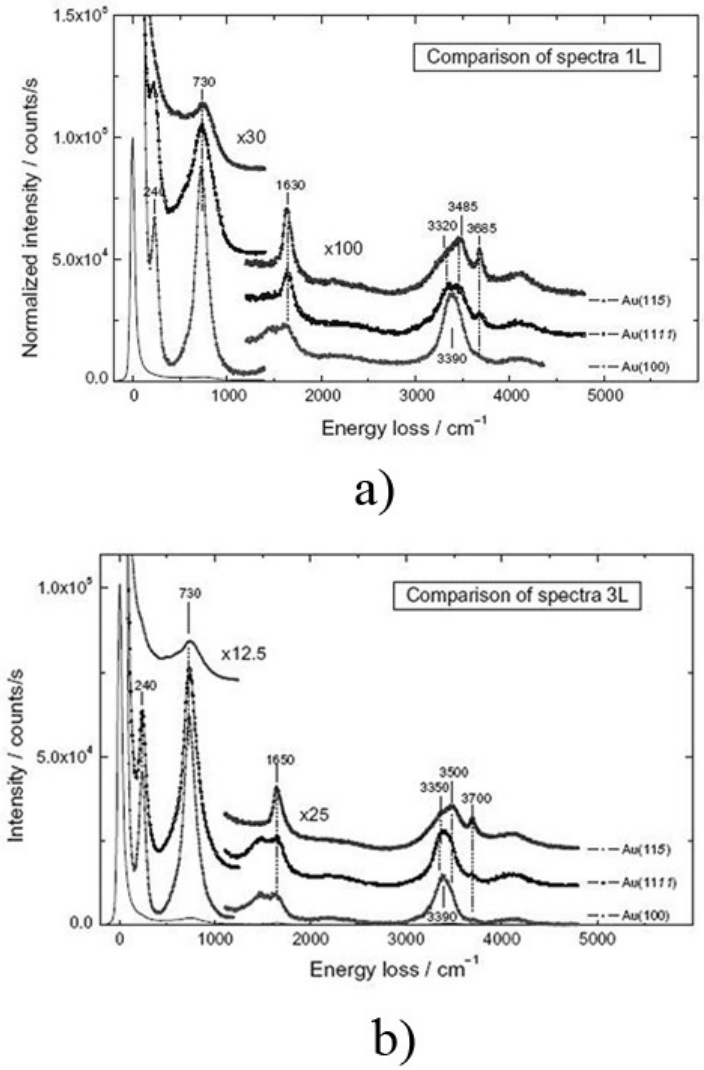


Fig. 5.1.1 Experimental results of energy loss spectra of Au(100), Au(1111) and Au(511) surfaces at 140 K. a) with 1L of water, b) with 3L of water[5.5].

In single adsorbed water layers, not all hydrogen atoms of the water molecules can be hydrogen-bonded to other water molecules. For example, in the ice-like hexagonal bilayers on (111) substrates every second water molecule has a hydrogen atom pointing either up (H-up) or down towards the surface (H-down). These water structures have comparable energies, their stability depends on the particular substrate [5.6, 5.27]. In vibrational spectra of water layers, the presence of the hydrogen-bonded (HB) hydrogen is reflected by a mode at about 3400 cm^{-1}, whereas non hydrogen-

bonded (NHB) hydrogen leads to a peak at 3700 cm^{-1} [5.5, 5.34]. The EELS spectra of water adsorbed on Au(100) at 140 K display in the O-H-stretch regime only a peak at 3390 cm^{-1}. The absence of the NHB hydrogen peak was taken as an evidence for a H-down water layer on Au(100) [5.5]. On stepped Au surfaces, on the other hand, significantly different vibrational spectra were found. Most importantly, the spectra contain a peak close to 3700 cm^{-1} which has been attributed to the presence of NHB hydrogens. Based on these findings, Ibach proposed three different structural models for a water layer on Au(511) involving distorted hexagonal rings which were all assumed to be consistent with the observed vibrational spectra [5.5]. However, a final assessment of the true water structure solely based on the vibrational spectra could not be made.

These experimental data can be seen as a object of reference to investigate the metal-water interface, especially the water structures at stepped surfaces. In this chapter, the properties of single water molecule adsorbed on different metal surfaces are discussed first. Then, considering water layers on flat and stepped gold surfaces, we have addressed structural and electronic properties of water layers on Au(100) and Au(511) by performing periodic density functional theory (DFT) calculations. The stability of several water structures has been evaluated. In addition, ab initio molecular dynamics (AIMD) simulations have been performed at temperatures of 140 K and 300 K in order to assess the thermal stability of the water layers and to derive vibrational spectra. Furthermore, we have analyzed the electronic structure of the water–Au systems. Additionally, the water-silver interface has been investigated. Silver has rather similar properties as gold, such as the lattice constant. A comparison between experimental and theoretical results will also be shown. At last, the lead-water interface will be addressed.

In the electronic structure theory, the d-band model has been proved particularly useful in the understanding of the breaking and making bonds at metal surfaces. This model can be simply described as follow:

When a molecule adsorbs on a transition metal surface, depending on the shape of the band which the metal states form, the interaction will result in a broadened single resonance if the metals states are broad and delocalized or split into bonding and anti-bonding resonances of the states are narrow and localized. The second one will form a strong chemical interaction.

5.2 Adsorption of single water molecule on metal surfaces (Au, Ag and Pb)

Although it is almost impossible to get any experimental data about the adsorption of a single water molecule on metal surfaces, it is necessary to investigate this system as the first step in the study of metal-water interfaces. Before we start to address the water structure, some basic data are needed. And more importantly, it could help us to get the key point of the interaction between the water molecules and the substrate from a complex water-metal system in the following.

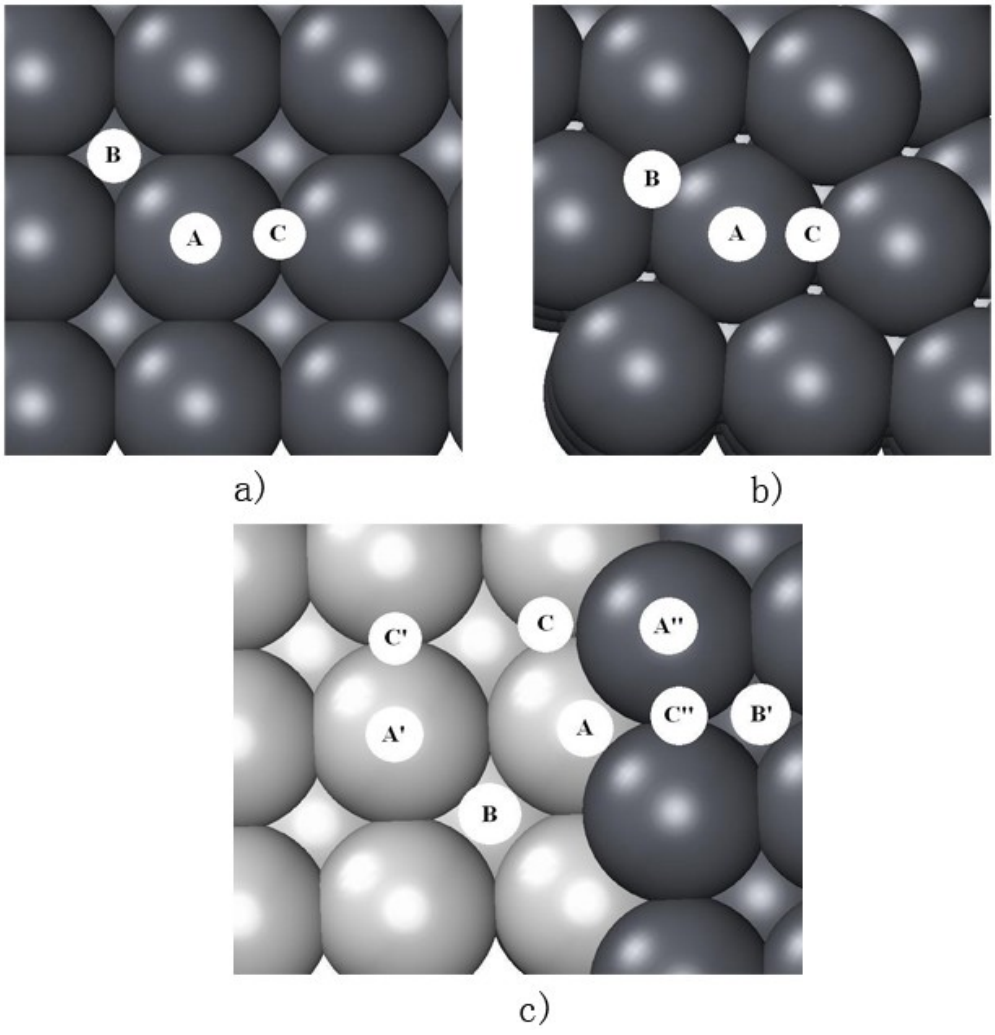


Fig.5.2.1: The possible adsorption position of a water molecule on a) (100) surface b) (111) surface c) (511) surface as a example of stepped surfaces.

Generally speaking, water molecules are assssumed to adsorb at the top ssite of the metal surface through their oxygen atoms, which is also been proved by our investigation. But there are only few investigations about water molecule at stepped surfaces, experimentally or theoretically. In our work, many starting positions of water molecule on both flat and stepped surfaces have been tried, as shown in figure 5.2.1.

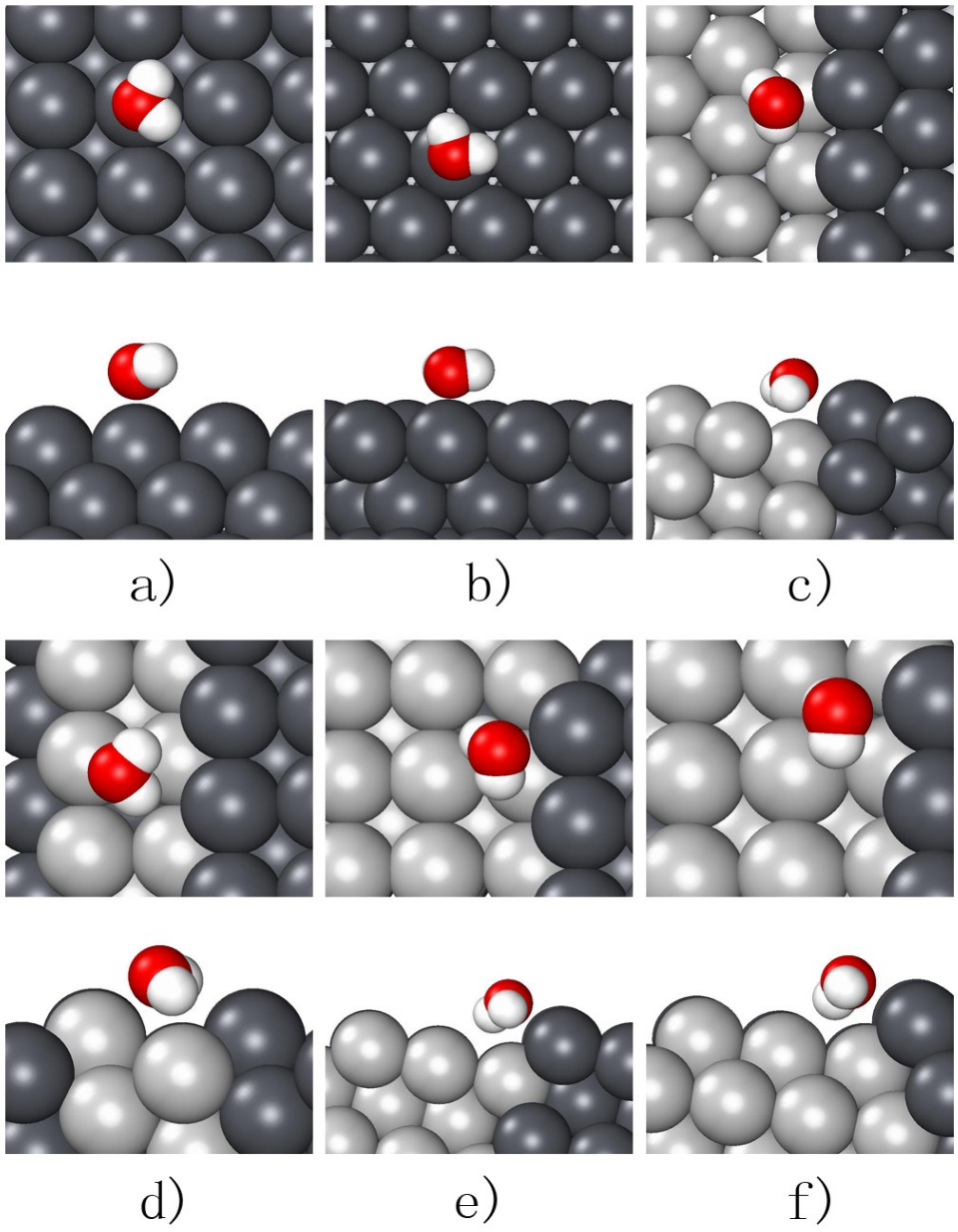


Figure 5.2.2: Top and side view of the relaxed single water molecule adsorbed on a a) Pb(100) surface, b) Pb(111) surface, c) Pb(211) surface, d) Pb(311) surface, e) Pb(511) surface and e) Pb(711) surface.

Figure 5.2.1 shows the possible adsorption position of a water molecule on a) (100) surface b) (111) surface c) (511) surface as an example of stepped surfaces. A, B and C positions are the top site, homo-site and bridge site, respectively. For stepped surfaces, the top site of atoms with different environment are signed as A, A' and A''. And also the adsorption condition of the water molecule is considered, like Hydrogen atom pointing up (H-up) or down (H-down) towards the substrate and parallel to the surface.

First, we address the results on flat surfaces. All of the calculations indicate the same result: top site is the favorable adsorption position for single water molecule not only on lead surfaces (shown in figure 5.2.2 a) and b)) but also on gold and silver. The water molecules are always parallel to the surfaces. Although Au(100) surfaces are not stable usually, in order to compare with other metals, and to get the trend we still investigate water on unreconstructed Au(100).

5.3 Water structures on flat and stepped gold surfaces

5.3.1. Geometry

First we address the water structure on the flat (100) surface. Water structures on (100) surfaces are significantly less frequently studied than water structures on the hexagonal (111) surfaces [5.10, 5.19].

Au(100) surfaces prepared in ultrahigh vacuum are always reconstructed with the uppermost layer forming an incommensurate, approximately hexagonal structure [5.5, 5.42]. Because of the difficulties associated with describing incommensurate structures within a periodic supercell approach, we have not made any attempt to model the reconstructed Au(100) surface. Rather, the results of Ibach for the Au(100) surface might be compared to simulations for water layers on Au(111) [5.6]. In contrast, the Au(511) surface which consists of (100) terraces does not reconstruct [5.43]. In order to have a reference for water on the (100) terraces, we consider a water layer on unreconstructed Au(100).

According to a DFT study using an Au12 cluster to model the Au(100) surface [5.44], an isolated water molecule is most strongly bound to bridge and on-top positions. However, to the best of our knowledge, except for the recent study of Ibach [5.5] there are no studies addressing the microscopic structures of water layers on Au(100). Water on Pt(100), on the other hand, has been the subject of a few studies [5.34, 5.45, 5.46]. Typically it has been assumed that water forms a rectangular structure with every surface atom covered by a water molecule on Pt(100) [5.45, 5.46]. For Au(100), we have adopted a similar structure as our starting point. The optimized structure obtained within a 2×2 geometry assuming an H-down configuration is illustrated in Fig. 5.3.1. There are two inequivalent water molecules per unit cell, one with a hydrogen atom pointing down, the other one bound with the oxygen atom to the underlying Au atom. Still, the water structure is rather flat with the distance between oxygen atoms of the water molecules and the underlying Au atom being about 3.6 Å. Every water molecule is bonded to two neighboring water molecules with a O-O distance of 2.8 Å which is quite typical for the H-bonded oxygen atoms. The O-O distance to the other two neighboring water molecules is 0.5 Å larger so that they can be regarded as not being bonded. This results in a water structure formed by an H-bonded zigzag chain.

The choice of the water structures on Au(511) considered as the initial configurations for the structure optimization was motivated by the suggestions proposed by Ibach [5.5]. In addition, we tried several other structures. However, all these structures relaxed basically towards the structures shown in Fig. 5.3.1. The structures depicted in Fig. 5.3.1 b and c possess a 1×3 periodicity whereas the structure in Fig. 5.3.1 d corresponds to a 1×2 periodicity. The water coverage is the same in all structures with six (Fig. 5.3.1 b and c) and four (Fig. 5.3.1 d) water molecules per unit

cell. The adsorption energies per water molecule are listed in Table 5.3.1. The most stable structure corresponds to the one shown in Fig. 5.3.1 b but the one depicted in Fig. 5.3.1c is within the accuracy of our calculations practically degenerate.

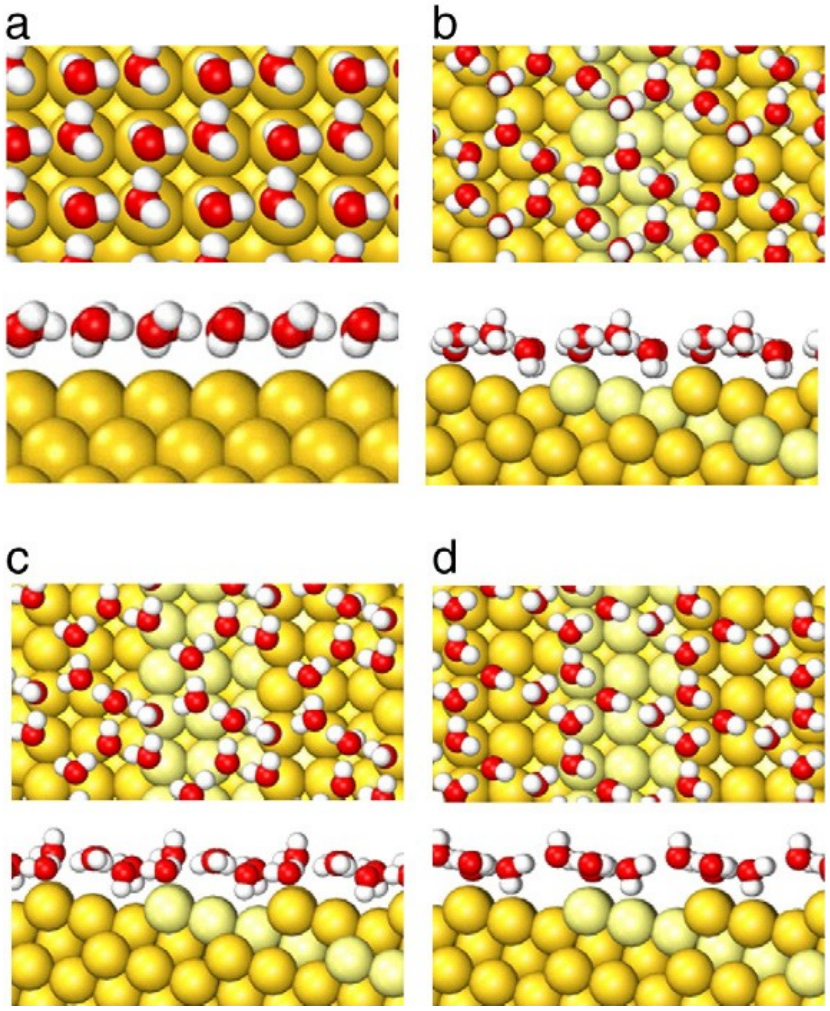


Fig. 5.3.1 Top and side view of the relaxed water structure on Au(100) (a) and Au(511) (b–d).

These two structures are rather similar, they only differ in the position of the H-up water molecules. In the following, we concentrate on the structure shown in Fig. 5.3.1 b which is in fact rather close to the one proposed by Ibach (Fig. 8a in Ref. [5.5]). It is formed by a complete hexagon located on the (100)-like terraces. Hexagons of adjacent terraces are connected by distorted rectangles and octagons. Note that the water molecules at the lower step edge are in an H-down configuration. Thus the water layer can become rather smooth with all oxygen atoms located almost in one plane. The

distances of the oxygen atoms to the underlying metal atoms are 3.30 Å, 4.17 Å and 3.84 Å, starting from the water adsorbed at the upper site of the step edge towards the one adsorbed at the lower site. The water molecules at the middle of the terrace are rather far away from the surface, even 0.33 Å further than those above the lower site of the step edge. Still, the height difference with respect to a (511) plane within the water layer of about 0.3 Å is much smaller than the height difference between the uppermost substrate atoms (0.7 Å). Note that there is only one H-up and one H-down molecule per unit cell, the other water molecules are oriented more or less parallel to the surface. The average distance between the oxygen atoms of two neighboring water molecules on the same terrace is 2.78 Å, whereas it is enlarged to 3.13 Å across the step edge. Finally, the optimized water structure within the 1×2 geometry (Fig. 5.3.1 d) is significantly less stable than the structures within the 1×3 geometry so that it is rather unlikely that it is realized.

Table. 5.3.1
Water adsorption energies in eV per H_2O molecule on Au(100) and on Au(511) for the structures illustrated in Fig. 5.3.1.

Structure	Au(100)	Au(511)b	Au(511)c	Au(511)d
Eads (eV/H2O mol.)	-0.39	-0.44	-0.43	-0.3

5.3.2. Ab initio molecular dynamics simulations

Recently it has been shown that the observed work function change of metal surfaces upon the adsorption of a water layer can only be understood if a thermally induced random orientation of the water molecules is assumed [5.6]. In order to assess the stability of the water layers on Au(100) and Au(511) at finite temperatures and to derive the vibrational spectrum, AIMD simulations at 140 K and 300 K have been performed for a run time of 8 ps. Snapshots of the initial configuration and the final configuration at both temperatures are shown in Fig. 5.3.2.

On Au(100), the rectangular structure obviously dissolves at 140 K (see Fig. 5.3.2b). Instead, a more open hydrogen-bonded network of water molecules evolves with almost all water molecules oriented in a plane perpendicular to the (100) surface. At 300 K which is in fact above the desorption temperature of water monolayers from Au surfaces, the resulting structure becomes even more open, reflecting the fact that the adsorbed water layer is not thermodynamically stable at room temperature. The run time of the simulations has just not been long enough for the desorption to be completed.

The water structure on (100) surfaces certainly deserves further attention. However, here we rather focus on the water structure on stepped Au for which a proposal for a

possible structure exists based on the limited width of the terraces. Interestingly enough, on Au(511) the water layer hardly changes its structure at 140 K, and even at room temperature, there is no indication of any structural rearrangement prior to desorption which sooner or later should occur at this temperature. In addition, there is no sizable reorientation of the water molecules which has been observed on (111) surfaces, also for more strongly interacting substrates such as Pt or Ru [5.6]. Single water molecules are only bound with an adsorption energy of −0.088 eV to the Au(100) surface which is even lower than the adsorption energy of −0.13 eV calculated for the water monomer bound to Au(111) [5.27]. At the lower step edge of the Au(511) surface, however, we find a much larger water monomer adsorption energy of −0.257 eV. Obviously, the water molecules strongly bound to the step edge atoms pin the water structure and lead to a high thermal stability of the water monolayer on Au(511).

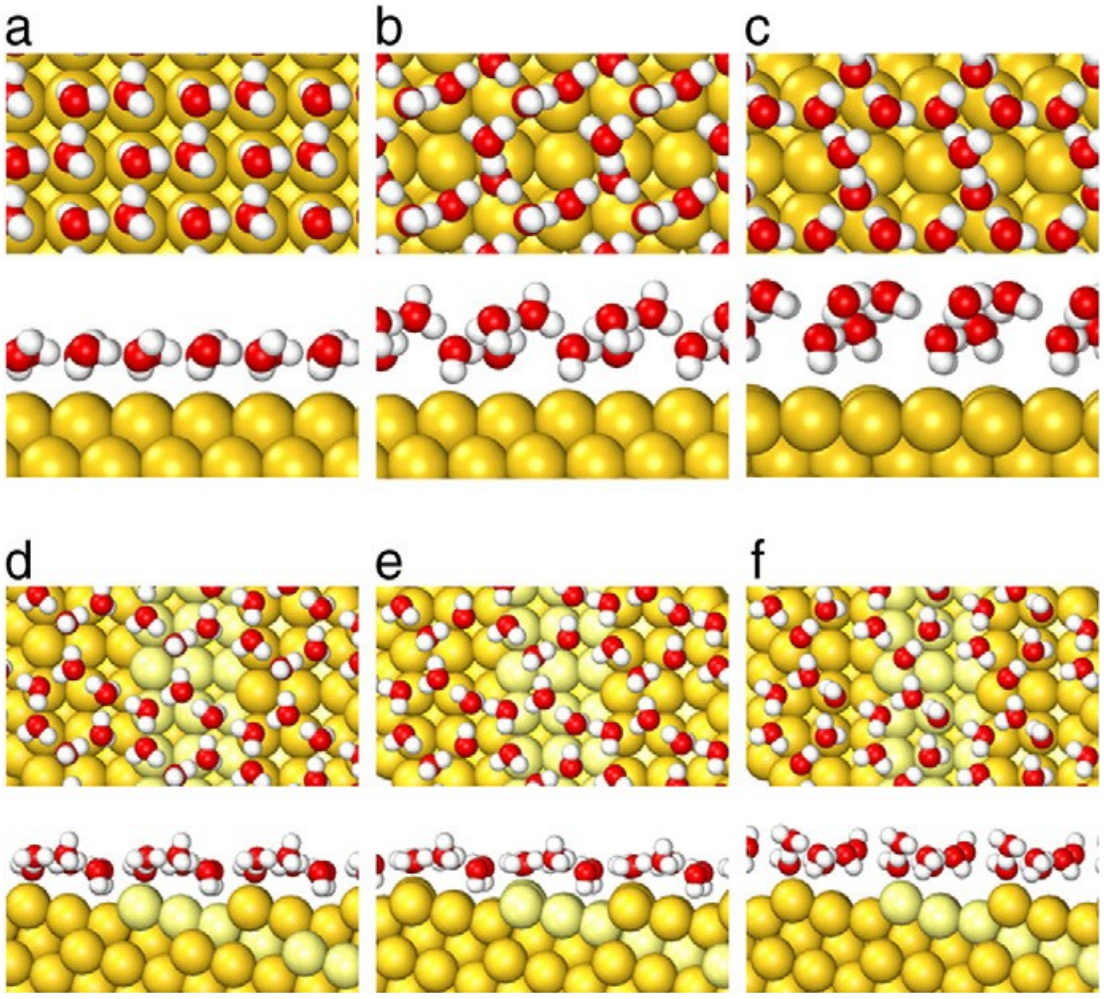


Fig. 5.3.2. Snapshots of the AIMD simulations on Au(100) (a,b,c) and Au(511) (d,e,f) in top and side view. Panels a and d: initial conditions; b and e: t=8 ps, T=140 K; c and f: t=8 ps, T=300 K.

As mentioned above, the oxygen atoms of the water molecules at the upper side of the steps are located much closer to the Au atoms than the oxygen atoms above the terrace sites. This means that the interaction of these water molecules at the terraces with the underlying Au atoms is much weaker. This much weaker binding might then conversely lead to a stronger water–water binding. Thus it is very likely that in total the thermal stability of the water layers at Au(511) is caused by the pinning of the water molecules at the steps together with the weaker metal–water and the stronger water–water interaction above the terraces.

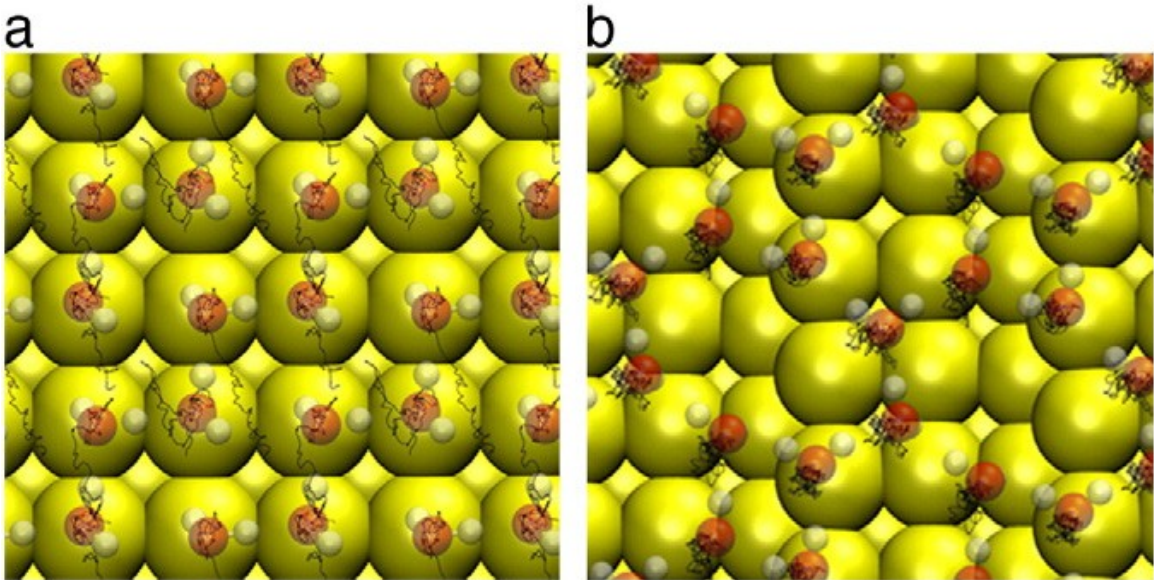


Fig. 5.3.3. Trajectories of the oxygen atoms of the water molecules indicated by the dark lines derived from the AIMD simulations at 140 K on Au(100) (a) and Au(511) (b).

Since snapshots can sometimes be deceiving, in Fig. 5.3.3 we have plotted the trajectories of the oxygen atoms of the water molecules along the AIMD runs at 140 K on Au(100) and Au(511). On Au(100), the trajectory shows that the water molecules leave the initial position and wander around, which means the water reconstruction and desorption has already started at 140K. The trajectories confirm the picture already derived from Fig. 5.3.2 : on Au(100), there is a substantial restructuring of the water layer. This shows a weak interaction between the water layer and the surfaces and also the instability of the water structures on flat gold surface, which indicates a liquid-like properties near the gold flat surfaces.

In contrast, on Au(511) the water molecules are rather stationary, in particular those at the step edge. It is clear that the water molecules vibrate around the equilibrium position. It shows a rather high stability of water structure at 140K and indicates a crystal-like properties near the gold stepped surfaces.

Using the Fourier transform of the velocity auto-correlation function, we derived the vibrational spectrum of the water layers on Au(100) and Au(511) in order to allow for a direct comparison with the experiment [5.5]. In order to reduce the dependence of the calculated spectra from the initial conditions, the results shown in Fig. 5.3.4 have been averaged over five different configurations after the thermalization of the water layer was completed.

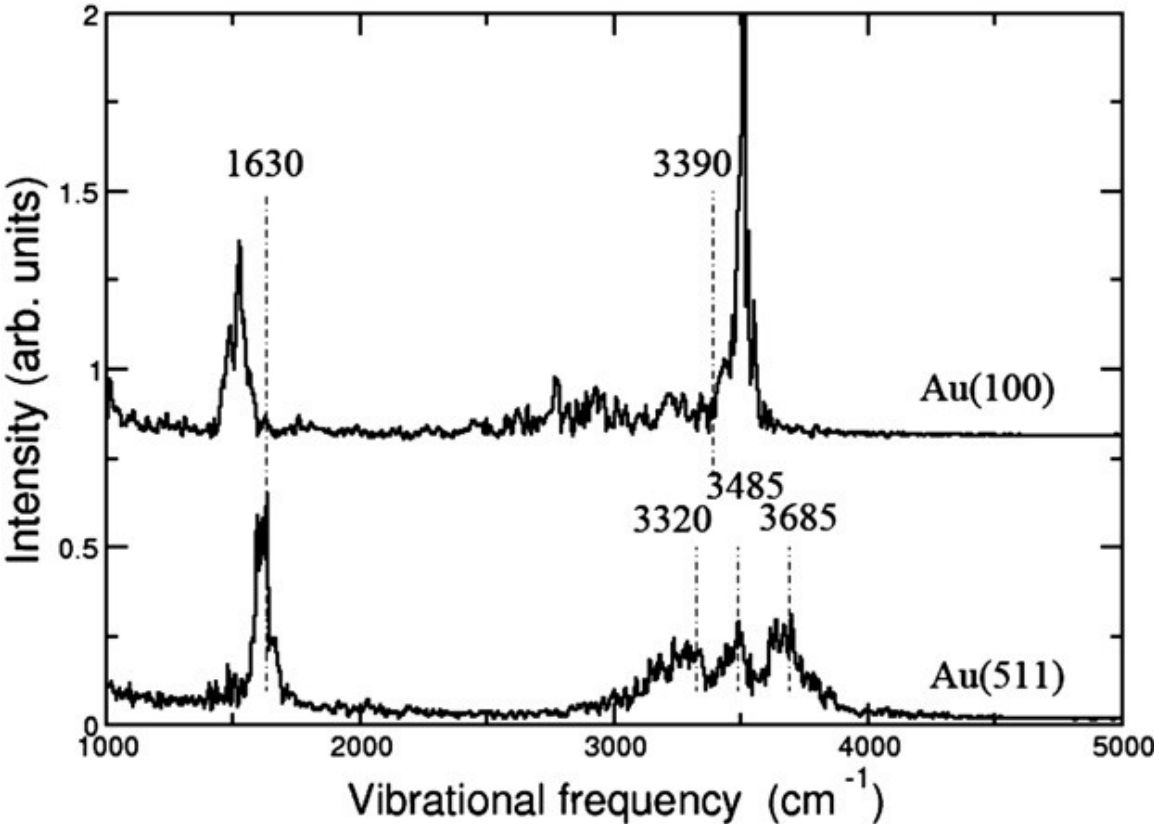


Fig. 5.3.4. Calculated vibrational spectra of the water layer on Au(100) and Au(511) derived from the Fourier transform of the velocity auto-correlation function. Experimentally observed modes [5.5] are indicated by dashed lines.

One of the prominent features observed in the experiments is a hydrogen scissor mode at 1630 cm^{-1} on both Au(100) and Au(511). In the O-H stretch regime, on Au(100) there is a single mode at 3390 cm^{-1}, whereas three modes have been identified on Au(511), two stretching modes at 3320 cm^{-1} and 3485 cm^{-1} which have been attributed to H-bonded (HB) hydrogen, and a stretching mode at 3685 cm^{-1} associated with non-H-bonded (NHB) hydrogen [5.5]. These modes are indicated as dashed lines in Fig. 5.3.4.

On Au(100), we find two sharp features in the calculated vibrational spectrum at about 1600 cm^{-1} and 3500 cm^{-1} which are related to the hydrogen scissor mode and O-H stretching mode, respectively. Interestingly enough, in spite of the rather open structure of the water layer (see Fig. 5.3.2b) with hydrogen atoms being non-bonded and bonded both to Au and to oxygen atoms, there is only one distinct peak in the O-H stretch region. The frequencies of the non-H-bonded hydrogen atoms might be red-shifted, as already suggested to explain the experimental results with only one peak in the O-H stretching region [5.5]. Note that AIMD simulations of water on Au(111) performed at 300 K yield similar results as those obtained here for Au(100), namely one hydrogen scissor mode at about 1600 cm^{-1} and also only one broad peak centered around about 3500 cm^{-1} [5.6].

Although DFT-derived vibrational frequencies often exhibit discrepancies compared to the experiment [5.47], the fact that both a red-shift and a blue-shift are obtained indicates that water on Au(100) might be not an appropriate model to describe water on reconstructed Au(100) (according to the experiment results, mostly like Au(111) surfaces).

For Au(511), on the other hand, there is a rather good agreement between measured and calculated water vibrational frequencies. This agreement might to a certain degree be fortuitous. Furthermore, it should be noted that the height of the peaks do not agree with the experiment which is not surprising considering the fact that we have not included the dipole selection rules in the simulation of the vibrational spectra. Still, the fact that the hydrogen scissor mode as well as the three-fold splitting of the O-H stretch mode is qualitatively and quantitatively reproduced indicates that the structural model for the water layer on Au(511) illustrated in Fig. 5.3.1b should be correct.

5.3.3. Electronic properties

In order to obtain a deeper understanding of the properties of water layers on Au(100) and Au(511) we have also analyzed their electronic structure. In Fig. 5.3.5, the d-band local density of states (LDOS) is plotted for a Au atom in the uppermost layer of Au(100) and Au (511) in the absence and the presence of a water layer where the energy minimum structures of water depicted in Fig. 5.3.2a and d have been used. Note that on clean Au(511) and in the presence of water there are inequivalent surface atoms. In order to keep Fig. 5.3.5 clearly laid out, we have selected one specific surface atom for both Au(100) and Au(511), namely one located below a hydrogen atom, however, the findings for the other surface atoms are rather similar. Fig. 5.3.5 in fact confirms what has already been found in the case of water layers on Pt(111) [1.6, 1.28]. Because of the relatively weak interaction between water molecules and metal atoms, the LDOS of the metal surface is hardly influenced by the presence of water.

In spite of the small change in the LDOS of the metal substrate, there is still a significant polarization of the water molecules upon the adsorption of the water layer [1.6]. This is illustrated in Fig. 5.3.6 where isosurfaces of the charge density differences

upon water adsorption on Au(100) and Au(511) are plotted. On Au(100), there is a particular strong charge accumulation of electron density below the water molecule being oriented parallel to the surface and bound via the oxygen atom to the Au atom whereas there is a considerable charge depletion below the H-down water molecule (Fig. 5.3.6c). On Au(511), the charge rearrangement is mainly localized at the step edge, however, qualitatively a similar pattern of charge depletion and accumulation as on Au(100) arises (Fig. 5.3.6d). This charge rearrangement also contributes to the water-induced work function change.

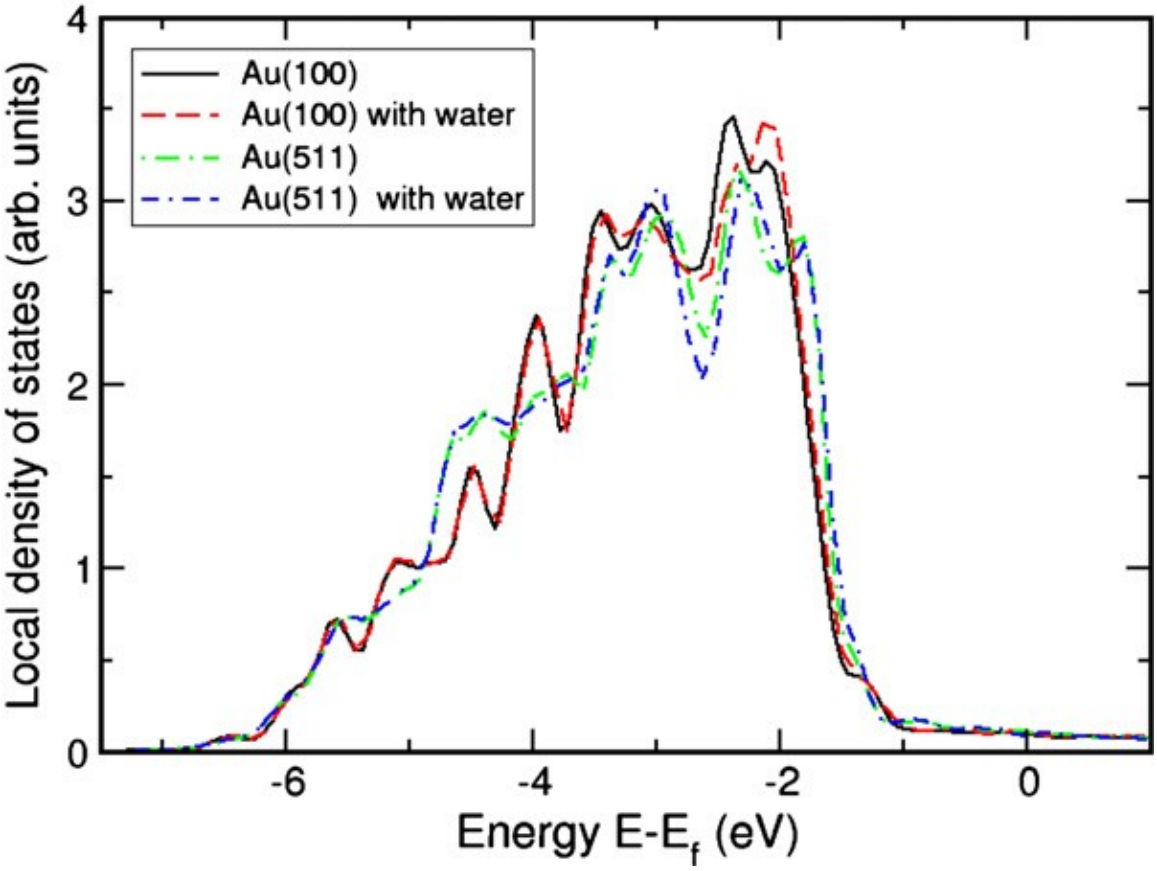


Fig. 5.3.5. Local density of states (LDOS) of the d-states of a Au atom in the uppermost layer of Au(100) and Au(511) in the absence and the presence of a water layer in the energy minimum structures.

In Table 5.3.2, the work function of clean and water-covered Au(100) and Au(511) is listed together with the water-induced work function change $\Delta\Phi$ which corresponds to the difference of these two values. Experimentally, for Au(100) a work function of 5.22 ± 0.04 eV was measured [5.48]; our calculated value of 5.022 eV compares reasonably well with the experiment. However, the calculated water induced work function changes of -0.093 eV and -0.057 eV for Au(100) and Au(511), respectively, seem at first sight to be surprisingly small considering the large polarization of the

water layers just discussed. In order to understand this result one has to take into account that both water layers correspond to H-down layers, i.e. the water molecules not oriented parallel to the surface bind with their hydrogen atoms to the surface. In the water layer on Au(511), there is also one H-up water molecule but two H-down water molecules per unit cell. H-down water layers have an intrinsic dipole moment that would increase the work function [5.6]. The fact that we find slight work function decreases upon the water adsorption indicates that the intrinsic water dipole moment is over compensated by the strong polarization of the water layers illustrated in Fig. 5.3.6. Similar results have been found for water layers adsorbed on strongly interacting hexagonal substrates such as Ru(0001) [5.6].

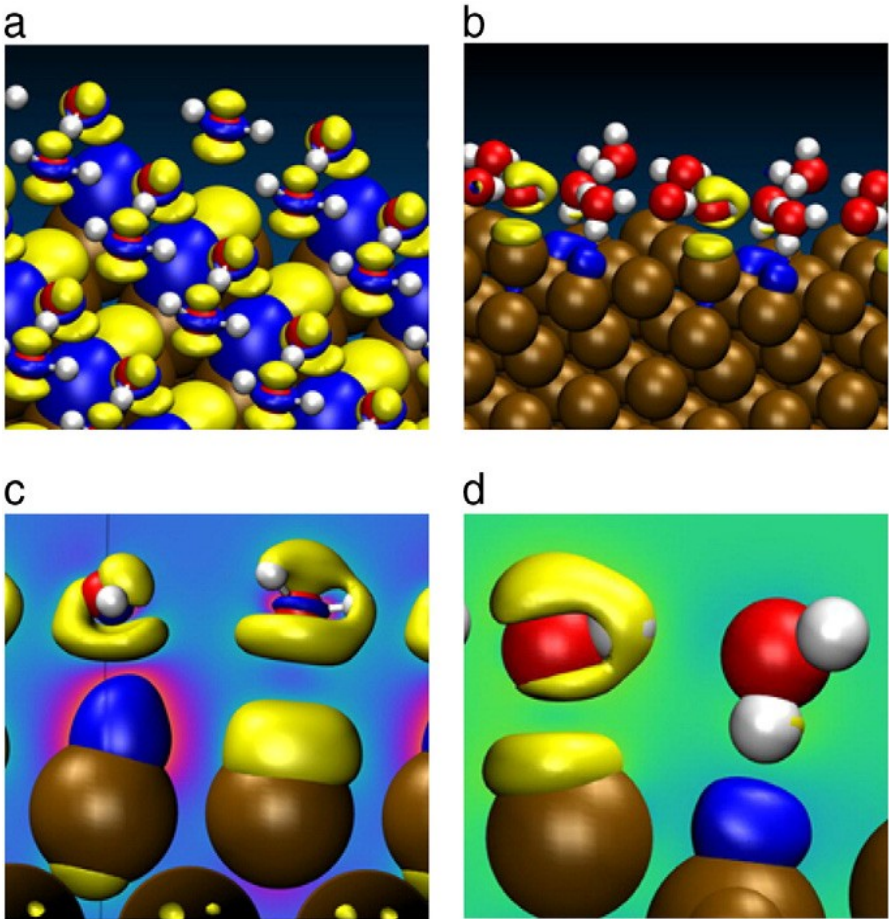


Fig. 6. Isosurface plots of charge density differences upon water adsorption on Au(100) (panels a and c, value 0.004 e/Å^3) and Au(511) (panels b and d, value 0.009 e/Å^3). Charge accumulation, i.e. accumulation of electron density, is plotted in yellow, charge depletion in blue. In contrast to the previous figures, the Au atoms are colored in brown. Panels c and d show a close-up of the regions with the largest charge rearrangement. (For interpretation of the references to color in this figure legend, the reader is referred to the web version of this article.)

At stepped Au and Ag surfaces, a reduced Helmholtz capacitance has been found compared to the corresponding flat surfaces [5.13]. It has been speculated that this reduction is due to a lower polarizability of the water molecules at the steps [5.13]. Now we have not performed any calculations for varying external electric fields or electrode potentials which is beyond the scope of the present paper; hence we cannot directly derive any facts with respect to the polarizability of the water layers. Still it is interesting to note that according to Fig. 5.3.6b on Au(511) the water layers are only polarized close to the steps. The water molecules above the terraces hardly show any polarization which can be related to the fact that their position is further away from the metal atoms so that they are only weakly interacting with the substrate. On unreconstructed Au(100), on the other hand, all water molecules in the first water layer are strongly polarized (see Fig. 5.3.6a).

It is now tempting to assume that the polarizability of the water molecules is related to the strength of their interaction with the metal substrate. Hence it might well be that not the water molecules at the steps exhibit the smaller polarizability but rather the water molecules above the terraces which are located further away from the metal atoms. A definite statement, however, can only be made after the polarizability of the water molecules has been explicitly determined.

Table 5.3.2

Work function in eV of clean and water-covered Au(100) and Au(511) and water induced work function change ΔΦ.

Surface	Φ(Au)	Φ(H2O/Au)	ΔΦ
Au(100)	5.022	4.929	−0.093
Au(511)	5.041	4.984	−0.057

5.4 Single water layer on Ag surfaces

After the successfully investigated water structures on Au(100) and Au(511) surface, Ibach focussed on the similar metal silver [5.49] which also exhibits the peculiar reduction of the Helmholtz capacitance by Beltramo [5.50]. From our DFT simulation, we found that only the water molecule above the step edge directly bonds to Au(511) surface, while water molecules above terraces are located at an relatively large distance to the surface atoms. In other words, they are not bonded directly to the surface atoms, which might be an explanation for the low capacitance [5.51]. Because of the similar lattice constant and surface properties, we could expect that the water structure on Ag(511) should be similar to the one on Au(511). However, these two surfaces also have characteristic differences which might cause different water structures. That's what we are interested in.

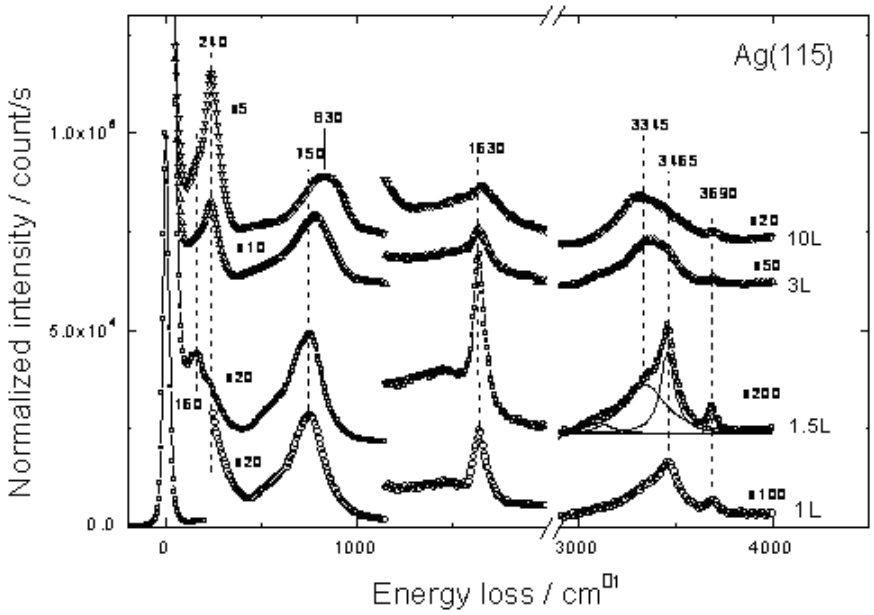


Fig.5.4.1 Spectra of water adsorbed on Ag(115) for 1L, 1.5L, 3L, and 10L exposure are displayed as circles, squares, up-triangles and down-triangles, respectively. The decomposition of the OH-stretching regime into 4 modes is shown for 1.5L by the solid lines

The experiments were performed in an ultra-high vacuum chamber (below 1×10^{-11} mbar) using thecylindrical mirror Auger-spectrometer, low energy electron diffraction (LEED) and an electron energy loss spectrometer (EELS) [5.52-5.54]. The stepped surface was first sputtered to clean the layer that was damaged by the polishing procedure, then heated to 1100K and then annealed. At last the surface was checked through measuring the LEED patterns.

Water layers were deposited with the sample placed near the water vapor inlet with the sample kept at about 130K. Note that 1×10^{-6} mbars correspond to 1L (1L = 1 Langmuir, originally defined as 1×10^{-6}Torrs). As the density of water molecules in a single layer is about $5\times10^{14}cm^{-2}$, in the experiment about 1.5L yields a surface coverage equivalent to a single water layer [5.49].

Fig. 5.4.1 shows us the main results of spectra of water adsorbed on Ag(511). Note that the spectrum of 1.5L also shows 4 peaks, a hydrogen scissor mode at 1630 cm^{-1} , two stretching modes at 3345 cm^{-1} and 3465 cm^{-1} which have been attributed to H-bonded (HB) hydrogen, and a stretching mode at 3690 cm^{-1} associated with non-H-bonded (NHB) hydrogen. This result is almost the same as on Au(511), where the four modes are at 1630 cm^{-1} , 3320 cm^{-1} , 3485 cm^{-1} and 3685 cm^{-1} . This result confirms that the water structure on Ag(511) should also be similar to the one on Au(511).

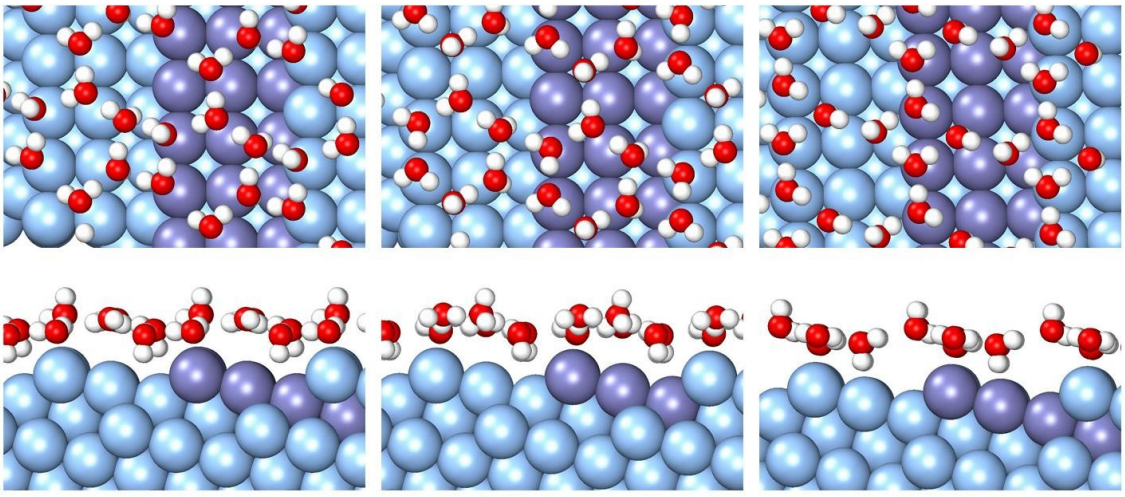


Fig. 5.4. 2 Top and side view of the relaxed water structure on Ag(511) surface.

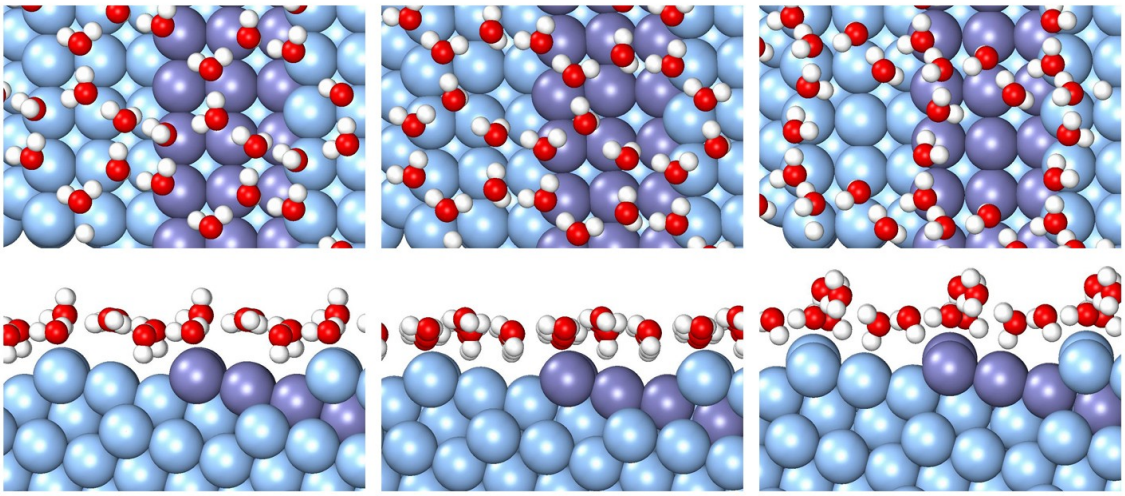
The first step of the DFT investigation is still to determine the most stable water structure on Ag(511). Several different initial structures were calculated in 1x2 and 1x3 supercells. The most stable structure is shown in Fig.5.4.2, which different initial structures assumed automatically after optimization.

As the first step, still, the water structure on Ag(511) is determined. Several different structures are tried in both 1 x 2 and 1 x 3 supercell including the same struture as the most stable water structure on Au(511) surface. Fig. 5. 4.2 shows the structures that all initial structures change automatically to after relaxzation. Fig. 5.4.2 a and b correspond to a 1 x 3 periodicity and fig.5.4.3 c is in a 1 x 2 supercell. The water coverage rate is the same as on Au(511), which is with six in 1 x 3 periodicity and four in 1 x 2 periodicity. The most stable structure is shown in Fig. 5.4.2 a, but Fig. 5.4.2 b has quite similar adsortion energy (table 5.4.1).

Table. 5.4.1
Water adsorption energies in eV per H_2O molecule on Ag(511) for the structures illustrated in Fig. 5.4.2.

Structure	Ag(511)a	Ag(511)b	Ag(511)c
Eads (eV/H_2O mol.)	-0.43	-0.42	-0.30

Since the lattice contant of Ag is rather similar to the one of Au, it is no surprise that the most stable structure on Ag(511) is almost the same as Au(511), which is formed by a hexagon located on the (100)-like terraces connected with other hexagons by rectangles and octagons. Although the water layer is not as flat as on Au(511), the structure which has two H-down water adsorbed at lower site of step edge make the whole water layer rather flat and smooth. The average distance between the O and the underlying metal atoms are 3.8Å , 3.86 Å and 2.96 Å corresponding to the water molecules adsorbed on the lower site of step edge, terrace and higher site of step edge, respectively. Interestingly enough, the O-O distance between water molecules above the terrace is 3.03 Å, whereas it reduces to 2.85 Å across the step edge. The relatively weak interaction between water molecules in the same terrace is the most significant difference between the structures on Ag(511) and Au(511). It indicates a stronger interaction between the water molecule and upper site of the step edge that one of the water molecule above the the upper site of step edge is about 0.5 Å closer than the one on Au(511), which can be seen clearly in Fig. 5.4.2 a. The water structure within the 1 x 2 supercell is formed by a rectangles and octagon located across the step edge, there is one water molecule above every surface atom at the upper site of the step edge, which also indicates the relatively strong water-metal interaction at the step edge. But this structure is relatively unstable, as it has a rather low adsoption energy.



a) 0K b) 140K c) 300K

Fig. 5.4.3 Snapshots of the AIMD simulations on Ag(511) in top and side view at different temperature. Panels a : initial conditions; b : t=8 ps, T=140 K; c: t=8 s, T=300 K.

The snapshots of AIMD results after 8ps at both 140K and 300K are shown in Fig.5.4.3. At 140K, the water structure hardly changed compared to the initial configuration, it exhibits a rather good stability, just like we observed on Au(511). But interestingly enough, the water structure totally dissolves, and note that some water molecule start to escape from the surface, a more open water structure forms. This indicates that the desorption of water has already started at 300K.

We are rather interested in the different stability of water structures on Au(511) and Ag(511). From the DFT calculation, we get the adsorption energy of a single water molecule on Ag(511) adsorbing on the upper site of the step edge, which is -1.40 eV. It is much larger than the one on Ag(111) (-0.56 eV). The water at the step edge strongly interact with the substrate, which make the water molecules located at a unfavorable position to form a Hydrogen bond, in other words, the water -water interaction is weaker. This weaker water-water interaction lead to the breakdown of the water structure, and water used to adsorb at the terrace move around and start to desorb,

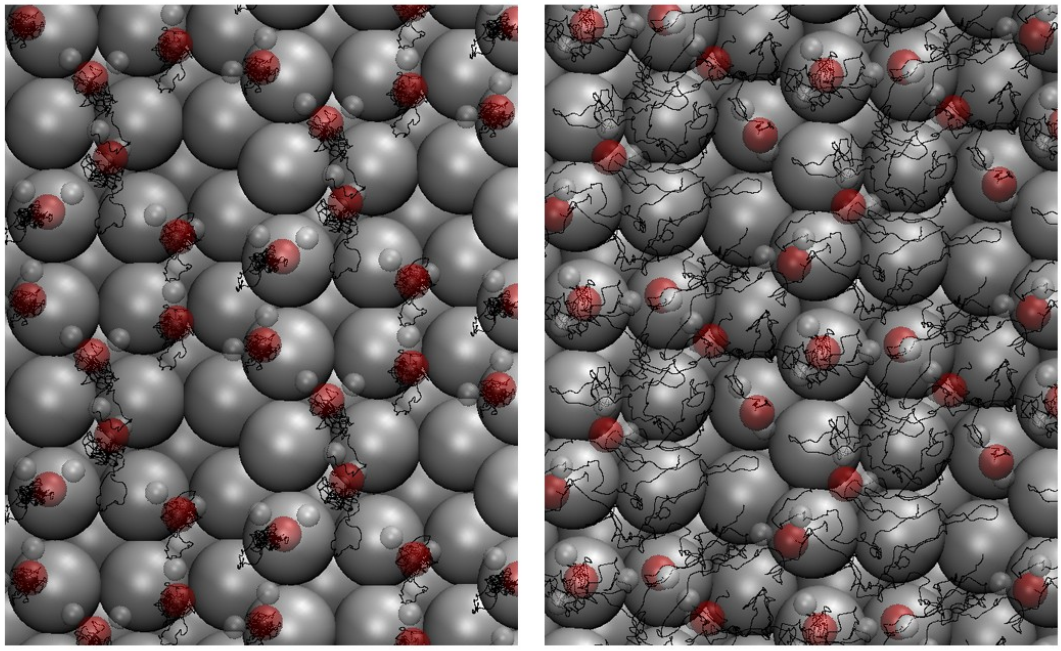


Fig. 5.4.4. Trajectories of the oxygen atoms of the water molecules indicated by the dark lines derived from the AIMD simulations on Ag(511) surface at 140 K (a) and 300K (b).

The trajectories at 140K and 300K shown in Fig.5.3.4 are even more illustrative. The water molecules, in particular, water at the step edge, are rather stationary at 140K, but still the vibration of other water molecules are stronger than on Au(511). Some water molecule even left the equilibrium position, though it went back finally, this point is what we can not get from the snapshot. It indicates the onset of the break up of this structure. The trajectory confirm the picture already derived fromFig. 5.3.3, at 300K the water structure totally dissolves, water molecules go everywhere and start to desorb from the surface.

Fig. 5.3.5 shows us the vibrational spectra of water layer on Ag(511) at 140K using the Fourier transform of the velocity auto-correlation function, so that we could compare with the experimental data directly. The spectra has already been averaged over five different initial configuration in order to reducer the dependence from a single initial structure.

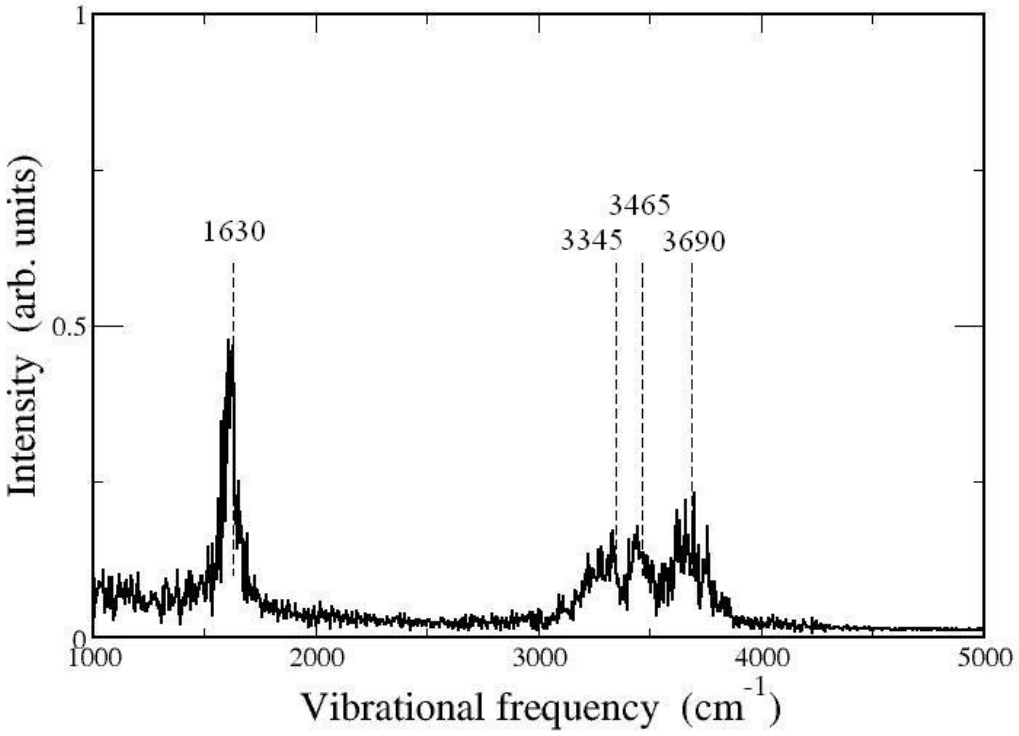


Fig. 5.4.5. Calculated vibrational spectra of the water layer on Ag(511) at 140 K derived from the Fourier transform of the velocity auto-correlation function. Experimentally observed modes [5.49] are indicated by dashed lines.

On Ag(511), four peaks were found in the calculated vibrational spectrum at 1630 cm^{-1} , 3345 cm^{-1} , 3465 cm^{-1} and 3690 cm^{-1} . The four features were related to the experimentally observed mode separately: a hydrogen scissor mode, two stretching modes which are attributed to H-bonded hydrogen and a stretching mode associated with non-H-bonded hydrogen. It also shows a rather good agreement between experimental and calculated water vibrational sprectra, which is rather similar to the one on Au(511). Although the height of the peaks do not agree with the observed data because dipole selection rules were not considered in the simulation, the agreement of both Au(511) and Ag(511) indicate that the structure shown in fig. 5.3.2 a is correct. The structural model is quite stable on Au(511) and Ag(511), and shows a crystal-like properties at 140K.

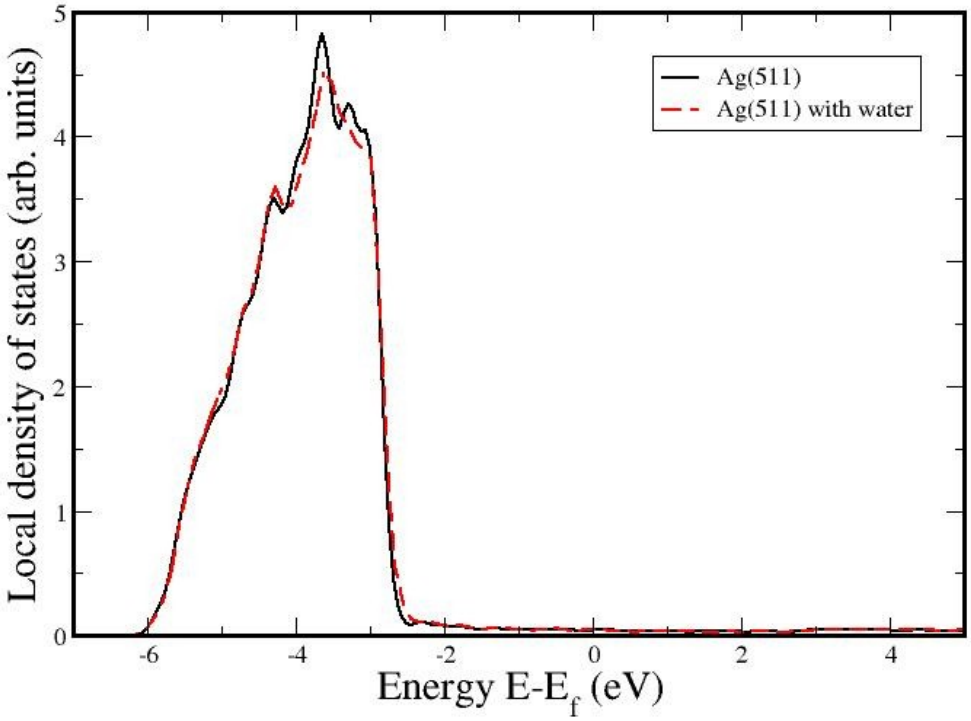


Fig. 5.4.6 Local density of states (LDOS) of the d-states of a Ag atom at the upper step edge on Au(511) surface in the absence and the presence of a water layer in the minimum structures.

The Local d-states density of state of one Ag atom at the upper step edge in the presence of a water molecule is compared with the Ag atom located in the same position on a clean substrate surface in Fig. 5.4.6. As we expect, the relatively weak physical adsorption of water molecules hardly influence the LDOS of the metal surfaces.

Comparing with water layer on Au(511), the charge density difference shows similar results: Since the water molecule above the terrace is relatively far away from the substrate, the water molecule and the terrace hardly polarize, which also indicates the weak interaction between these two. On the other hand, the water layer at the upper site of the step edge polarized even stronger than on Au(511), showing a strong interaction between them. Compared with the charge density difference of clean Au(511), the charge strongly polarized at the upper site of the stepped edge.

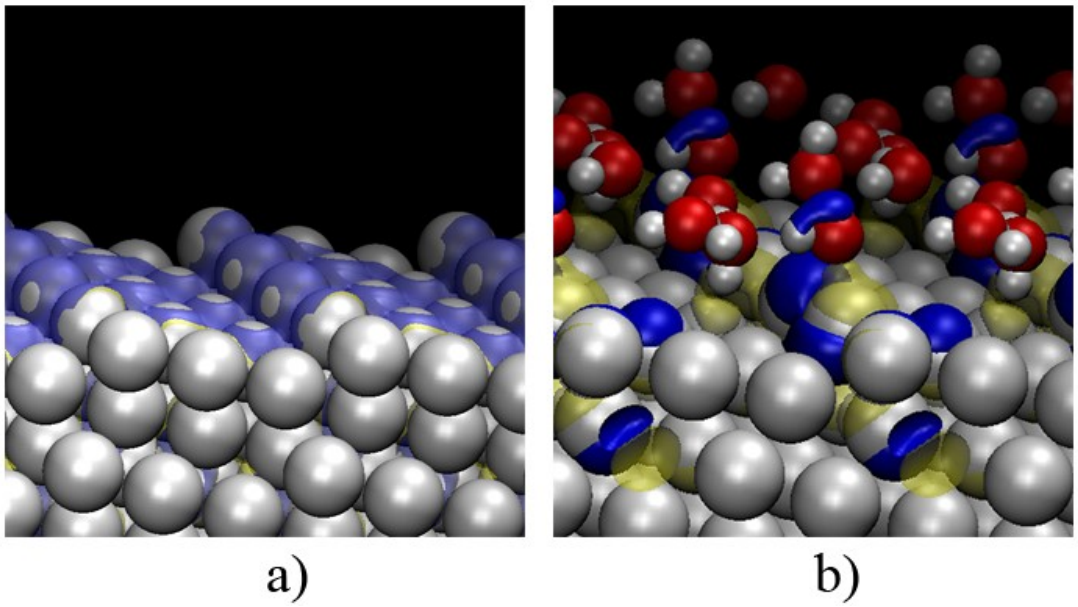


Fig. 5.4.7 Isosurface plots of charge density differences upon clean Ag(511) surface(panel a, value 0.01 e/Å3) and water adsorption on Ag(511) (panels b, value 0.01 e/Å3). Charge accumulation, i.e. accumulation of electron density, is plotted in blue, charge depletion in yellow. In contrast to the previous figures, the Ag atoms are colored in grey.

5.5 Water layers on flat Pb surfaces

For lead surfaces, the situation is a little bit different compared with silver and gold. There are only few experiments addressing this metal, in particular with respect to the liquid solid interface. So there is little information about the water structures on Pb surfaces, especially at stepped surfaces. As we have already determined the structures on Au and Ag surfaces, it seems to be a good idea to use the trends of the water layers on stepped surfaces derived from the results of gold and silver, then assume similar structures, like we have done on silver surfaces. And this is what we tried first, but then we found it impossible. The lattice constant of Pb is 5.02Å , which is 20% larger than those of Ag (4.17Å) and Au (4.16 Å), note that there is hardly any difference between Au and Ag. The results of this part will illustrate the water structure difference caused by the larger lattice constant.

It is really hard work to derive the water structure at the stepped surfaces, even if we decide to get the structures by putting the water molecules one by one onto the surfaces. As the stepped surfaces (n11) can be seen as a combination of (111) and (100), we decided to obtain the water structures on flat Pb surfaces in order to get a general idea for stepped surfaces.

Generally speaking, the ice-like hexagonal water structure is considered as the normal structure on the metal (111) surfaces at low temperature[5.6, 5.55, 5.56]. On some metal which have stronger water- metal interaction like Pt (111), this structure is stable even at room temperature [5.6]. So the ice-like layer was chosen as the initial water structure on the Pb (111) surface. We tried H-up, H-down structures and the H-up/H-down mixture structures. After the relaxation, whatever the starting structure is, the optimized water structure changed into the H-down one automatically. Obviously, the H-down structure is more favorable.

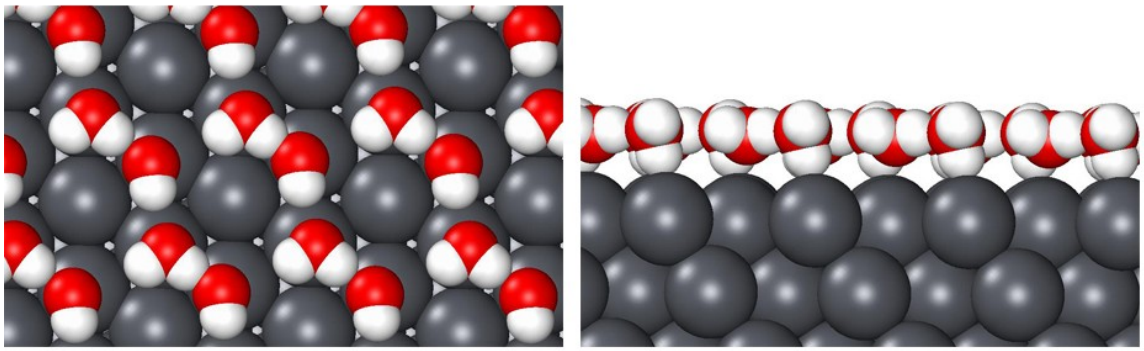


Figure 5.5.1 Top and side view of the relaxed ice-like water structure on Pb(111). The Pb ,O and H are colored by grey, red and white.

Figure 5.5.1 shows us the most stable ice-like water structure on Pb(111) after relaxation. The water layer is formed by hexagons. There are two kinds of water molecules, one bounds to two other water molecule through an H-bond, the other has a hydrogen atom pointing down towards the metal surface. All of the water molecules adsorb at the top side of the Pb atoms, as is also true for single water molecules adsorbed on the other metal surfaces.

From the side view figure, we note that the water layer is rather flat, which is a basic requirement to determine weather it is a complete water layer. The distance between the oxygen and metal surface is about 3.7Å . The distances between oxygen atoms are not all the same. The shortest one is about 3.01Å, and the average distance is 3.5Å. The angle of O-H-O is almost 180 degree. Generally speaking, the bonding distance of H-bond is 2.0Å to 3.8Å, and the angle of O-H-O should be between 120º and 180º. The larger the angle is and the shorter the H-bond is, the stronger the H-bond is.[5.10] Hence, the water layer on Pb(111) form a rather weak H-bond. The reason will be discussed later.

When we checked the adsorption energy of the water layer, we obtained as surprisingly low value at only -0.25 eV/water molecule. It is a very small value which is only almost one half of the water layer adsorption energy on Ag(111). We will show that the reason of this small value is not any weak interaction between lead and water molecule. According to the results for single water molecules adsorbed on Ag(111) and Pb(111), the value is almost the same. And the distance between the O atom and the surface is also in the usual range compared with Ag and Au surfaces.

The adsorption energy per water molecule is calculated by the formula

$$E = (E_{tot} - nE_{substrate} - NE_{H_2O})/N \qquad (5.5.1)$$

where E_{tot} is the total energy of our system, $E_{substrate}$ is the energy of the substrate per unit cell, n is the number of metal atoms in unit cell which formed the supercell, N is the number of water molecule in the supercell, E_{H2O} is -14.22eV.

From this formula, it is not difficult to understand that this adsorption energy is not “pure” adsorption energy but includs the water-water interaction. To determine the “pure” water metal interaction, the isolated water layer with the same geometry of the metal water system should be calculated (table 5.5.1). This E_{H2O} layer energy is obtained by the following formula

$$E_{H_2O\,layer} = (E_{isolated\ water\ layer} - NE_{H_2O})/N \qquad (5.5.2)$$

The physical meaning of $E_{H2O\ layer}$ is the strength of water-water interaction (H-bond) per water molecule.

As shown in tab. 5.5.1, the difference between the adsorption energy on Pb(111) and Ag(111) is about 0.196 eV, it is almost the same as the energy difference from the hydrogen bonding within the water layer on these two metal surfaces (0.174 eV), which means that the interactions between water molecules and the Pb/Ag surfaces are almost

the same, the difference is only about 0.02 eV. This result indicates that the low adsorption energy on Pb(111) is mainly caused by the weak interaction between the water molecules. As mentioned above, water molecule prefer to adsorb at the top of the metal surface atom. The lattice constant of Pb is 20% larger than for Ag and Au. This causes the distance between the water molecules to be larger, in other words, it will make the hydrogen bond between water molecules weaker.

Table 5.5.1 The difference between adsorption energy on Pb(111) and Ag(111) compared with the energy difference for the isolated water layers

	Eads/H2O(eV)	Ewater-water(eV)	Lattice constant(Å)
Pb(111)	-0.254	-0.221	4.95
Ag(111)	-0.450	-0.395	4.09
Diff	0.196	0.174	21%

Because of the large lattice constant, it is likely that the most stable water structure on Pb is different compared to the one on Au/Ag surfaces. Hence we regarded water structures with a higher coverage.

Unfortunately, it seems that there are only few studies about the (100) surfaces. According to these studies, most of them agree that the water structure should be formed by rectangles, which means that there is a water molecules adsorbed on top of every surface metal atoms. Compared with our results, the top site is always the most favorable site on Pb surfaces. So this rectangle structure guess is reasonable. Hence, we have started with this structure on Pb(100) (fig.5.5.2).

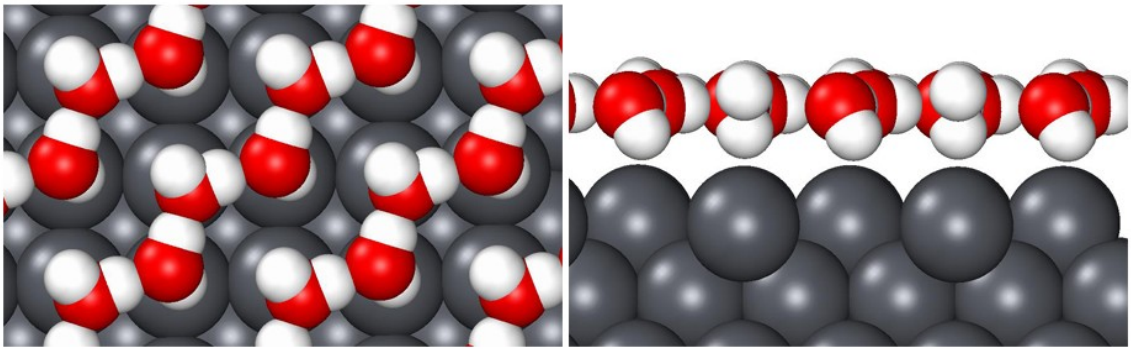


Fig. 5.5.2 Top (a) and side view (b) of the water structure on Pb(100) with 100% coverage.

According to our calculations, the water structure on Pb(100) does not form rectangles like on Cu(100) [4.4] or on Au(100). The water molecules accumulate and

form parallel zigzag water chain. There are two kinds of water molecule in the chain, a H-up and a H-down water molecule. The average distance between two neighboring oxygen is 2.75Å . There is no hydrogen pointing towards the water in other chain. The nearest O-O distance between two neighboring water chain is 4.38Å , which is much too large for a H-bond. Hence, there is no H-bond formed between the water chain. This structure can also be explained by the large lattice constant of Pb.

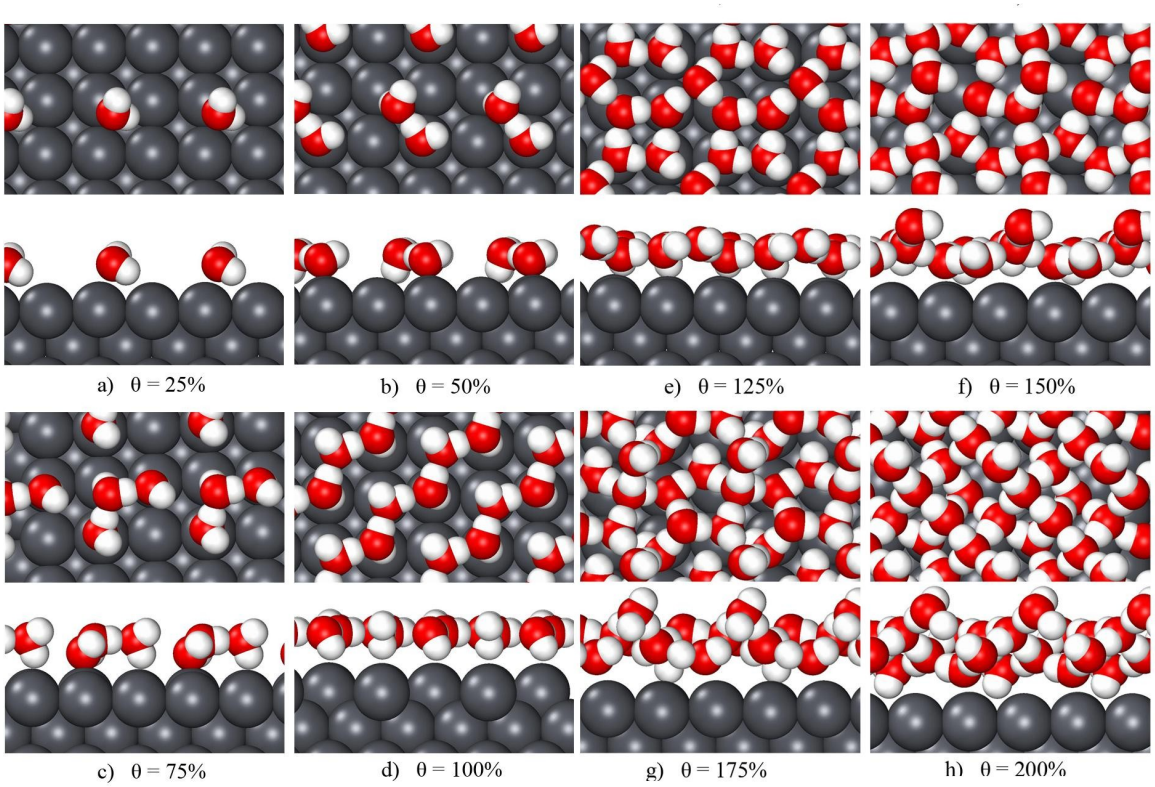


Fig. 5.5.3 Top (up-site figures) and side views (down-site figures) of the water structures on Pb(100) with different coverage

Note that, it is really hard to unambiguously define a complete water single layer. Both the water-metal and water-water interaction exist, and the values of these two contributions are in the same order of magnitude. More importantly, these two parts are not independent. Generally speaking, the stronger one part is, the weaker the other one is. To determine a complete water layer, in particular, to compare two water layers with different coverage, the adsorption energy can not be considered as the only standard, but only as a reference point. More water molecules will form more H-bonds. Hence, it is also rather important to have a look at the water structures, like whether the layer is still flat, or what is the distance between two water molecules.

Using a 2x2 supercell, water structures with different water coverage are calculated, from 25% to 200%.The definition of the water coverage is the number of water molecules divided by the number of the metal atoms in the first layer. So the

water layer we showed in fig. 5.5.2 corresponds to 100% coverage. Figure 5.5.3 shows us the most stable one for every water coverage.

A single water molecule adsorbs at the top site of the surface atom, as I mentioned earlier. The second water molecule adsorbs at the hollow site. Although the top site is the most favorable site of water adsorption, the distance between two top sites is too large to form a H-bond. So these two water molecules favor the balance of the water-water and water-metal interaction – to adsorb at the second most favorable site, hollow site, and form a much stronger H-bond (O-O distance 2.80Å) . The adsorption energy at 50% coverage is 3 times larger than the one at 25% (table 5.5.2). Three water molecules form a triangle structure. The water molecules roughly stay at the top site, but slightly closer than the Pb atoms to form the H-bond. The O-O distance is 2.78 Å, and the angle of these three water molecules is 113 degree.

The 100% coverage water structure has already been analyzed above. Two zigzag water chains without any H-bond bonded with each other are formed in the supercell. Hence we suppose that the 100% coverage water structure still is not the complete single layer on Pb(100), and higher water coverages should be checked. The results justify our guess.

The 125% coverage water layer is formed by hexagons and rectangles. One rectangle is connected by four hexagons. Comparing with the 100% layer, one more water molecule adsorbs at the hollow site between two zigzag chain. From the side view of fig. 5.5.3 e, it is clear that the water layer is rather flat. The average O-O distance is 2.98 Å, the shortest bond is 2.87 Å, and the largest one is 3.23 Å. Obviously, the water-water interaction is much stronger than for the 100% structure.

When the number of water molecules continuously increases, the second water layer starts to form. One water molecule adsorbs at a position much higher than the other, and the whole water layer becomes rough (fig. 5.5.3 f). The water structures with even higher coverage rate show clearly that the second water layer is formed gradually, a complex hydrogen-bonded network of water molecules results. From table 5.5.2, note that the adsorption energy per water molecule increases when the water coverage gets larger. This can be explained by the increasing number of H-bonds, when one more water molecule adsorbs on the surface.

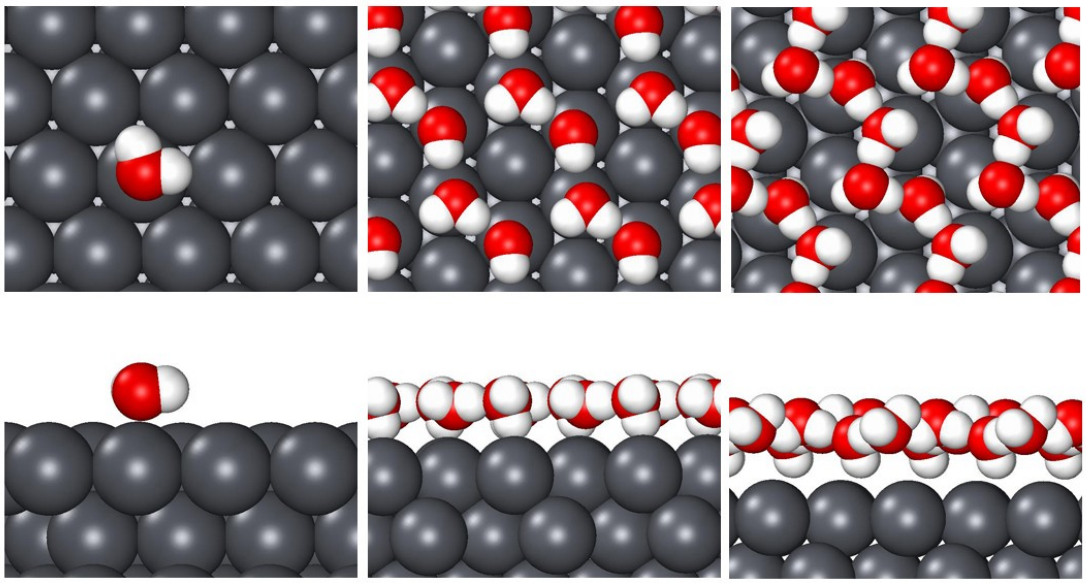


Fig. 5.5.4 Top (up-site figures) and side views (down-site figures) of the water structures on Pb(111) with different coverage

Table 5.5.2 The adsorption energy of water layers as a function of the coverage on Pb(100).

Water coverage	Adsorption energy (eV/ water molecule)
25%	-0.07
50%	-0.22
75%	-0.27
100%	-0.36
125%	-0.40
150%	-0.45
175%	-0.45
200%	-0.5

Furthermore, water layers with different coverages at Pb(111) is also calculated within a $\sqrt{3}\times\sqrt{3}$ supercell. Unlike other metals, for example Ag, Pt or Au, a higher coverage water layer can also form a single water layer on Pb(111) (Fig.5.5.4 c).

Table 5.5.3 The adsorption energy of the water layers with different water coverage on Pb(111) surface.

Water coverage	Adsorption energy (eV/ water molecule)
33%	-0.06
66%	-0.25
100%	-0.37

As mentioned earlier, one single water molecule prefers to adsorb at the top site, and the 66% coverage water molecules as well. The structure for 100% coverage is more interesting. The O atoms are located almost in one plane, and there are three different kinds of water molecules in a supercell, one H-up, one parallel and one H-down water molecule. The water molecules are no longer adsorbed on the top site of the surface, and the distance between O atom and substrate is 0.6 Å larger than for the 66% coverage structure, which indicates that the interaction between water layer and the surface is weaker than for the 66% one. But a much larger adsorption energy (0.12 eV/ water molecule) indicates a stronger water-water interaction (table 5.5.3). Water layers on both Pb(111) and Pb(100) shows rather different structures compared with other metals, hence we estimate the water structures on stepped surface should also be different.

Bibliography

[5.1] R. Guidelli, W. Schmickler, *Electrochim. Acta* **45** 2317 (2000).
[5.2] K. Andersson, A. Nikitin, L. G. M. Pettersson, A. Nilsson, H. Ogasawara, *Phys. Rev. Lett.* **93** 196101 (2004).
[5.3] C. Clay, S. Haq, A. Hodgson, *Chem. Phys. Lett.* **388** 89 (2004).
[5.4] D. N. Denzler, C. Hess, R. Dudek, S. Wagner, C. Frischkorn, M. Wolf, G. Ertl, *Chem. Phys. Lett.* **376** 618 (2003).
[5.5] H. Ibach, *Surf. Sci.* **604** 377 (2010).
[5.6] S. Schnur, A. Gross, *New J. Phys.* **11** 125003 (2009).
[5.7] P. J. Feibelman, *Science* **295** 99 (2002).
[5.8] X. Wu, A. K. Ray, *Phys. Rev. B: Condens. Matter* **65** 085403 (2002).
[5.9] A. Michaelides, K. Morgenstern, *Nat. Mater.* **6** 597 (2007).

[5.10] A. Hodgson, S. Haq, *Surf. Sci. Rep.* **64** 381 (2009).
[5.11] Y. Tiwary, K. A. Fichthorn, *Phys. Rev. B: Condens. Matter* **81** 195421 (2010).
[5.12] J. E. Goose, E. L. First, P. Clancy, *Phys. Rev. B: Condens. Matter* **81** 205310 (2010).
[5.13] G. Beltramo, M. Giesen, H. Ibach, *Electrochim. Acta* **54** 4305 (2009).
[5.14] M. Lischka, A. Gross, *Phys. Rev. B: Condens. Matter* 65 075420 (2002).
[5.15] S. Dahl, A. Logadottir, R. C. Egeberg, J. H. Larsen, I. Chorkendorff, E. Toernqvist Norskov, *Phys. Rev. Lett.* **83** 1814 (1999).
[5.16] A. Gross, *J. Comput. Theor. Nanosci.* **5** 894 (2008).
[5.17] H. Baltruschat, S. Ernst, *ChemPhysChem* **12** 56 (2011).
[5.18] P. A. Thiel, T. E. Madey, *Surf. Sci. Rep.* **7** 211 (1987).
[5.19] M. A. Henderson, *Surf. Sci. Rep*. **46** 1 (2002).
[5.20] M. Ito, M. Yamazaki, *Phys. Chem. Chem. Phys.* **8** 3623 (2006).
[5.21] S. Haq, C. Clay, G. R. Darling, G. Zimbitas, A. Hodgson, *Phys. Rev. B: Condens. Matter* **73** 115414 (2006).
[5.22] X. Wei, B. Miranda, Y. R. Shen, *Phys. Rev. Lett.* **86** 8 (2001).
[5.23] K. Andresson, A. Gomez, C. Glover, D. Nordlund, H. Oestroem, T. Schiros, O. Takahashi, H. Ogasawara, L. G. M. Pettersson, A. Nilsson, *Surf. Sci.* **585** 183 (2005).
[5.24] S. Meng, L. F. Xu, E. G. Wang, S. Gao, *Phys. Rev. Lett*. **89** 176104 (2002).
[5.25] S. Meng, E. G. Wang, S. Gao, *Phys. Rev. B: Condens. Matter* **69** 195404 (2004).
[5.26] A. Roudgar, A. Gross, *Chem. Phys. Lett.* **409** 157 (2005).
[5.27] A. Michaelides, *Appl. Phys. A* **85** 415 (2006).
[5.28] Y. Gohda, S. Schnur, A. Gross, *Faraday Discuss.* **140** 233 (2008).
[5.29] J. Kucera, A. Gross, *Beilstein J., Nanotechnology* **2** 384 (2011).
[5.30] S. Schnur, A. Gross, *Catal. Today* **165** 129 (2011).
[5.31] G. Materzanini, G. F. Tantardini, P. J. D. Lindan, P. Saalfrank, *Phys. Rev. B: Condens. Matter* **71** 155414 (2005).
[5.32] A. Michaelides, A. Alavi, D. A. King, *J. Am. Chem. Soc.* **125** 2746 (2003).
[5.33] A. Roudgar, A. Gross, *Surf. Sci.* **597** 42 (2005).
[5.34] H. Ibach, S. Lehwald, *Surf. Sci.* **91** 187 (1980).
[5.35] G. Kresse, J. Furthmueller, *Phys. Rev. B : Condens. Matter* **54** 11169 (1996).
[5.36] G. Kresse, J. Furthmueller, *Comput. Mater. Sci.* **6** 15 (1996).
[5.37] J. P. Perdew, K. Burke, M. Ernzerhof, *Phys. Rev. Lett.* **77** 3865 (1996).
[5.38] P. Vassilev, C. Hartnig, M. T. M. Koper, F. Frechard, R. A. Van Santen, *J. Chem. Phys.* **115** 9815 (2001).
[5.39] J. Vande Vondele, F. Mohamed, M. Krack, J. Hutter, M. Sprik, M. Parrinello, *J. Chem. Phys.* **122** 014515 (2005).
[5.40] P. Cabrera-Sanfelix, D. Sanchez -Portal, A. Mugarza, T. K. Shimizu, M. Salmeron, A. Arnau, *Phys. Rev. B : Condens. Matter* **76** 205438 (2007).
[5.41] M. Schmitz, P. Tavan, *J. Chem. Phys.* **121** 12247 (2004).
[5.42] B. M. Ocko, D. Gibbs, K. G. Huang, D. M. Zehner, S. G. J. Mochrie, *Phys. Rev. B : Condens. Matter* **44** 6429 (1991).

[5.43] M. Sotto, J. Boulliard, *Surf. Sci.* **214** 97 (1989).
[5.44] A. Ignaczak, J. Gomes, *J. Electroanal. Chem*. **420** 209 (1997).
[5.45] X. Xia, M. L. Berkowitz, *Phys. Rev. Lett.* **74** 3193 (1995).
[5.46] I. -C. Yeh, M. Berkowitz, *J. Electroanal. Chem.* **450** 313 (1998).
[5.47] I. S. Ulusoy, Y. Scribano, D. M. Benoit, A. Tschetschetkin, N. Maurer, B. Koslowski, P. Ziemann, *Phys. Chem. Chem. Phys.* **13** 612 (2011).
[5.48] G. V. Hansson, S. A. Flodstroem, *Phys. Rev. B : Condens. Matter* **18** 1572 (1978).
[5.49] H. Ibach, *Surf. Sci.,* **606**, 19 (2012).
[5.50] G. Beltramo, M. Giesen, H. Ibach, *Electrochim. Acta* **54** 4305 (2009).
[5.51] X. Lin, A. Groß, *Surf. Sci.*, **606**, 886 (2012).
[5.52] H. Ibach, Journal of Electron Spectroscopy and Related Phenomena 64/65, 819 (1993).
[5.53] H. Ibach, M. Balden, S. Lehwald, *J. Chem. Soc., Faraday Trans.* **92**, 4771 (1996)
[5.54] H. Ibach, J. Rajeswari, *J. Electr. Spectros. Rel. Phen.* **185**, 61 (2012).
[5.55] Michaelides A., *Appl. Phys. A* **85**, 415 (2006).
[5.56] Thiel P. A. and Madey T. E., *Surf. Sci. Rep.* **7**, 211 (1987).

Chapter 6
self-diffusion on Pb flat and stepped surfaces

In this chapter, some results have been taken from the pulication which has been published in Electrochim Acta 140, 505-510 (2014).

As I mentioned in the first chapter, the main goal of my investigation is to understand the principle of the quantum switch. The fundamental elementary process occurring in the switch is the deposition of metal atoms from the electrolyte to the metallic electrodes and the formation of a contact. The specific metal structure growing on the electrode upon metal deposition is controlled by diffusion processes. Hence a crucial part in the modeling of the atomic-scale switch is the determination of metal self-diffusion paths and the corresponding diffusion barriers.

As a possible mechanism, a novel switching mechanism has beens uggested that is based on the collective deposition of metal atoms from the electrolyte onto the switch[6.1, 6.2, 6.5]. Still, the exact nature of the collective process was not clarified. Here we report the results of a theoretical effort in order to elucidate elementary steps in the collective switching mechanism on an atomic scale and to develop concepts to describe the corresponding processes.

The fundamental elementary process occurring in the switch is the deposition of metal atoms from the electrolyte onto the metallic electrodes and the formation of a contact. The specific metal structure growing on the electrode upon metal deposition is controlled by diffusion processes [6.6- 6.10]. Hence, a crucial part in the modeling of the atomic-scale switch is the determination of metal self-diffusion paths and the corresponding diffusion barriers[6.11].

As the first step, Monte Carlo simulations [6.12] of the breaking of contacts in a two-dimensional geometry based on simple model potentials have already been done. These simulations provide insights into the statistical nature of the motion of the electrode atoms. In particular, they show how the elementary processes – atoms moving over diffusion barriers – transform into collective many-body processes when the junction is (slowly) closed. These simulations also suggest that exchange processes play an important role in the contact formation at the nanoscale.

In order to check whether exchange processes indeed occur at realistic electrode surfaces, we have then determined metal diffusion paths using total-energy calculations based on density functional theory (DFT). As the specific metal, we have considered lead which has also been used as an electrode material in the quantum conductance switch [6.13]. To the best of our knowledge, diffusion processes on stepped Pb surfaces

have not been addressed yet by DFT calculations, but by a computational study [6.14] based on embedded atom potentials.

Note that the controlled formation of nano-structures at metal surfaces is of critical importance not only for the realization of the electrochemical quantum conductance switch, but also for several further applications at surfaces and interfaces, including heterogeneous[6.15- 6.20] and electro-catalysis [6.21- 6.23], quantum [6.24- 6.27] and magnetic data storage [6.28, 6.29]. However, in spite of the fact that such important diffusion processes have been studied in detail [6.30- 6.32], it is fair to say that the atomic level understanding of these processes, in particular at complex, structured surfaces, is still limited. It is also important to note that the formation of the contact in the switch occurs at the electrochemical solid/liquid interface which adds further complexity to the system [6.33- 6.35].

6.1 single atom adsorbed on Pb surfaces

Barriers for self-diusion of Pb on Pb substrates were calculated due to the importance of diffusion for growth processes. After metal deposition on a surface, the resulting surface structure is determined by the fact whether the deposited atoms propagate further on via diffusion and how facile the diffusion is. Generally speaking, there are two kinds of diffusion mechanisms, the hopping mechanism and the exchange mechanism which are illustrated in Figs.6.1a and b, respectively. The hopping mechanism is typically considered as the usual mode of the diffusion by which atoms move between the adjacent equilibrium sites. It is mainly operative on closed packed metal surfaces. In the exchange mechanism, the adatom displaces a surface atom which then becomes the adatom. It has typically been observed on (100) surfaces such as Pt(100) [6.36] or Ir(100) [6.37]. Whereas in the hopping mechanism the transition state corresponds to the hopping atom in a two-fold coordination, in the exchange mechanism there are two atoms in a three-fold coordination at the transition state on a (100) flat surface. Which mechanism is operative is hence determined by the fact whether one atom in a two-fold situation is more favorable than two atoms in a three-fold configuration. Thus the exchange mechanism is operative at flat metal surfaces that favor a three-fold coordination with the three-valent aluminum being the prototypical example. On stepped surfaces, however, the diffusion across a barrier is hindered by the relatively large Schwoebel-Ehrlich barrier while the exchange mechanism might involve rather high-coordinated congurations.

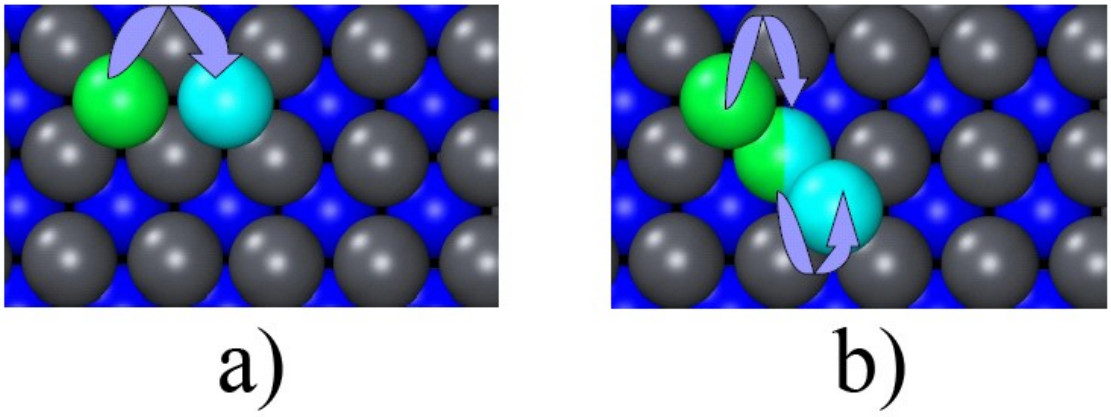


Fig.6.1 illustration of a) hopping diffusion, b) exchange diffusion on a (100) surface. The original and final adatoms are colored by green and light blue.

As the first step to address the diffusion paths, we determined the optimum adsorption position of a Pb adatom on flat and stepped Pb surfaces (see Fig.6.3). For these surfaces, all possible positions ,including the top sites, bridge sites and hollow site located at the upper site of the step edge were considered. The lower ste of the step edge and the terrace (Fig. 6.2), are evaluated to find the initial position of and meta-stable transition poition of the diffusion processes, in particular, for stepped surfaces. For Pb(111) and Pb(100) we find, as expected, that the equilibrium geometry corresponds to the three fold hollow site (Fig.3 a) and the four fold hollow site (Fig.3b), respectively. On Pb(111), the adatom adsorption height is 2.23Å , the distance to the nearest neighbors is 3.13 Å which is 12% shorter than the interatomic distance in the bulk. As for Pb(100), the adatom adsorption height is 1.96Å , and the distance to the nearest neighbors is 3.21 Å which is 9% shorter than the interatomic distance in the bulk. These trends are typical for adsorbed metal atoms and can be explained in terms of the correlation between bond strength and coordination [6.38].

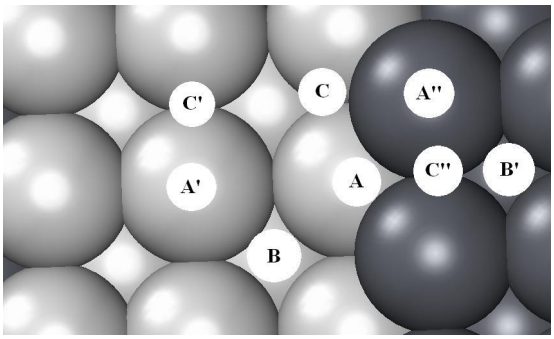


Fig. 6.2 Possible initial and meta-stable transition position that have been simulated at stepped surface, including top sites (A), bridge sites (B) and hollow sites (C)

As all other considered (n11) stepped surfaces with odd n have rather similar properties, the results of diffusion processes are also similar. We focus in the discussion on the Pb(511) surfaces and just report the results for the other stepped surfaces. On Pb(511), the adatom prefers to adsorb at the lower side of the step edge in direct contact with one step atom in an bridge-like site with respect to the atoms of the lower terrace (Fig.3c). Because of this bridge-like conguration, the adsorption height is 3.27 Å with respect to the lower terrace, and the distance between the adatom and the step edge is 3.39Å .

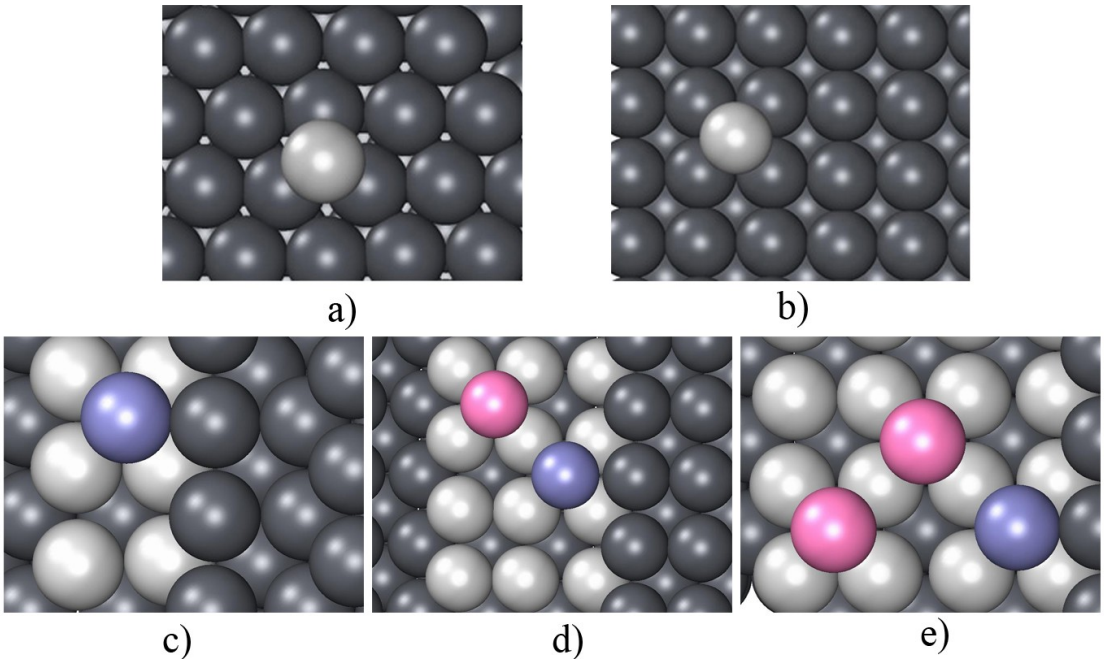


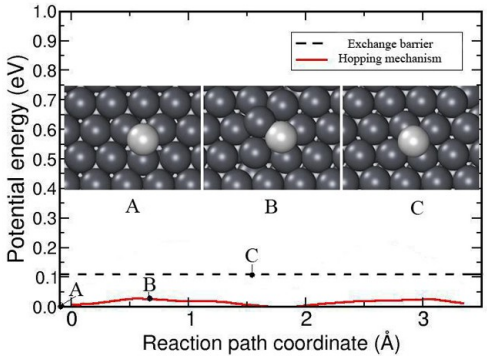
Fig6.3 Optimized position of Pb adatoms on different surfaces. The adatoms in the most stable position are depicted in light grey in a) and b) and is blue in c) which surface atoms are shown in dark grey and the adatoms in meta-stable transition position are shown in light red (for d, e).
a) Pb(111) surface, b) Pb(100) surface, c) Pb(311) surface, d) Pb(511) surface and e) Pb(711) surface.

The meta-stable transition position is also very important for the diffusion process in perpendicular direction at stepped surfaces. As could have been expected, the meta-stable transition position of stepped surface is at the four-fold hollow sites of the terrace, as the terrace can be regarded as a piece of (100) surface.

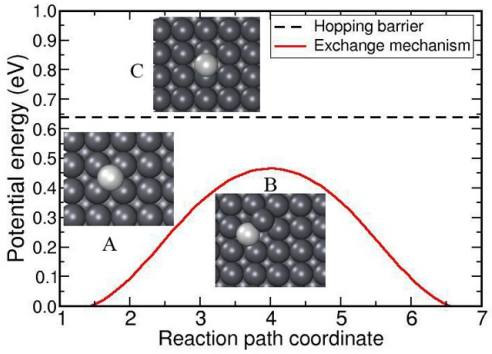
6.2 diffusion processes of self-diffusion

6.2.1 self-diffusion on flat surfaces

Table 6.2 shows the diffusion barriers on the flat Pb(100) and Pb(111) surfaces. On the Pb(111) surface, we obtained an energy barrier of only 0.01 eV for the hopping mechanism and 0.11 eV for the exchange mechanism which is about 10 times larger than for the hopping process. But interestingly enough, on Pb(100) the diffusion barrier of the exchange mechanism is 0.47eV which is 0.17eV lower than for hopping one indicating that the exchange diffusion is the favorable mechanism on Pb(100).



a)



b)

Fig. 6.4 shows us the minimum energy path of favorable mechanism on Pb(111) (a) and Pb(100) (b) surfaces. The configuration A, B and C are related to the initial state, intermediate state of favorable mechanism and the other mechanism.

Table 6.2 The diffusion barriers on Pb flat surfaces

	hopping(eV)	exchange(eV)
Pb(111)	0.01	0.11
Pb(100)	0.64	0.47

The diffusion constant is given by the Arrhenius formula:

$$D = D_0 \exp(-E_d / K_B T) \quad ,$$

where E_d is the diffusion barrier. Many studies show that the prefactor D_0 for exchange diffusion is usually 10 – 15 times larger than the one for hopping diffusion [6.39, 6.40] , hence the exchange is obviously favored for Pb(100), which is similar for Au(100). The large barrier difference between the hopping and exchange diffusion is easy to understand, as the (111) surface is the closed packed surface, the distance between the neighbouring surface atom is the smallest, so for a surface atom to break the bond and move out cost energies, and that is the reason why the exchange diffusion process is rather unfavouable. But for (100) surface, this process becomes much easier. Note that the two atoms exchanging each other are rather close to each other at the transition state, only about 3.15Å . Furthermore, the dimer is only 1.44 Å above the surface, so that the two atoms can be described as practically being five fold coordinated. Hence it is obviously this high coordination that makes the exchange diffusion on Pb(100) more favorable than the hopping diffusion.

6.2.2 self-diffusion on stepped surfaces

At stepped surfaces, the diffusion paths are much more complex than on the flat surfaces. First of all, one has to distinguish diffusion along the step edge from diffusion perpendicular to the step edge, i.e. across the step edge. For the exchange mechanism along and across the step edge, there are several possibilities. All the atoms in light grey and white in Fig.6 may be partners in the exchange diffusion of the adatom along and perpendicular to the step.

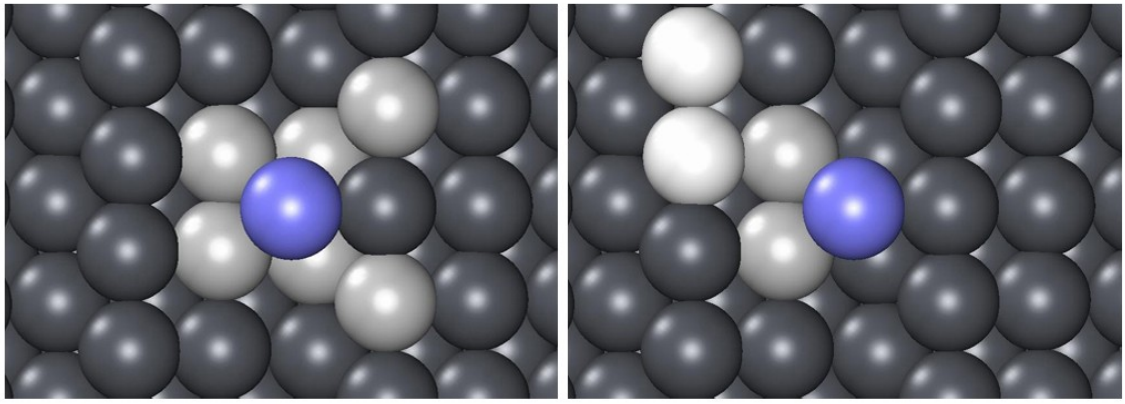


Fig.6.5 Surface atoms (in light grey) which might exchange with the adatom (in blue). a) diffusion along the step edge. b) diffusion perpendicular to the step edge. The atoms colored in light grey may be involved in the diffusion across the terrace while the atoms colored in white may be part of the exchange mechanism across the step.

The minimum energy diffusion paths on Pb(511) are illustrated in Figs.5 and 6. As shown in Fig.5, for the diffusion along the step edge, the barrier of hopping diffusion is 0.39eV lower than for the exchange mechanism. The hopping process occurs close to the step edge (inset B of Fig.5) and involves some relaxation of the step edge atoms. This relatively low barrier can be explained by the fact that the coordination of the hopping atom does not change signicantly along the diffusion path. In the exchange mechanism, on the other hand, the step edge atom has to detach almost entirely from the lower terrace making this mechanism rather unfavorable. The mechanism is quite similar to the diffusion process on Al(110) in the so-called in-channel diffusion [6.39].

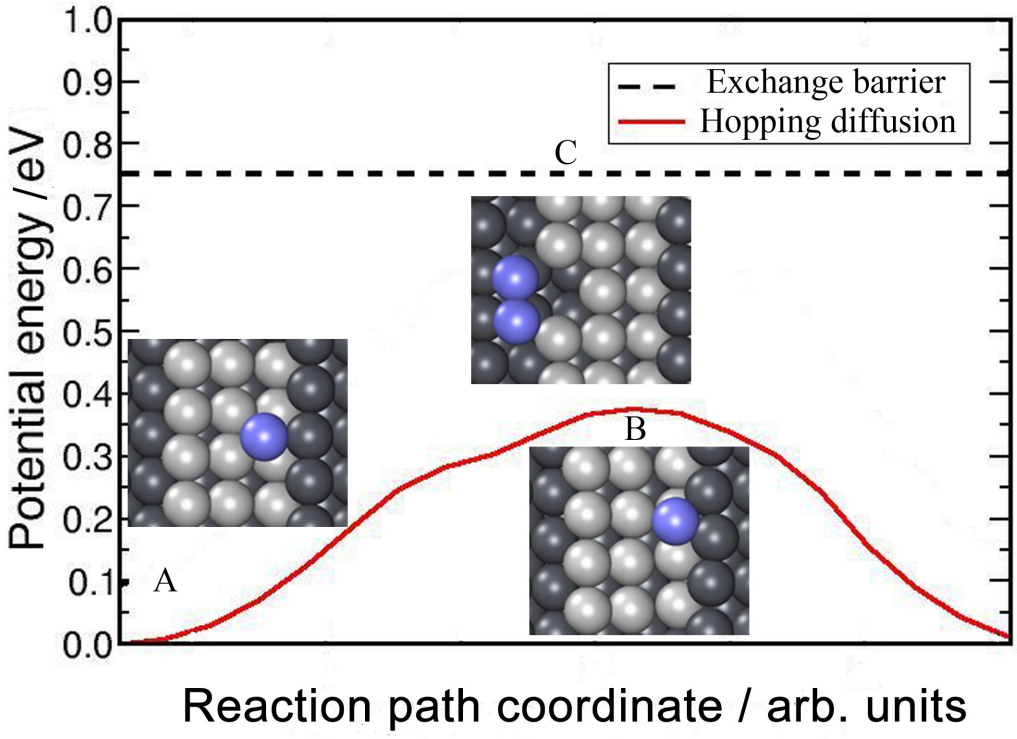


Fig. 6.6 Minimum energy path of the hopping mechanism for the diffusion along the
step at Pb(511). Insets A and B illustrate the initial and transition state of the hopping mechanism. The barrier for the exchange mechanism is indicated by the dashed line, its configuration is shown in inset C

For the diffusion across the terrace perpendicular to the step edge, the exchange mechanism is most favorable, as Fig.6 shows. The diffusion in the middle of the terrace is almost the same as the diffusion process on the flat Pb(100) surface with a very similar energy barrier. Across the step edge, the energy barrier for the exchange process is much lower than for the hopping mechanism. The high barrier in the hopping mechanism of 0.93eV is caused by the low coordination at the transition state, whereas in the exchange process (inset A of Fig.6), the coordination number of the adatom is only reduced from five at the initial state at the lower edge of the step to four at the transition state leading to a relatively low diffusion barrier.

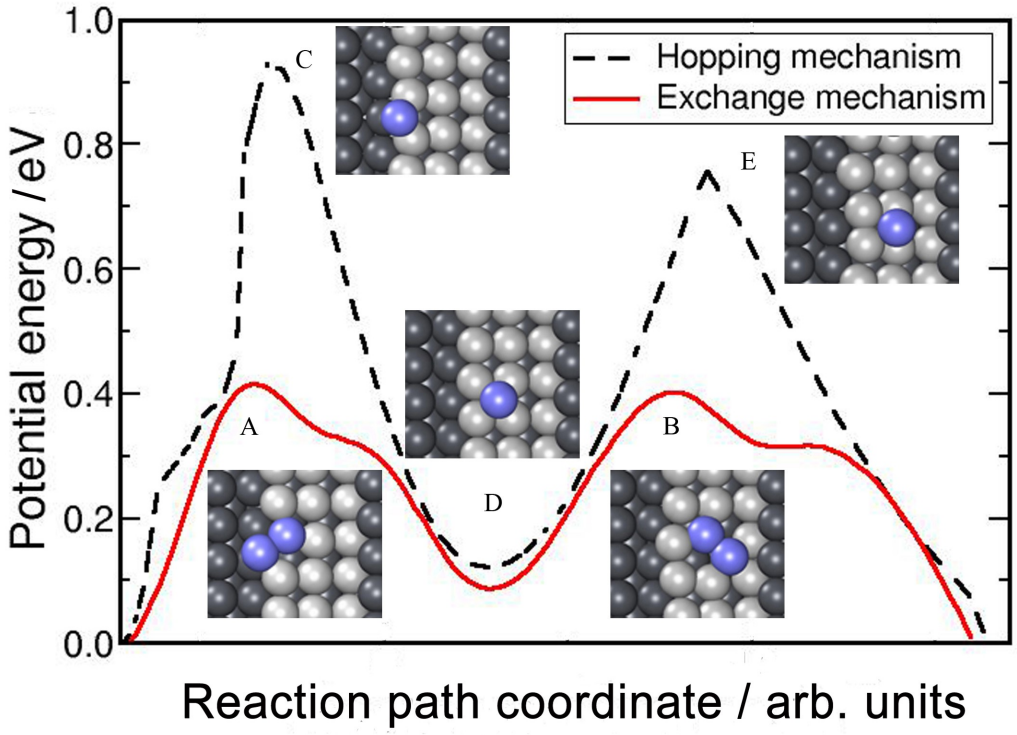


Fig. 6.7 Minimum energy path of the hopping and exchange mechanisms on Pb(511) across the step edge. Insets A and B show intermediate states of the exchange diffusion whereas insets C and E illustrate intermediate states in the hopping diffusion. Inset D shows the metastable intermediate on the terrace.

Table 6.2 Diffusion barriers at stepped Pb surfaces for diffusion along the steps (para) and across the steps (perp).

surface	Hopping (eV)	Exchange (eV)
Pb(311)para	0.33	0.36
Pb(311)perp	0.95	0.57
Pb(511)para	0.36	0.75
Pb(511)perp	0.93	0.41
Pb(711)para	0.37	0.73
Pb(711)perp	0.97	0.56

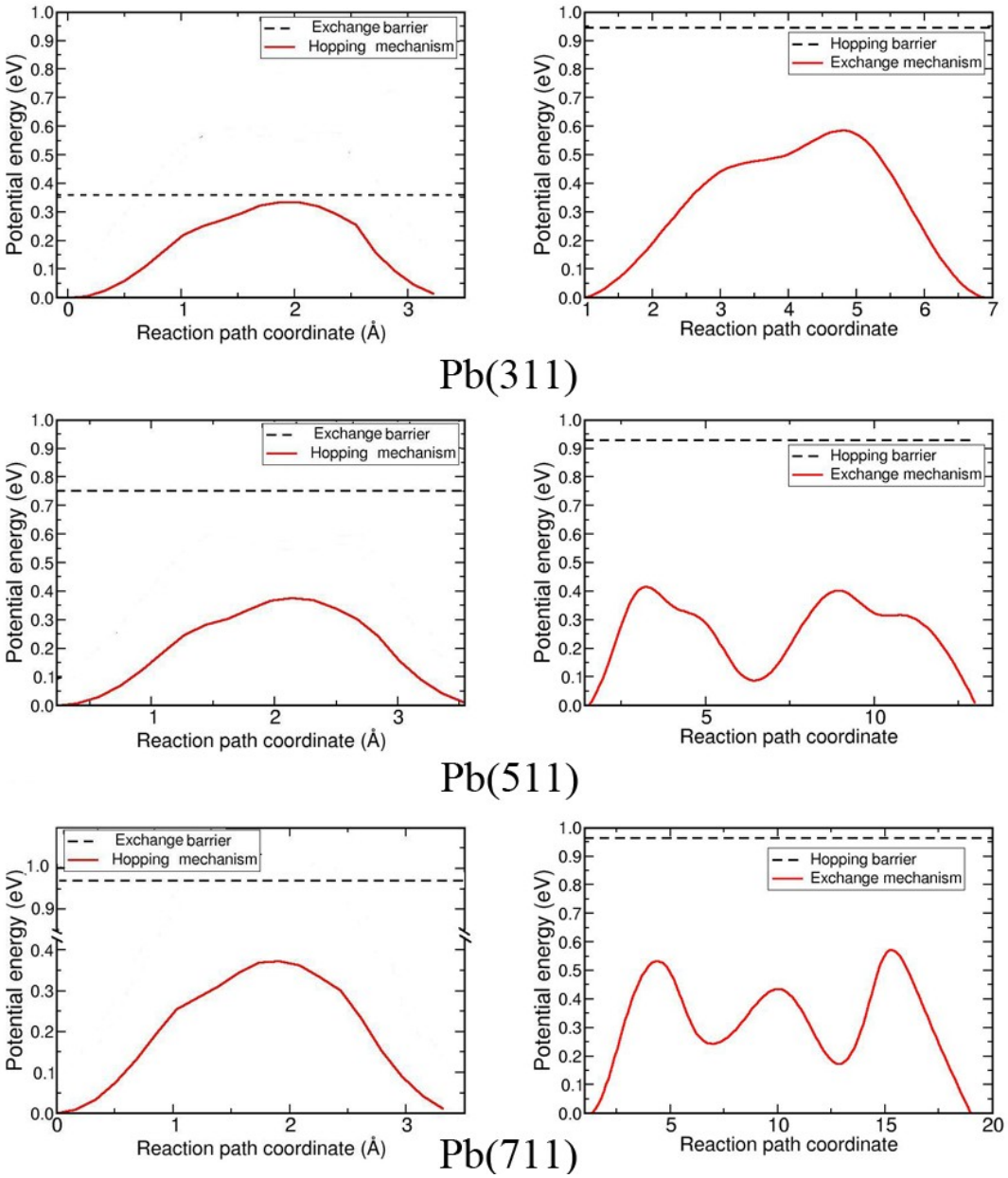


Fig. 6.8 The minimum energy path of diffusion at stepped surfaces both along the step edge (left panels) and across the step edge (right panels). The barriers of unfavorable mechanism are shown in dashed line

All calculated diffusion barriers at the considered stepped Pb surfaces, Pb(311), Pb(511) and Pb(711), are listed in Table 6.2. As already mentioned above, all of the

stepped surfaces have rather similar properties, as far as diffusion is concerned. Whereas along the steps the hopping mechanism is favored, across the steps the diffusion occurs in a exchange mechanism. These results are in qualitative agreement with previous calculations using the embedded atom method [6.14]. As a consequence, the diffusion barriers along and across the steps do not differ substantially facilitating the particle transport on the surface.

Fig.6.8 shows the minimum energy path of diffusion at stepped surfaces. As we have already mentioned, the properties of the stepped surfaces are similar. The shape of the curves are rather similar with each other. Another interesting point is that the longer the terrace is, the more similar diffusion process is with the one on the (100) surface. Note that the middle peak of Pb(711) diffusion across the step edge, the curve is almost the same as the (100) one, not only with respect to the barrier but also with respect to the shape.

Upon changing the electrode potential and thus the charge state of the surface, a new
equilibrium structure of a nanostructured electrode might result [6.41, 6.42]. To assume the new equilibrium configuration, deposition and transport processes have to occur. It is true that also the diffusion barriers can vary as a function of the electrode potential [6.43, 6.44], and we are currently addressing this issue in an ongoing project. Also the structure of the aqueous electrolyte at stepped surfaces is modified compared to flat electrodes [6.45, 6.46]. However, it has been estimated from the dipole moments of the diffusing metal particles in the initial and the transition state that diffusion barriers do not change substantially as a function of the electrode potential [6.44]. Thus the already rather low diffusion barriers for Pb self-diffusion on flat and stepped surfaces enable fast structural changes upon changing the equilibrium conditions. Hence our results are consistent with the proposed atomic mechanism occurring in the electrochemically controlled atomic-scale quantum conductance switch[6.1, 6.5, 6.13].

Bibliography

[6.1] F. -Q. Xie, L. Nittler, C. Obermair, and T. Schimmel, *Phys. Rev. Lett.* **93** 128303 (2004).

[6.2] F. -Q. Xie, R. Maul, C. Obermair, E. Starikov, W. Wenzel, G. Schoen, and T. Schimmel, *Nano Letters* **8** 4493 (2004).

[6.3] F. -Q. Xie, R. Maul, C. Obermair, W. Wenzel, G. Schoen, and T. Schimmel, *Adv. Mater* **22** 2033 (2010).

[6.4] R. Maul, F. -Q. Xie, C. Obermair, G. Schoen, T. Schimmel, and W. Wenzel, *Appl. Phys. Lett* **100** 203511 (2012).

[6.5] C. Obermair, H. Kuhn, and T. Schimmel, *Beilstein J. Nanotechnol.* **2** 740 (2011).

[6.6] T. Michely, M. Hohage, M. Bott, and G. Comsa, *Phys. Rev. Lett.* **70** 3943 (1993).
[6.7] M. Kalff, G. Comsa, and T. Michely, *Phys. Rev. Lett.* **81** 1255 (1998).
[6.8] P. Ruggerone, A. Kley, and M. Scheffler, *Prog. Surf. Sci.* **54** 331 (1997).
[6.9] H. Brune, *Surf. Sci. Rep.* **31** 121 (1998).
[6.10] M. E. Quayum, S. Ye, and K. Uosaki, *J. Electroanal. Chem.* **520** 126 (2002).
[6.11] H. Jonsson, Annu. *Rev. Phys. Chem.* **51** 623 (2000).
[6.12] D. Frenkel and B. Smit, Understanding Molecular Simulation: From Algorithms to Applications, Academic Press, San Diego, (1996).
[6.13] F. -Q. Xie, F. Hueser, G. Pauly adn Schoen, C. Obermair, and T. Schimmel, *Phys. Rev. B* **82** 075417 (2010).
[6.14] Y. Han, G. -H. Lu, B. -J. Lee, and F. Liu, *Surf. Sci.* **602** 2284 (2008).
[6.15] S. Dahl, A. Logadottir, R. C. Egeberg, J. H. Larsen, I. Chorkendorff, E. Toernqvist, and J. K. Norskov, *Phys. Rev. Lett.* **83** 1814 (1999).
[6.16] M. Lischka and A. Gross, *Phys. Rev. B* **65** 075420 (2002).
[6.17] F. Buatier de Mongeot, A. Toma, A. Molle, S. Lizzit, L. Petaccia, and A. Baraldi, *Nanoscale Res. Lett.* **2** 251 (2007).
[6.18] T. E. Madey, W. Chen, H. Wang, P. Kaghazchi, and T. Jacob, *Chem. Soc. Rev.* **37** 2310 (2008).
[6.19] A. Gross, *J. Comput. Theor. Nanosci.* **5** 894 (2008).
[6.20] P. Jakob, K. Anhut, S. Schnur, and A. Gross, *Phys. Rev. Lett.* **101** 206101 (2008).
[6.21]A. Abd-El-Latif, E. Mostafa, S. Huxter, G. Attard, and H. Baltruschat, *Electrochem. Acta* **55** 7951 (2010).
[6.22] M. F. Juarez and E. Santos, *J. Phys. Chem. C* **117** 4606 (2013).
[6.23] J. G. Howalt, T. Bligaard, J. Rossmeisl, and T. Vegge, *Phys. Chem. Chem. Phys.* **15** 7785 (2013).
[6.24] D. Loss and D. P. DiVincenzo, *Phys. Rev. A* **57** 120 (1998).
[6.25] L. Wang, A. Rastelli, S. Kiravittaya, M. Benyoucef, and O. G. Schmidt, *Adv. Mater.* **21** 2601 (2009).
[6.26] M. Nomura, N. Kumagai, S. Iwamoto, Y. Ota, and Y. Arakawa, *Nature Phys.* **6** 279 (2010).
[6.27] H. Oka, P. A. Ignatiev, S. Wedekind, G. Rodary, L. Niebergall, V. Stepanyuk, D. Sander, and J. Kirschner, *Science* **327** 843 (2010).
[6.28] J. I. Martin, J. Nogues, K. Liu, J. L. Vicent, and I. K. Schuller, *J. Magn. Mater.* **256** 449 (2003).
[6.29] S. Baud, C. Ramseyer, G. Bihlmayer, and S. Bluegel, *Phys. Rev. B* **73** 104427 (2006).
[6.30] P. J. Feibelman, *Phys. Rev. Lett.* **65** 729 (1990).
[6.31] T.-Y. Fu and T. T. Tsong, *Surf. Sci.* **454** 571 (2000).
[6.32] T. -Y. Fu, L. -C. Cheng, Hwang, Y. J., and T. T. Tsong, *Surf. Sci.* **507** 103 (2002).
[6.33] S. Schnur and A. Gross, *New J. Phys*. **11** 125003 (2009).
[6.34] S. Schnur and A. Gross, *Catal. Today* **165** 129 (2011).
[6.35] T. Roman and A. Gross, *Catal. Today* **202** 183 (2013).

[6.36] G. L. Kellogg and P. J. Feibelman, *Phys. Rev. Lett.* **64** 3143 (1990).
[6.37] C. Chen and T. T. Tsong, *Phys. Rev. Lett.* **64** 3147 (1990).
[6.38] B. D. Yu and M. Scheffler, *Phys. Rev. B* **56** R15569 (1997).
[6.39] R.Stumpf and M. Scheffler, *Phys. Rev. B* **53** 4958 (1996).
[6.40] K. C. Pandey, *Phys. Rev. Lett.* **57** 2287 (1986).
[6.41] K. P. Bohnen and D. M. Kolb, *Surf. Sci.* **407** L629 (1998).
[6.42] A. Y. Lozovoi and A. Alavi, *Phys. Rev. B* **68** 245416 (2003).
[6.43] K. Poetting, N. B. Luque, P. M. Q. H. Ibach, and W. Schmickler, *Electrochim. Act* **54** 4494 (2009).
[6.44] N. B. Luque, H. Ibach, K. Poetting, and W. Schmickler, *Electrochim. Act* **55** 5411 (2010).
[6.45] H. Ibach, *Surf. Sci.* **604** 377 (2010).
[6.46]X. Lin and A.Gross, *Surf. Sci*. **606** 886 (2012).

Conclusions

My work has focussed on the water-metal interface and the diffusion processes on stepped and flat Pb, Au, Ag surfaces, in order to understand the quantum switching processes at the electrode.

We first tested the parameter for modeling the surface system and for the accuracy of DFT calculation. Then some basic properties of clean flat and stepped surface have been addressed including the lattice constant, surface energy, interlayer distance, charge density difference and density of states.

For a better understanding of the water – metal interaction, a single water molecule adsorbed on different surfaces has been simulated. The strength of the metal-water interaction depends on the properties of the metal. Generally speaking, the adsorption energy of single water molecule on the stepped surfaces is much larger than on the flat surfaces.

The structural, electronic and vibrational properties of a water layer on Au(100) have been addressed, Au(511) and Ag(511) have been studied by first principles total energy calculations and ab initio molecular dynamics simulations. On Au(100) a structural model based on a (2 x 2) surface unitcell does not seem to be realistic.

We obtained the most stable water structures on Au(100), Au(511) and Ag(511). From the calculated vibrational spectra, several fundamental aspects have been derived. On Au(100), an OH stretching mode can be found at 3500 cm^{-1} and no NHB hydrogen stretching mode was obtained which might be caused by the weak interaction between water layers and the Au(100) surface.

On stepped surfaces, three peaks can be found around 3500 cm^{-1} (3300 cm^{-1} ,3500 cm^{-1} and 3600 cm^{-1} for Au(511), 3345 cm^{-1} ,3465 cm^{-1} and 3690 cm^{-1} for Ag(511)), where the appearance of two HB hydrogen stretching modes might be caused by the influence of the step edge. The simulation results with respect to the positions of the peaks agree with the experimental data quite well.

AIMD simulations show that at 140K on Au(100) the rectangular structure is thermodynamically not stable whereas on Au(511) and Ag(511) the calculated structure is quite stable at 140K, there is even hardly any change of the structure on Au(511) at 300K. The charge density difference shows a rather localized and strong polarization of water at the step edge on Au(511) and Ag(511). All of the phenomena indicate a strong interaction between step edge and water layer, and rather different electronic properties compared with flat metal surfaces.

As the lattice constant of Pb is much larger than Au and Ag, we find different water structures of a single layer on Pb(100) and Pb(111) surfaces. We also addressed the water structures with different coverage on both surfaces.

Using first principles electronic structure calculations we have addressed elementary processes that may be relevant to the collective switching mechanism

occurring in the atomic-scale quantum conductance switch. The DFT calculations indeed revealed that diffusion processes across the steped edges of nanostructured surfaces are facilitated through the exchange mechanism making diffusion across the steps almost as facile as along the steps. This can be helpful to elucidate the atom transfer at the electrode during the switching process.

Appendix A

Inter-Layer distance of Au, Ag and Pb surfaces after the DFT-GGA relaxations. All of the value in this table is in the unit of Å.

surface	d_{12}	d_{23}	d_{34}	d_{45}	d_{56}	d_{67}	d_{78}	d_{89}	dbulk
Au(111)	2.44	2.40	---	---	---	---	---	---	2.41
Au(100)	2.07	2.09	---	---	---	---	---	---	2.08
Au(211)	0.64	0.74	1.06	0.78	0.86	0.86	---	---	0.85
Au(311)	1.00	1.41	1.21	1.28	---	---	---	---	1.26
Au(511)	0.67	0.59	1.05	0.71	0.81	0.82	---	---	0.80
Au(711)	0.49	0.53	0.39	0.84	0.55	0.51	0.62	0.60	0.58
Ag(111)	2.41	2.41	---	---	---	---	---	---	2.40
Ag(100)	2.06	2.11	---	---	---	---	---	---	2.08
Ag(211)	0.75	0.78	0.93	0.84	0.85	0.86	---	---	0.85
Ag(311)	1.11	1.32	1.25	1.27	---	---	---	---	1.25
Ag(511)	0.73	0.70	0.89	0.77	0.81	0.82	---	---	0.80
Ag(711)	0.52	0.58	0.49	0.67	0.57	0.56	0.60	0.60	0.58
Pb(100)	2.37	2.59	---	---	---	---	---	---	2.50
Pb(111)	2.74	2.93	---	---	---	---	---	---	2.89
Pb(211)	0.88	0.92	1.06	0.98	0.99	1.14	---	---	1.02
Pb(311)	1.22	1.54	1.45	1.59	---	---	---	---	1.51
Pb(511)	0.89	0.97	0.87	1.03	1.00	0.97	---	---	0.96
Pb(711)	0.56	0.74	0.56	0.74	0.62	0.73	0.73	0.75	0.70

Appendix B

The surface energy of Ag(111) surface with different exchange-correlation functional and basis sets.

method	Surface energy (J/m2)
PBE/PAW(our study)	0.80
PBE/NAO[4.6]	0.77
PBE/EMTO[4.10]	0.89
PBEsol/EMTO[4.10]	1.23
RPBE/PAW[4.6]	0.57
RPBE/NAO[4.6]	0.58
LDA/FP-LMTO[4.8]	1.21
LDA/FCD-LMTO[4.9]	1.17
Experimental Ag (T0/Ta/Tm) (J/m2)[4.7]	1.38/1.30/1.05

Appendix C
surface energy of metal Cu

Surface	Surface energy (J/m2)
Cu(100) [4.4]	1.45
Cu(111) [4.4]	1.30
Cu(311) [4.11]	1.82
Cu(511) [4.11]	1.68

Acknowledgments

Financial support by the Baden-Wuerttemberg-Stiftung tugh the network "Functional Nanostructures" is gratefully acknowledged. Computer time has been provided by the BW-Grid of the federal state of Baden-Wuerttemberg and by a computer cluster financed through the stimulus programme "Electrochemistry for Electromobility" of the German Ministry of Education and Science (BMBF).